Dissolved Organic Fouling on Nanofiltration Membranes

by

Kai Lee

A thesis submitted in partial fulfillment of the requirements for the degree of

Master of Science

in

Chemical Engineering

Department of Chemical and Materials Engineering
University of Alberta

Abstract

The fluids produced from a thermal enhanced recovery process such as steam assisted gravity drainage (SAGD) and cyclic steam stimulation (CSS) are pumped to the surface where bitumen and water are separated. This initial fluid is known as SAGD-PW (produced water). A potential way to effectively treat SAGD-PW is to use membrane filtration technology. Membrane filtration technology has the potential to remove the dissolved organics present in SAGD-PW. Current conventional water treatment (main components include warm lime softener and weak acid cation exchanger) of SAGD-PW cannot remove effectively the dissolved organics. This treated water with still dissolved organics has the potential to foul equipment downstream of the water treatment plant. This was the motivation to investigate using membranes to treat SAGD-PW. The focus of this study was to investigate organic fouling and performance for nanofiltration (NF) membranes used to treat SAGD-PW. NF membranes were considered over other membranes (RO, UF, MF) due to the ability to remove dissolved organics and the lower energy requirements. This study also focused on the membrane surface properties (roughness, wettability, and material composition) of the six commercially available NF membranes and its impact on membrane fouling and fluid flux. The cross flow filtration fouling experiment were all conducted at the 45^{o}C and same hydrodynamic flowing conditions and most the majority of the experiments; the synthetic feed water was identical. Two special feed water samples were used in two separate experiments to investigate the effect of salt and emulsified oil presence in the feed water. The results showed that NF membranes were capable of removing high amount (>90%) of dissolve organics present in the feed water. Both the membrane initial surface roughness and the membrane material composition played a role in overall performance and fouling behavior. The addition of salt in the process water increased the fouling and produced

lower permeate rates (32% drop in permeate rate after 20 hours of filtration) compared to the case where no addition salt was added to the process water. Similarly, when the process water contains emulsified oil, the fouling was severe and permeate rate was reduced (70% drop in permeate rate after 20 hours of filtration) compared to the case where no emulsified oil was present in the process water. The fouling experimental data generated was then used to model the effect of roughness resistance. The roughness resistance was a proposed resistance that can be used to improve the predictive fouling capabilities of the conventional filtration theory equation. The development of the resistance model and validation of the predictive capability showed that it is conceivable that the membrane surface roughness plays an important role in membrane fouling. It is recommended that future studies add more complexities to the feed water composition and eventually using real SAGD-PW samples to evaluate performance and fouling characteristics. To scale up the membrane filtration process and bring the technology closer to pilot scale testing, it is also recommended that subsequent studies should integrate spiral wound membrane elements into their lab testing facility. This increases the membrane active surface area and allows for scale up to commercial applications and conditions. To further understand the fouling mechanisms that occur between membrane and foulant, future studies could investigate the interaction forces that arise during the membrane fouling process. Future studies could also advance the concept of a roughness resistance and further validate and improve the roughness resistance (R_r) model developed in this study.

Preface

In this study, cross-flow filtration of synthetically made SAGD produced water was conducted by using NF membranes to remove dissolved organics and salt. The membrane surface properties before and after the fouling experiment were analyzed to observe the effect of fouling on these surface properties. A new concept of roughness resistance was proposed and a new parameter related membrane roughness was incorporated into the existing filtration theory. This can then be used to predict the fouling behavior during filtration. This thesis is an original work done by Kai Lee. No part of this thesis has been previously published.

Acknowledgement

I would like to express my sincere gratitude to my U of A supervisor Dr. Hongbo Zeng and to my Innotech Alberta supervisor Mr. Ross Chow for their guidance and support throughout my research. It was an interesting process of expanding ones knowledge and improving their researching skills. I would also like to thanks my work colleagues: Dr. Shad Siddiqui and Dr. Pablo Contreras from (Innotech Alberta) for their continued mentoring and guidance through this unique opportunity presented to me by Innotech Alberta to improve myself. All the academic and industrial experience from these individuals mentioned above was essential to accomplish this study.

I would also like to acknowledge Innotech Alberta for their support and giving me the opportunity during these 3 years to improve my capabilities especially my manager (Dr. Haibo Huang).

I extend my appreciation to the students and members of Dr. Hongbo Zeng's research group for their suggestions, advice, and technical support during my research.

Finally but equally important, a special thanks to my wife, family and friends for their constant encouragement to continue to improve myself and become a better researcher.

TABLE OF CONTENTS

LIST OF TABLES

LIST OF FIGURES

NOMENCLATURE

Abbreviations

SAGD	Steam assisted gravity drainage
CSS	Cyclic steam stimulation
SAGD-PW	Steam assisted gravity drainage produced water
TDS	Total dissolved solids
TOC	Total organic content
BFW	Boiler feed water
OTSG	Once through steam generator
OSPW	Oil sands produced water
IST	Innovative steam technologies
DOM	Dissolved organic matter
MF	Microfiltration
UF	Ultrafiltration
NF	Nanofiltration
RO	Reserve Osmosis
MD	Membrane distillation
XDLVO	Extended Derjaguin-Landau,Verwey-Overbeek theory
PES	Polyethersulfone
TMP	Transmembrane pressure
MWCO	Molecular weight cut off
PSIG	Pounds per square inch gauge
Re	Reynolds number

BPR	Back pressure regulator
DI	Deionized
AFM	Atomic force microscopy
RMS	Root means square
ATF-FTIR	Attenuated total reflectance-fourier transform infrared spectroscopy
SEM-EDX	Scanning electron microscopy-energy dispersive X-ray
ASTM	American Society for Testing and Materials
IC	Ion chromatography
ICP-OES	Inductively coupled plasma-optical emission spectroscopy
CCD	Charged coupled device
EDL	Electric double layer

Symbols

Q	Permeate rate
A	Membrane active area
P	Pressure
μ	Fluid viscosity
R	Resistance
V	Permeate volume
α	Specific cake resistance
C	Concentration
I	Cake Resistivity
J	Permeate flux
t	Experiment time

K	Resistance coefficient
n	Blocking index
N	Total number of open pores per membrane area
x	Number of foulant blocking pores per permeate volume
k	Proportionality constant
r	pore radius
u	flowrate
L	Thickness of membrane
K’	Permeability
ρ	Density
D	Hydraulic radius
U	Cross flow velocity
a	Membrane rectangular slot dimension
b	Membrane rectangular slot dimension
η	Dynamic viscosity
ζ	Zeta potential
λ_D	Debye length
e	Elementary charge
Z	Charge number
T	Temperature

Subscripts

m	Membrane
c	Cake

b	Complete blocking
s	Standard blocking
i	Intermediate blocking
o	Initial
rel	Relative
eff	Effective
tot	Total
r	Roughness
H	Hydraulic
w	Water
max	Maximum
y	Percent the permeate rate decreased compared to initial value

1.0 INTRODUCTION

1.1 BACKGROUND AND LITERATURE REVIEW

The fluids produced from a thermal enhanced recovery process such as steam assisted gravity drainage (SAGD) and cyclic steam stimulation (CSS) are pumped to the surface where bitumen and water are separated. This initial fluid is known as SAGD-PW (produced water). Figure 1.1 shows a typical SAGD water treatment plant with specification for SAGD-PW feed and the clean water feed going into the steam generator. This indicates that the total dissolved solids (TDS) and total organic content (TOC) throughout the water treatment process does not change significantly. In the water treatment process, the bitumen and produced water are first separated using gravity and flotation cells. This is followed by skim tanks and induced static flotation to separate the remaining residual oil from the produced water. The de-oiled water is then treated in a warm lime softener to remove primarily calcium and magnesium by using chemicals. The chemicals used are soda ash (Na_2CO_3) and sodium hydroxide. During this warm lime softening process, significant amount of silica (~90%) is removed from the water due to attachment of the silica particles to the precipitated magnesium ions. Finally multivalent cations (like Ca^{2+} and Mg^{2+}) are removed via a weak acid cation exchanger. During this process, the de-alkalization of the produced water is done by using weak acid cation resins. The resins are usually carboxylic type acids [Singh (2006), Pingale (2005)]. The treated water can then be used as boiler feed water (BFW) in once through steam generators (OTSG). Figure 1.2 shows the layout of an OSTG. It should be noted that the process water temperature entering the warm lime softener is typically between 80^{o}C to 90^{o}C. This high temperature is above most commercial membrane operating limits which is typically around 45^{o}C to 50^{o}C. Table 1.1 shows the typical OSTG

boiler feed water specification. Table 1.2 shows another comparison between SAGD-PW and oil sands produced water (OSPW). The OSPW is the waste water generated during the mining extraction process for bitumen reservoirs.

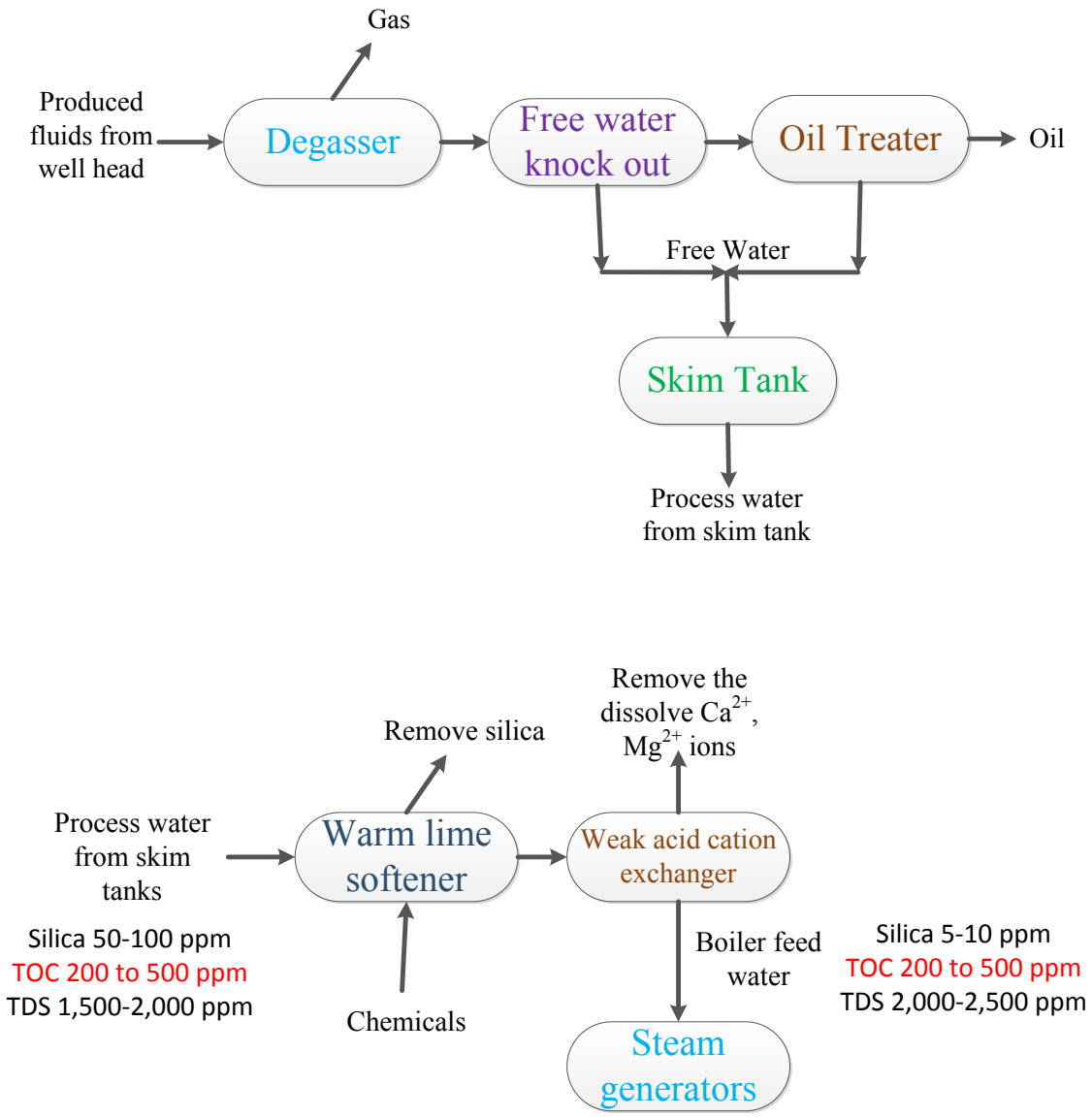

Figure 1.1: Typical conventional SAGD water treatment plant [Wang et al. (2005)]

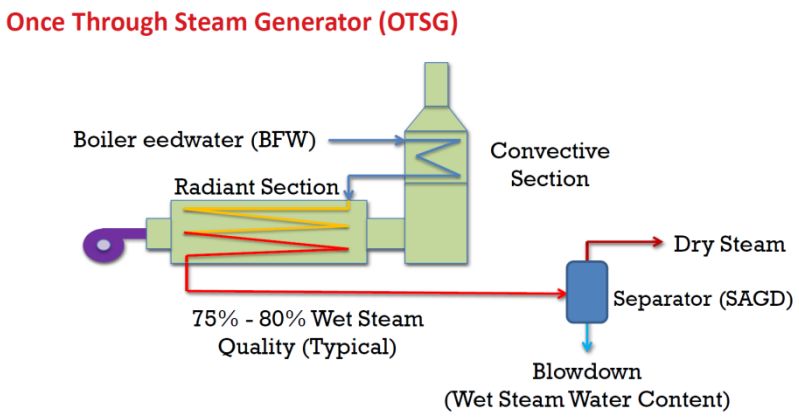

Figure 1.2: General layout of an OSTG (Image taken from Canadian Heavy Oil Conference presentation by Innovative Steam Technologies (IST))

Table 1.1: Typical SAGD OTSG BFW specification [Sadrzadeh et al. (2015)]

Parameter	Spec	Units
TDS	<0.5	mg/L as $CaCO_3$
Silica	<75	mg/L as SiO_2
Electrical Conductivity	<12	mS
Bitumen content in water	<0.5	mg/L
Iron	<250	µg/L as Fe
Turbidity	<7.5	NTU

Table 1.2: Comparison of SAGD-PW, OSPW, and boiler blow down water [Thakurta et al. (2013)]

Characteristic	SAGD-PW	OSPW
pH	7.11	8.6 to 9.1
Conductivity, µS/cm	1,540	2,370 to 3,459
TDS, ppm	1,005	2,477
TOC, ppm	232	48 to 83

This conventional water treatment setup lacks a treatment for the effective removal of total dissolved solids (TDS) and dissolved organic material (DOM). In Figure 1.1 the total organic content and TDS in the water relatively unchanged throughout the treatment process. OTSGs are used to generate steam from BFW due to ability to operate at water feed quality with higher contaminants like TDS and Ca/Mg/Si. The steam quality from these OTSGs are generally low (~80%) to counter balance for the low quality BFW. This means less steam is being produced (i.e. less steam vapour and more liquid water coming out of the OTSG) and a larger volume of boiler blowdown water is being recycled back to the water treatment plant. This can affect the economics of an SAGD process. Operations that lead to higher than 80% steam quality could lead to scale formation in the OTSG due to the contaminants. The scaling can lead to overheating and eventual failure of the equipment.

Deviation from BFW specifications can result in heat exchanger and boiler tubing fouling. The fouling materials found on these heat exchangers were a combination of organic carbon and Ca/Mg/Si [Sadrzadeh et al. (2015), Hayatbakhsh et al. (2016)]. Wang et al. (2005) and Guha et al. (2013) have studied the effect of fouling during SAGD operation from the contaminants in feed water. They discuss organic fouling to heat exchangers and boiler tubes as a result of high contaminant content (TDS and organics) in feed water composition.

The organic component in the SAGD-PW can be different from the process water from mining operations. This is known as oil sands process affected water (OSPW). Many earlier studies have reported that OSPW consists primarily of naphthenic acid like compounds [Masliyah et al. (2004), Perez et al. (2011)]. In contrast, it was reported that the organic component in SAGD-

PW was demonstrated to be more representative of humic acid which can affect membrane performance [Thakurta et al. (2013)].

1.1.1 Potential Technologies for Treatment of SAGD Produced Water

The goal of SAGD operators when treating produced water is to remove as much organics as possible including the dispersed and dissolved organics. The dispersed organics can be in the form of emulsions where the fine oil droplets are suspended and quite stable in the water phase. A majority of the dispersed organics or oils can be removed via an initial de-oiling step. However, the dissolved organics are not removed during this initial step. Operators also want to remove suspended particles and sand, chlorides, dissolved gases, and remove excess water hardness [Daniel et al. (2005)]. Some of the potential technologies that operators may apply as standalone or combined treatment processes include the following:

- Membrane filtration technology – Membranes are porous films with specific pore size ratings which selectively separate undesirable solute from the main solution. There are four main established membrane separation processes including microfiltration (MF), ultrafiltration (UF), nanofiltration (NF), and reverse osmosis (RO). RO membranes are able to effectively desalinate water. NF membranes are capable of removing dissolved organics and ions. UF membranes can separate macromolecules like proteins and viruses. MF membranes are effective at separating suspended particles. Membrane processes are pressure driven processes with RO membranes requiring the highest transmembrane pressure to drive the process compared to MF membranes where transmembrane pressures are much lower. Membrane technology can operate in either dead end filtration mode or in cross flow filtration mode (Figure 1.3). In dead end filtration, the feed enters

one side of the membrane and exits on the other side due to the applied pressure drop. In cross flow filtration, the feed is flowed across the membrane surface and part of the feed water is passed through the membrane due the applied transmembrane pressure. In most commercial applications of water treatment, the filtration mode utilizes cross flow filtration.

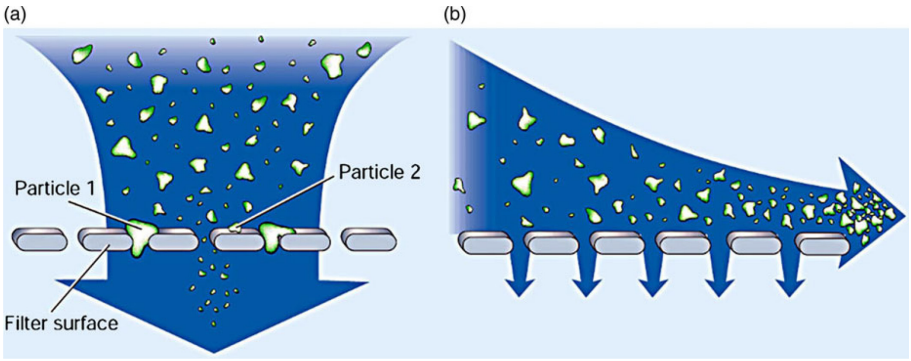

Figure 1.3: Membrane filtration modes: (a) dead end filtration mode and (b) cross flow filtration mode [Igunnu and Chen, 2014]

- Adsorption – The use of adsorbents can be an effective method to polish the produced water and remove organics, oils, and heavy metals present in the water [Igunnu and Chen, 2014]. However these adsorbents can be easily overloaded by organics and require replace or regeneration of the adsorbent material. The types of adsorbents include activated carbon, organoclays, activated alumina and zeolites [Allen (2008), Swenson et al. (2012)]. The cost of clean/regeneration, potential low capacity of most adsorbents and environment issues of waste disposal after adsorption are the principle drawbacks of using adsorbents for large scale water treatment processes.

- Ion exchange technology – Ion exchange is a technology used in industrial operations for various purposes. It is been shown to be useful in removing monovalent and divalent ions present in treating produced water [Igunnu and Chen (2014), Clifford (1999)]. However, the lifespan for this technology is ~ 8 years and usually requires a pre-treatment step to remove solids.
- Membrane Distillation (MD) – Membrane distillation is an emerging technology for treating process water from oil production. This technology has been around for more than 40 years and there have been recent interest in potentially using it to treat process water from oil sands mining and in-situ extracted oil [Souhaimi and Matsuura (2011), Elsayed et al. (2015)]. This technology is a thermally driven transport of vapour through a non-wetted hydrophobic porous membrane. The driving force is mainly due to the vapour pressure difference between the two sides of the membrane. There is simultaneous heat and mass transfer involved in this process. The feed solution is heated up to moderate temperatures but below the boiling point at the feed pressure condition. The produced water vapour than travels across preferentially through the hydrophobic membrane and condenses on the other side of the membrane to form the clean permeate stream. One benefit of treating SAGD produced water with this technology is that the stream is already heated to elevated temperatures. This can reduce the cost of heating the feed solution before treatment. However, with most membrane type processes, the membranes are susceptible to fouling from the contaminants in the feed water [Elsayed et al. (2015), Lokare et al. (2017), Malmali et al. (2017)].

1.1.2 Focus on Membrane Filtration Technology

A potential way to effectively treat SAGD-PW is to use membrane filtration technology. Membrane filtration technology has the potential to remove the dissolved organics present in SAGD-PW. Current conventional water treatment of SAGD-PW mentioned above cannot remove effectively the dissolved organics. This treated water with still dissolved organics is then fed to the steam generators where potential fouling of this equipment can happen due to the organics. This is the motivation to investigate using membranes to treat SAGD-PW.

Membrane separation is a pressure driven process that have been used to treat produced water due to their advantages of low energy consumption, lower operating cost, and effective removal of contaminants. However, membranes processes suffer from fouling on membrane surfaces due to deposition of contaminants. There have been studies indicating that organic material is the main contributor to membrane fouling [Lin et al. (2014)]. The membranes used range from finely porous structures to nonporous and can remove contaminants such as bacteria and macromolecules down to ions. Another advantage of membrane technology is its ability to be modular and range from large scale to lab scale applications. There are a number of different types of membranes classification.

Table 1.3 highlights the typical application of these membranes [Zioui et al. (2015)].

Table 1.3: Types of membranes

Membrane Process	Application	Membrane Material	Pore Size	Molecular weight cut-off	Typical Filtration Pressure
Microfiltration (MF)	Removal of suspended solids and colloids	Ceramic, Polymeric	<0.1 μm	>5000 kDa	< 2 bar
Ultrafiltration (UF)	Removal of viruses and macromolecules	Polymeric	100 to 2 nm	5 to 5000 kDa	1 to 10 bar
Nanofiltration (NF)	Removal of organic compounds and multi-valent ions	Polymeric	2 to 1 nm	0.1 to 5 kDa	3 to 20 bar
Reverse Osmosis (RO)	Removal of salts/ single valent ions	Polymeric	<1 nm	<100 Da	10 to 80 bar

To improve the steam quality (i.e. OSTG operating a higher efficiency), reduce boiler blow down recycle water, and prevent equipment fouling, there is a need to target the removal of TDS and organic material. NF and RO membranes can potentially accomplish this given the specifications in Table 1.2. The important difference between the two types of membranes is the operating conditions. RO membranes operate at high transmembrane pressures (TMP) compared to NF membranes. This is due to the filtration pore size. Thus there needs to be a balance between effectively removing DOM and TDS in relation to operating pressure. Higher operating pressure equates to higher operating cost.

In fact, in recent studies RO and NF membranes were tested with SAGD-PW to determine DOM and TDS rejection [Sadrzadeh et al. (2015), Hayatbakhsh et al. (2016)]. At these experimental conditions, they observed similar contaminant removal in both NF and RO membranes (DOM, salt, and silica > 98% removal). The DOM that did pass through the membranes was hydrophilic

by nature. These experiments also showed that the membrane surfaces were fouled due to inorganic (silica and iron) and organic (carbon and oxygen) materials and that the pH of the feed had an impact on flux and membrane fouling. At higher pH (10.5) feed conditions, less fouling was observed on the membrane surface and the flux decline was not as severe compared to the lower pH (8.5) condition. An investigation into using ultrafiltration (UF) membranes to treat SAGD-PW was done by revealed poor salt, silica, and DOM removal compared to NF and RO membranes [Hayatbakhsh et al. (2016)]. The pore size feature of these UF membranes was not suitable for this type of feed water.

In terms of understanding membrane fouling from SAGD-PW, there have been very little studies looking into specifically the mechanism or causes on membrane fouling when dealing with SAGD-PW. The types of contaminants that are formed on membrane surfaces from SAGD-PW feed have been identified [Sadrzadeh et al. (2015), Hayatbakhsh et al. (2016)]. These two studies however did not relate membrane surface properties to the observed fouling performance.

An important membrane characteristic that has not been deeply explored in literature is the impact of NF membrane wettability (wettability affected by surface roughness, contact angle and zeta potential measurement of wettability) on organic fouling.

However, there have been a number of studies looking at membrane surface characteristics and its interaction with different foulants. For instance, Xiao et al. (2011) investigated interactions between polyvinylidene fluoride MF membranes and foulants representing polysaccharides, proteins, and humic substances. They measured the contact angle and zeta potential of the

fouling participants (membrane and foulants) and also used a semi-empirical model derived from the extended Derjaguin-Landau,Verwey-Overbeek (XDLVO) theory to describe the membrane-foulant interactions. The important conclusion from their study was that the hydrophobic interactions rather than electrostatic interactions may be the predominant mechanism affecting adsorptive fouling. Maruf et al. (2013) studied the effect of nanoimprinted surface patterns on UF membranes and its ability to resists deposition of colloidal silica particles. They concluded that the imprinted surface pattern had a positive effect on reducing fouling. The cause for this observation was unknown. Low et al. (2015) explored enhancing antifouling properties of polyethersulfone (PES) ultrafiltration membranes by coating the membrane with nanoporous titania nanoparticles. These particles enhanced the wettability of the membrane by reducing the surface free energy and reduced the observed contact angle. These modified membranes showed higher resistance to fouling.

1.2 MEMBRANE FILTRATION THEORETICAL BACKGROUND

Looking into the theoretical aspect of membrane fouling, the conventional filtration theory has been used by researchers to describe the membrane performance and its relation to foulant cake formation on the membrane surface. It relates feed flow to the transmembrane pressure (TMP). For the cross flow filtration case, Equation 1 is used to related flow rate to TMP [Koo et al. (2013)].

$$Q = \frac{A\Delta P}{\mu(R_m+R_c)} \qquad (1)$$

Where Q=flowrate, A=membrane active area, ΔP=transmembrane pressure, μ=fluid viscosity, R_m=membrane resistance, R_c=cake resistance.

Here R_m is related to the membrane characteristics and this is related to the overall porosity. R_c is a variable that is related to the membrane fouling. Equation 1 can be shown to be derived from Darcy's Law and uses the resistance-in-series model to represent the total resistance [Koo et al. (2013)]. The total resistance, R_{tot}, is equal to the sum of the individual resistances (R_m and R_c).

The cake resistance, R_c, is due to foulant deposition and is the product of the permeate flux, the filtration time, and the cake resistivity.

$$R_c = JtI \qquad (2)$$

Where J=permeate flux, t=filtration time, and I=cake resistivity.

Substituting Equation 2 back into Equation 1, we obtain Equation 3.

$$\frac{Q}{A} = \frac{\Delta P}{\mu(R_m + JIt)} \qquad (3)$$

Since Q/A is equal to J, equation 3 can be re-written as:

$$J = \frac{\Delta P}{\mu(R_m + JIt)} \qquad (4)$$

The cake resistivity should be a related to the type of contaminant present in the feed and membrane surface properties. However, in this conventional filtration theory which was original

derived for fine particle filtration, there is no direct or indirect variable that captures the membrane surface wettability characteristics.

The conventional cake filtration theory can be evaluated under a constant pressure case [Koo et al. (2013), Iritani and Katagiri (2016)]. Equation 5 shows the relationship between permeate accumulated volume versus the pressure difference across the membrane. The basis for this equation is from Darcy law [Koo et al. (2013), Iritani and Katagiri (2016)].

$$\frac{t}{V} = \frac{\mu R_m}{\Delta P A} + \frac{\mu I}{2\Delta P A^2} V \qquad (5)$$

Where V=Accumulated permeate volume.

At plot of t/V versus V results in a straight line and the slope is used to calculate the cake resistivity. This analysis will be used in Chapter 4 where the generated experimental fouling data is used to determine the cake resistivity.

Classical filtration theory described three types of physical blocking mechanisms that can occur during membrane filtration in addition to cake filtration mechanism [Rezaei et al. (2011), Iritani et al. (2016), Hermia (1982)]. The proposed model consists of four different filtration mechanisms: complete blocking, standard blocking, intermediate blocking, and cake filtration. Figure 1.4 shows a general schematic of each mechanism under a simplified membrane structure with four parallel pores with constant diameter and length.

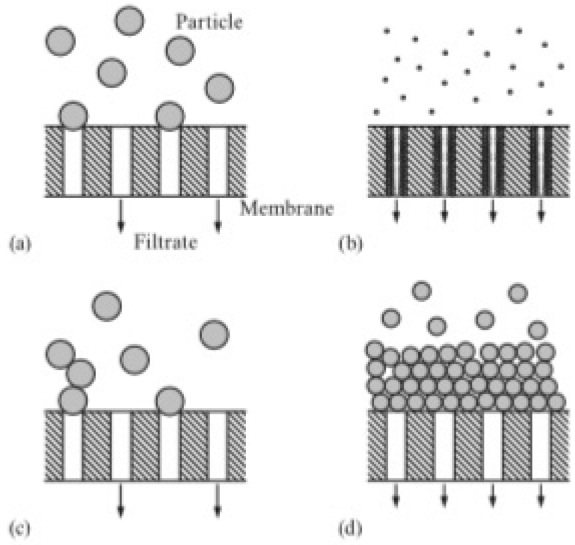

Figure 1.4: Membrane filtration mechanisms. (a) Complete blocking, (b) standard blocking, (c) intermediate blocking, and (d) cake filtration [Iritani et al. (2016)]

For complete and intermediate blocking, the foulants usually reaches the top surfaces of the membrane and cause a reduction in permeates flow through the membrane. In these two cases, the foulant is typically larger than the average pore sizes in the membrane. In complete blocking, it is assumed that the foulant completely blocks the membrane pores. For the standard blocking mechanism, the foulant tends to initially cause a pore constriction within the membrane pores by depositing onto the pore walls. This again causes a reduction in the permeate flow through the membrane. In this standard blocking mechanism case, the foulant present in the feed usually contains foulant that is smaller than the average pore size of the membrane. These four blocking mechanisms are modelled under a general model presented by Hermia (1982) and shown in the differential Equation 6 where t is the filtration time, V is the permeate volume per membrane filtration area, K is the resistance coefficient, and n is the blocking index.

$$\frac{d^2t}{dV^2} = K\left(\frac{dt}{dV}\right)^n \quad (6)$$

For complete blocking, n=2 where the membrane pores are sealed by the foulant. For standard blocking, n=1.5 where the foulant is causing a constriction of the pore effective diameter due to foulant coating the pore walls. For intermediate blocking, n=1 where the foulant settles on top of each other over the membrane surface. For cake filtration, n=0 where fouling occurs through the formation of a layer of foulant on the membrane surface. The derived linearized blocking filtration equations based on Equation 6 and using the appropriate index is shown in Table 4. The equations in Table 1.4 are used in a Chapter 4 where the experimental fouling data is investigated.

Table 1.4: Blocking filtration equations for constant pressure filtration

Blocking Mechanism	Blocking Index	Equation #	Derived linear equations
Complete	2.0	7	$K_b v = J_o - J$
Standard	1.5	8	$\frac{t}{v} = \frac{K_s}{2}t + \frac{1}{J_o}$
Intermediate	1.0	9	$K_i t = \frac{1}{J} - \frac{1}{J_o}$
Cake filtration	0.0	10	$\frac{t}{v} = \frac{K_c}{2}v + \frac{1}{J_o}$

Where K_b=complete blocking coefficient, v=permeate volume per membrane area, J=permeate rate, J_o=initial permeate rate, t=time, K_s=standard blocking coefficient, K_i=intermediate blocking coefficient, and K_c=cake filtration coefficient.

These derived linear equations can be used to identify the membrane fouling mechanism. Plots of the experimental fouling data using Equations 7 to 10 can be analysed to determine the best fit where the curve is most linear. Figure 1.5 shows examples of the plots based on Equations 7 to 10 in Table 1.4 that can be used to observe the dominant blocking mechanism during the fouling experiments. From the slope of these plots, the corresponding blocking coefficient can be determined.

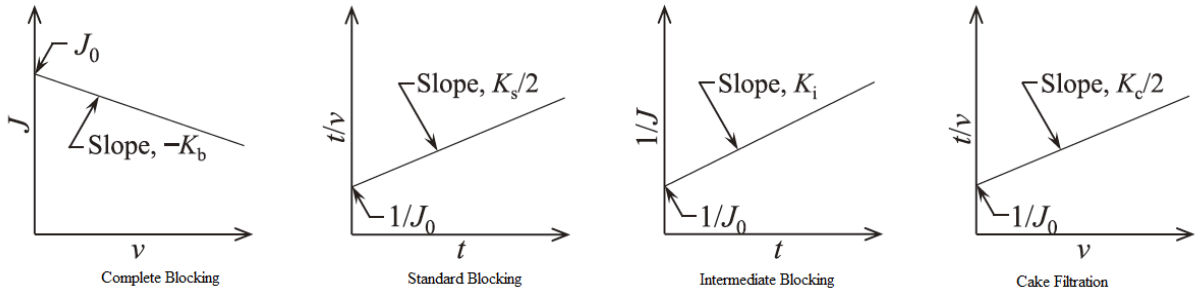

Figure 1.5: Graphical representation of the blocking filtration mechanisms for constant pressure system [Iritani and Katagiri (2016)]

Using an analogy from fluid flow in porous media, there could be potential to capture wettability characteristics of the membrane in the conventional filtration equations. In porous media, the fluid flow rate can be described by Darcy equation. In this equation the wettability characteristic of the porous media is indirectly capture by the effective permeability or relative permeability.

$$K'K'_{rel} = K'_{eff} \tag{11}$$

$$\frac{Q}{A} = \frac{-K'K'_{rel}\Delta P}{\mu L} \tag{12}$$

Where Q=flowrate, A=cross-sectional flow area, K'=absolute permeability, K'_{rel}=relative permeability, K'_{eff}=effective permeability ΔP=total pressure drop, μ=fluid viscosity, and L=length over which pressure drop is taking place.

The wettability of the porous media (somewhere between fully water wet to fully oil wet) is reflected in the relative permeability. As the fluid system changes during flow in the porous media (i.e. the water saturation changes), this affects the relative permeability which affects the overall flowrate. This analogy can be related to fouling in membranes over time. The initial roughness of the different membranes and corresponding roughness during the fouling experiment can vary and impact the degree of fouling. This change in roughness will change the wettability characteristic of the membrane surface and ongoing fouled surface. For example, as the filter cake starts to form and build on top of the membrane, this affects the total permeate flow rate or transmembrane pressure. Using this analogy, it is proposed that there needs to be a modification to the conventional filtration theory (Equation 1) to capture the wettability affects (i.e. surface roughness influence) of the membrane during the filtration process. Comparing Equation 3 to Equation 12, we can see that the relative permeability, K'_{rel}, which captures wettability and should be relatable to $1/(R_m + JIt)$. Here R_m is only a function of the membrane porosity. Therefore, membrane wettability could be potentially captured in a new third resistance term labelled R_r (Roughness resistance). Hence the denominator in Equation 3 would become $1/(R_m + JIt + R_r)$. The proposed modified form of the conventional filtration theory is shown in Equation 13.

$$\frac{Q}{A} = \frac{\Delta P}{\mu(R_m + JIt + R_r)} \qquad (13)$$

Where R_r=roughness resistance.

1.3 THESIS OBJECTIVES (TARGETING NANOFILTRATION MEMBRANES)

The objective of this study is to investigate organic fouling and performance for nanofiltration (NF) membranes used to treat SAGD-PW. The NF membranes are favoured over RO membranes due to similar performance reported in removing contaminants in SAGD-PW and have the advantage of lower pressure operating conditions. This study also focused on the membrane surface properties (roughness, wettability, and material composition) of the six commercially available NF membranes and its impact on membrane fouling and fluid flux. The fouling experimental data generated is also used to model the effect of roughness resistance presented in Equation 13. The outcome from this study is a further understanding and knowledge into membrane fouling and its relations to membrane surface wettability. It is envisioned that this could pave the road for future research work into mitigating membrane fouling due to organic material and aid in the improvement of current membranes or development of new membranes.

1.4 THESIS OUTLINE

In chapter 1, a general overview of the treatment of SAGD-PW and the potential technologies to treat the process water are discussed. A more detailed discussion of membrane filtration technology is also presented in this section. After that the membrane filtration theoretical back ground is given with the supporting equations and figures. The purpose and focus of the thesis is highlighted at the end of chapter 1.

In chapter 2, the experimental design basis and description of the cross flow filtration setup is presented. The design basis of the setup is highlighted along with the experimental methodology

and program. A description of the synthetic process was composition and the NF membrane used in this study is defined.

In chapter 3, the initial characterization of the clean membranes and synthetic process water is given. Here all the characterization methods are described and the testing conditions given. The results are all displayed in the chapter.

In chapter 4, all the fouling experiments are discussed including the high and low TMP conditions. Initially the membrane specific resistance is determined for each membrane and the results presented here. For both the high and low TMP experiments, the post analysis of the fouled membranes is presented here. The results of the two special fouling runs where the effect of salt and emulsified oil in the feed water are highlighted in the section. The last section of this chapter presents the modelling of the fouling experiment data and also the development of the roughness resistance model.

In the last chapter a summary and main outcomes of the thesis are provided and some suggested future research works are presented.

2.0 EXPERIMENTAL PROCEDURE AND METHODS

2.1 INTRODUCTION AND DESIGN BASIS

In this chapter the design of test setup, experimental procedure, and materials used in this study are described. The fouling experiments are all conducted in a bench scale cross flow membrane filtration setup. The feed water used in the experiments are generated synthetically and modeled of a typical SAGD-PW water specification for dissolved organics, sodium chloride and pH. Real SAGD-PW water samples are not used in this study due to the main objective of investigating the effect of dissolved organics on fouling and performance using NF membrane filtration. Addition of other components (e.g. silica, other ions, dispersed organics, etc.) in the feed water would make the water composition more complex and not allow the study to focus strictly on dissolved organics removal and its impact on membrane fouling. The membranes are purchased from commercially available NF membranes with varying molecular weight cut off (MWCO) specifications. The MWCO for membranes is a characteristic of each membrane relating to average pore size distribution and retention capabilities of the membrane. It is defined as the lowest molecular weight (in Daltons) at which greater than 90% of the solute or foulant is retained by the membrane. NF membranes with different surface features like pore size and roughness could lead to differences in membrane fouling and performance which is an objective of this study.

Further details of the test setup, feed water, and membranes, experimental plan and procedure are documented next in this chapter.

2.2 Design and Assembly of Cross Filtration Membrane Apparatus

The generated synthetic water is fed into a cross flow NF filtration system shown in the schematic below in Figure 2.1. Figure 2.2 shows the test setup on the lab bench. The main cross flow membrane filtration module is purchased from Sterlitech and was designed for flat sheet membranes with an active filtration area equivalent to 42 cm^2. The module is made of stainless steel with a maximum pressure rating of 1,000 PSIG and maximum temperature rating of 80^oC.

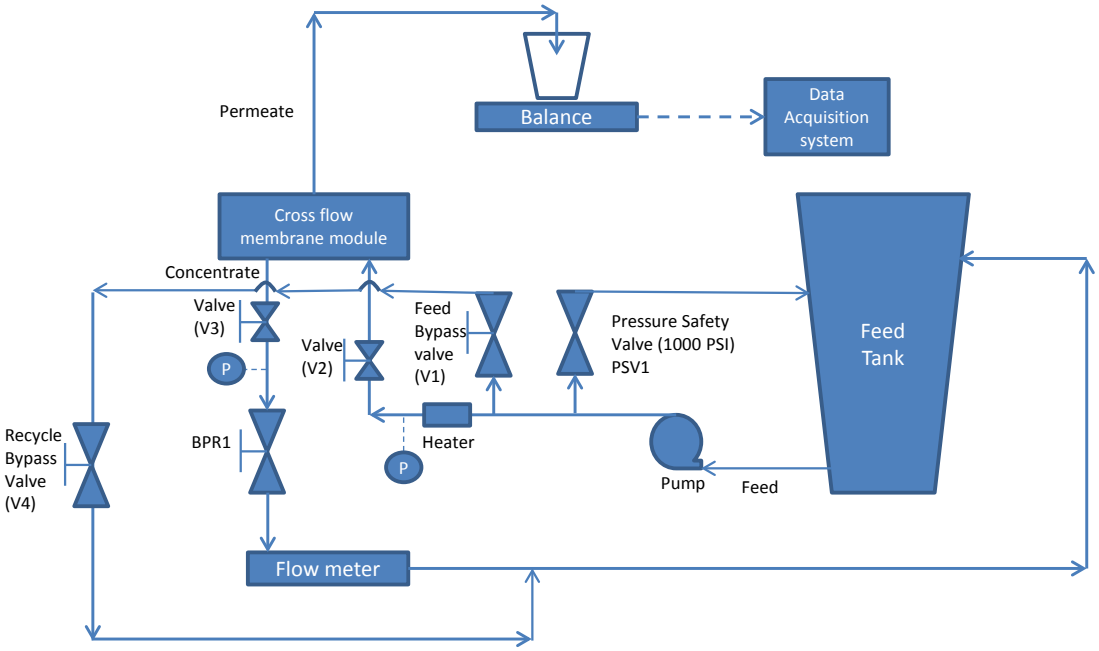

Figure 2.1: Schematic of NF membrane experimental setup

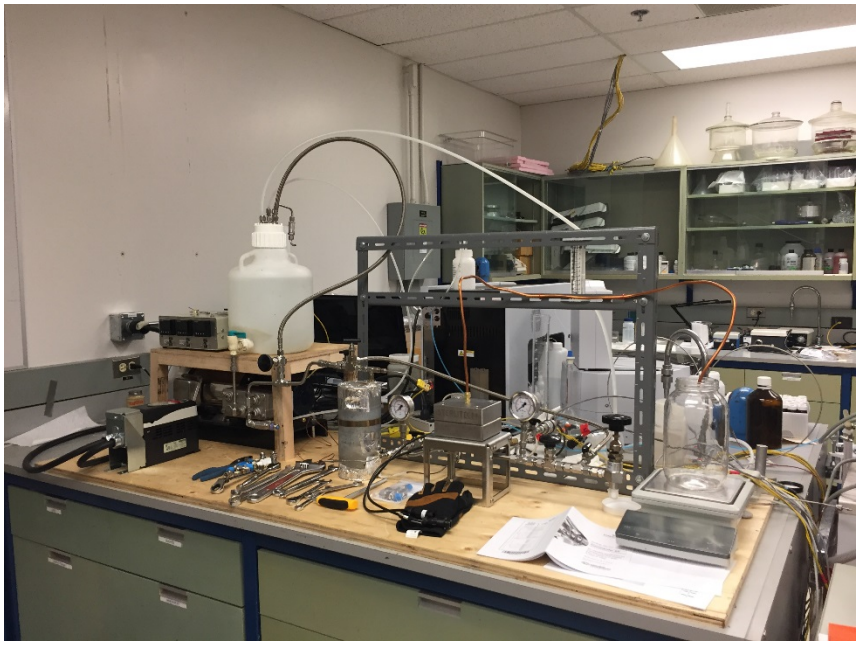

Figure 2.2: Cross flow filtration setup in lab

The filtration module is operated with the process feed entering from the bottom of the unit and flowing across the membrane. The feed water is either returned as a concentrate stream exiting the bottom of the module back to the feed tank or depending on the applied transmembrane pressure, the process water proceeds through the membrane and exit at the top of the filtration module as the clean permeate water stream. Figure 2.3 shows more details of the filtration module from Sterlitech. The images show the assembled module on the left side, the open module showing the inlet and outlet, and the module with the membrane. The permeate water is collected in a glass jar and weighed using a scale to determine the permeate flowrate and accumulated volume over time. Any foulant captured is accumulated on the bottom of the membrane.

Figure 2.3: Images of filtration module

Before the feed stream enters the filtration module, the process water is heated using an electrical rod heater. The feed tank is insulated and wrapped with electrical heaters. These electrical heaters are temperature controlled to the set temperature. In all experiments, the set temperature is 45^{o}C. Before each experiment, the test loop is set in bypass mode where process water is continuously recirculating and heating up to experimental conditions. The feed flowrate is monitored and set using the flowmeter. To adjust the feed flowrate, the pump variable frequency drive controller is set and adjusted. In all experiments, the feed flowrate is set to 500 cc/min. At this feed flowrate, the calculated average cross flow velocity through the membrane module for

the process water is 0.08 m/s. This is the feed flow velocity across the membrane surface. This cross velocity is similar in range with other studies using membrane filtration process and SAGD-PW feed [Sadrzadeh et al. (2015), Hayatbakhsh et al. (2016), Swenson et al. (2012)]. The cross flow velocity and membrane module slot dimensions are used to estimate Reynolds number for the process system. The calculations are based on using water density and viscosity at 45^{o}C. Equations 14 and 15 are used in this calculation. The calculated Reynolds number is 6,258 which indicated a turbulent flow regime across the membrane active area surface.

$$Re = \frac{\rho U D_H}{\mu} \quad (14)$$

Where Re=Reynolds number, U=cross flow velocity, D_H= hydraulic radius, and μ=fluid viscosity.

$$D_H = \frac{4ab}{2(a+b)} \quad (15)$$

Where a and b are the rectangular slot dimension for the fluid flow entering the membrane active area.

This turbulent flow regime is important during the fouling experiments as it limited the fouling resistance effect due to concentration polarization [Strathmann (2004), Baker (2012)]. Concentration polarization is a phenomenon where the emergence of concentration gradients at the membrane/process water interface resulting from selective transfer of some foulant through the membrane under pressure driving forces [Schafer (2001), Hoek et al. (2013)]. The concentration gradients form on either side of the membrane. For example, upstream of the membrane, foulant that is rejected by the membrane can accumulate and for a gradient with the

highest foulant concentration near the membrane surface. At the same time, downstream of the membrane, an opposite concentration gradient can form with the lowest foulant concentration existing near the membrane surface downstream. These two opposite concentration gradients cause additional diffusion fluxes which cause an overall negative effect on the permeate flowrate. Since the objective of this study is to investigate the effect of membrane surface properties on organic fouling, reducing the impact of concentration polarization resistance and preventing concentration gradient from forming is important. In the bypass mode, the transmembrane pressure across the module is zero and no process water is entering the membrane. Here the back pressure regulator (BPR) is fully open. To initiate the start of any experiment and to set the initial starting permeate flowrate, the BPR is adjusted to restrict flow back to the feed tank. Once this happens, flow through the membrane begins. The BPR is then adjusted to achieve the starting permeate flowrate and the fouling experiment begins. At this time the transmembrane pressure is monitored and recorded. Over the course of the experiment, the data acquisition system logs the temperature inlet and outlet from the tank and the membrane module, tracks the transmembrane pressure across the filtration module, and logs the accumulated permeate volume and average permeate flowrate.

2.3 SAMPLE PREPARATION OF SYNTHETIC FEED WATER

The synthetic process water feed is prepared using three primary components including deionized water, humic acid, and sodium chloride. Both the humic acid and sodium chloride are purchased from Sigma Aldrich. In a separate experiment to observe the effect of disperse emulsified organics in the feed on membrane fouling, diluted bitumen is used. The bitumen was obtained from a producer in the Athabasca oil sands region in northern Alberta. The viscosity and density of the bitumen at 20^{o}C is 450,000 mPa-s and 1,012 kg/m^{3} respectively. Hexane is

used as the solvent to dilute the bitumen. Hexane is used because in SAGD operations, condensate is usually added to the produced oil. The condensate is equivalent to Hexane. A 70:30 volume percent ratio of bitumen to hexane is used to generate the diluted bitumen. This ratio is used to represent a typical bitumen solvent dilution ratio observed in the emulsions present in the water during the treatment of SAGD-PW [Razi et al. (2016)]. The diluted bitumen is emulsified into the process water using an ultrasonic homogenizer probe.

The synthetic feed water for most experiments contains the initial concentration of humic acid and sodium chloride of 500 mg/L and 350 mg/L respectively. The experimental program shown later in this section in Table 2.3 highlights the exact composition of process feed water used for each experiment. Sodium hydroxide is used to assist the humic acid in dissolving into the water and the final pH is adjusted between 7 and 8. This pH is typical for SAGD-PW reported in literature [Sadrzadeh et al. (2015), Hayatbakhsh et al. (2016), Thakurta et al. (2013), Khorshidi et al. (2016)]. The synthetic process water is then carefully decanted and filtered through a 0.45 μm filter to remove any contaminants and undissolved components. From other past studies, the average range for the hydrodynamic diameter of humic acid is between 2 to 18 nm [Schafer (2001), Nghiem et al. (2010), Boussu et al. (2007)] and the average molecular weight is around 4,000 g/mol [Chin et al. (1994), Karanfil et al. (1996)]. The overall specification of the synthetic water used in the experiment is shown in Table 2.1.

Table 2.1: Synthetic process water specifications

Synthetic water specifications		
pH	7 to 8	
Water type	DI	
Humic acid	500	mg/L
NaCl	350	mg/L

2.4 DESCRIPTION OF NF MEMBRANES

Six polymeric NF membranes are used in this study. All the NF membranes are flat sheet membranes with average pore diameter ranging from 1 to 2 nm. Three of the membranes are composed mainly of polyamide as the active layer. One of the membranes has an active layer composed of polypiperazine-amide. Figure 2.4 shows the typical structure of an aromatic polyamide membrane and piperazine membrane. Both membranes are similar in structure and provide good chemical stability and durability [TriSEP (2016)]. The main difference between polyamide and piperazine membrane is that piperzine membranes contains trace additives that allow for different dissociation constants and thus provide different monovalent salts transporting characteristics through the membrane. For the purpose of this study, the three polyamide and one piperazine membranes are assumed to be similar in material composition and are referred as polyamide or amide type membranes. These four membranes have different surface roughness (results presented later in Chapter 3) and will provide a basis for studying the effect of membrane surface properties on organic fouling.

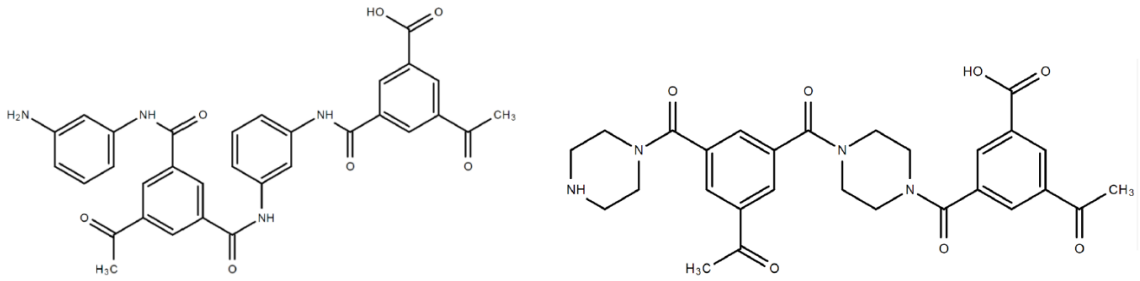

[a] [b]

Figure 2.4: Chemical structure of polyamide[a] and piperazine[b] membranes [TriSEP (2016)]

All four membranes are thin film composite membranes with three layers. A thin active layer (~0.2 μm), an intermediate microporous layer (~40 μm) and a mesoporous polyester support layer (~120 μm) [34]. The three layer configuration gives the desired properties of high rejection, good filtration rate, and good mechanical strength. Figure 2.5 shows a cross section of thin film composite membranes.

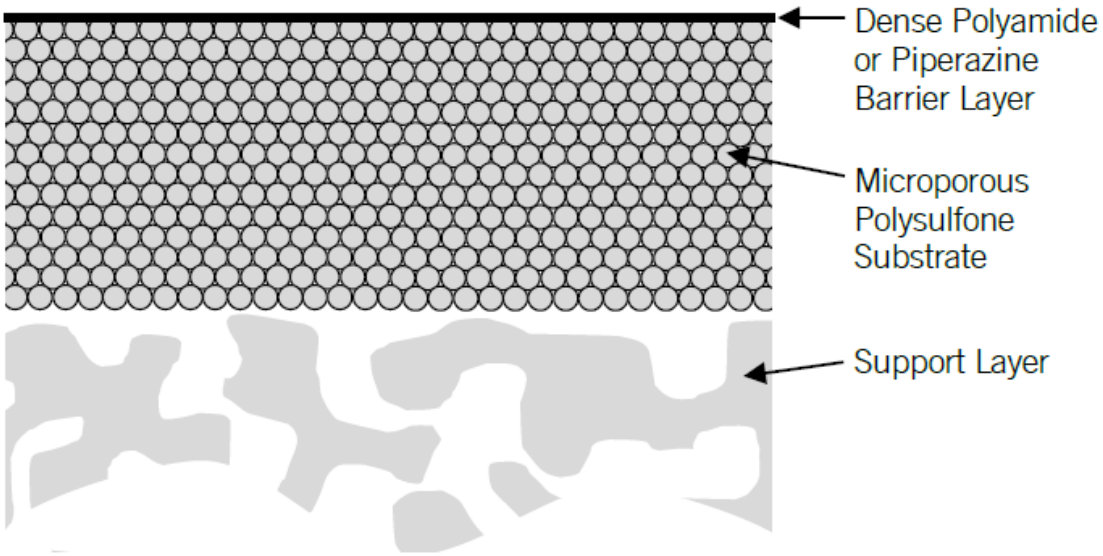

Figure 2.5: Cross section image of thin film composite membranes [TriSEP (2016)]

All six membranes are designed to treat industrial waste water with good organic and ion rejection. The other two membranes are made with active material comprising of cellulose acetate and polyethersulfone. Figure 2.6 shows a cross section image of the cellulose acetate membrane. The polyethersulfone membrane has a similar cross-sectional structure to the cellulose acetate membrane but the backing or support layer is composed of polypropylene. The overall thickness for the polyethersulfone membrane is approximately 210 to 250 μm. Table 2.2 shows the NF membranes used the fouling experiments. The reason for choosing the four amide

type membranes (Membranes #1 to #4) is to observe the fouling effect for similar material composition type membranes having different surface properties (i.e. wettability, roughness, and pore size). Membranes #5 and #6 which is non-amide type membranes is used to observe the effect of membrane material on fouling.

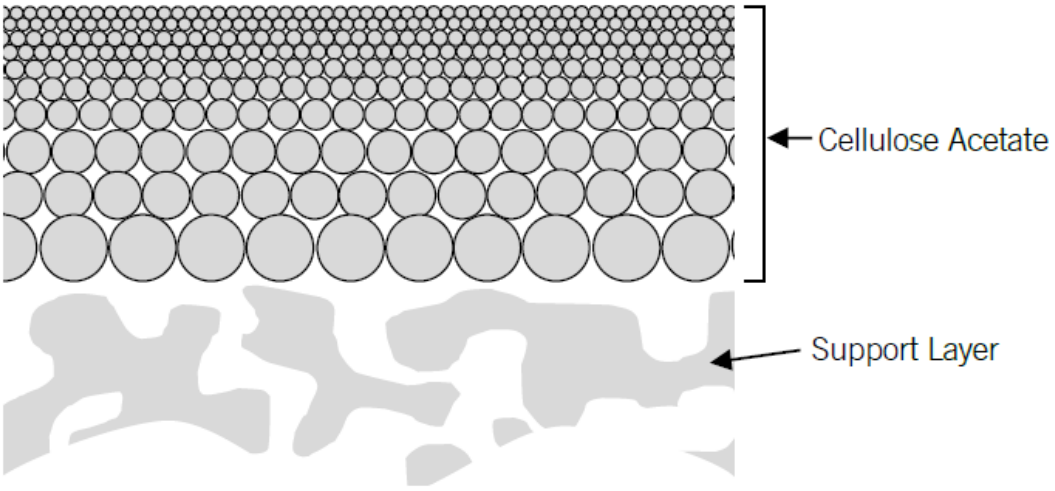

Figure 2.6: Cross section of a cellulose acetate membrane [TriSEP (2016)]

Table 2.2: List of NF membranes and specifications

NF Membranes									
Membrane #	**Manufacturer**	**Product Name**	**MWCO, Da**	**NaCl rejction %**	**Max Temp, C**	**pH range**	**Membrane active material**	**Max operating Pressure, PSI**	**Flux, GFD**
1	Dow Filmtech	NF90	200 to 400	90 to 96	45	2 to 11	Polyamide	600	40 to 60
2	Synder	NFX	100 to 250	40	50	3 to 10.5	Polyamide	435	20 to 25
3	TriSEP	TS80	100 to 200	80 to 90	50	2 to 11	Polyamide	600	20
4	TriSEP	TS40	200 to 300	40 to 60	50	2 to 11	Polypiperazine-amide	600	20
5	TriSEP	SB90	150	85	N/A	N/A	Cellulose acetate blend	435	30
6	Microdyn	NP030	500	30	95	0 to 14	Polyethersulfone (PES)	N/A	40 L/m^2hr

Before each experiment, the membrane is soaked in DI water for at least 24 hours (based on manufacture recommendations) and then compressed with DI water at 45^{o}C in the filtration module to achieve a stable permeate flux. Through this initial process of preparing the membrane before the fouling experiments, the membrane specific resistance is determined by varying different TMP and allowing the permeate flux to stabilize during the DI water run. Results of the membrane specific resistances for all the six membranes are highlighted later in this report.

2.5 EXPERIMENTAL METHODOLOGY

Prior to running any fouling experiments, the membranes and fluids are initially characterized. The techniques used, characterization results, and implications are highlighted in Chapter 3. As mentioned in the previous section, the membrane is allowed to presoak in DI water for a minimum of 24 hours. After which the membrane is compacted using the filtration module with DI water at 45^{o}C circulating and during this time the experimental setup is heated up. The TMP is set to three different values and at each TMP value, the permeate water flowrate is allowed to stabilize to a constant rate. A plot of permeate flux versus TMP allows for the determination of the specific membrane resistance.

For all the fouling experiments, the feed flow rate is set at 500 cc/min, the temperature is 45^{o}C, and the experimental duration is 20 hours. The experimental mode of operation is a constant TMP and allowing the permeate flux to decline over time due to fouling. The fouling experiments are grouped into two categories with experiments conducted at high TMP conditions and at low TMP conditions. For most experiments the process water feed composition is the same and the specifications are shown in Table 2.1. However two additional experiments are conducted at low TMP conditions to observe the effect of sodium chloride and the presence of

emulsified oil droplets. For the effect of sodium chloride, the different synthetic process water composition is used in this experiment and contained only RO water and dissolved humic acid. RO water is used instead of DI water to minimize the amount of monovalent ions (sodium and chloride) present initially in the water. To investigate the effect of dispersed or emulsified oil, another different synthetic process water composition is used in this experiment and contains the specifications in Table 2.1 plus the addition of 1 wt.% emulsified oil droplets. Water samples of the concentrate and permeate are collected during the experiments to observe the change in sodium ions, chloride ions, and dissolve organics content to evaluate the performance of the membranes.

For the high TMP experiments, the initial TMP are adjusted until the starting initial permeate flux is set to 10 g/min. For the low TMP experiments, the initial TMP are again adjusted until the starting initial permeate flux is set to 5 g/min. A summary of the entire experimental program for this study is shown below in Table 2.3.

Table 2.3: Summary of experimental program

Experimental Program												
Experiment #	**1**	**2**	**3**	**4**	**5**	**6**	**7**	**8**	**9**	**10**	**11**	**12**
Membrane #												
1	x						x				x	x
2		x										
3			x					x				
4				x								
5					x				x			
6						x				x		
Test conditions:	**High TMP**						**Low TMP**					
Temperature, °C	45	45	45	45	45	45	45	45	45	45	45	45
Feed Flow rate, cc/min	500	500	500	500	500	500	500	500	500	500	500	500
Initial Permeate flowrate, g/min	10	10	10	10	10	10	5	5	5	5	5	5
Test duration, hours	20	20	20	20	20	20	20	20	20	20	20	20
Synthetic water specs:												
Type of water used	DI	DI	DI	DI	DI	DI	DI	DI	DI	DI	RO	DI
Added Humic Acid, mg/L	500	500	500	500	500	500	500	500	500	500	500	500
Added NaCl, mg/L	350	350	350	350	350	350	350	350	350	350	0	350
Added Emulsified oil wt. %	0	0	0	0	0	0	0	0	0	0	0	1

3.0 INITIAL CHARACTERIZATION OF VIRGIN MEMBRANES AND PROCESS FLUIDS

3.1 INTRODUCTION

In this chapter the characterization techniques used to describe the membrane surface and synthetic process water properties are discussed. It is important to initially characterize the membranes surface and fluids properties to establish a baseline prior to the fouling experiments. The results from the fouling experiments are then compared to the initial membrane surface properties like roughness, wettability, and material composition to determine possible influence to membrane surface properties to filtration performance. The analysis of the clean membrane surface properties relating to the fouling experiments is discussed in Chapter 4. After each fouling experiments, the fouled membranes are again characterized to observe the difference in membrane surface properties after filtration.

3.2 CHARACTERIZATION METHODS AND RESULTS FOR MEMBRANES AND PROCESS FLUIDS

3.2.1 Characterization of Membranes

3.2.1.1 Atomic Force Microscopy

Atomic force microscopy is a method used to determine the average roughness on the membrane active surfaces. This surface scanning method is performed with an AFM cantilever with a silicon probe (Bruker Nano) with a spring constant of approximately 42 N/m and a resonance frequency of approximately 350 kHz. The AFM instrument is a Dimension Icon AFM by Bruker (Santa Barbara, Ca). The characterizations are conducted at 23^{o}C in air with an operation mode of PeakForce tapping Quantitative Nanoscale Mechanical (QNM). The AFM scanned membrane

area is 5 μm by 5 μm. This mode allows for the highest resolution and high speed mapping of the membrane structure. During the scanning process of the membrane surface, van der Waals-London interactions occur between atoms at the end of the tip and the atoms at the surface of the membrane. The created interactions are then detected by the probe. The average roughness of the scanned clean membranes is shown in Table 3.1. The results show that membrane #1 is the least rough of the polyamide type of membranes (#1 to #4). This could indicate that during the fouling experiments, membrane #1 would foul less compared to membranes #2 to #4. However, membrane #6 is the smoothest of all the membranes (amide and non-amide) and could be the most fouling resistance membrane. Figure 3.1 shows the 2D and 3D AFM images of the roughness profile for membrane #1. The additional AFM profile images for all other membranes are shown in Appendix A.

Table 3.1: Average roughness of clean membranes

Membrane #	Average Roughness, nm
1	3.4 ± 2.0
2	20.8 ± 2.9
3	49.0 ± 16.4
4	10.8 ± 1.8
5	5.4 ± 0.5
6	1.2 ± 0.3

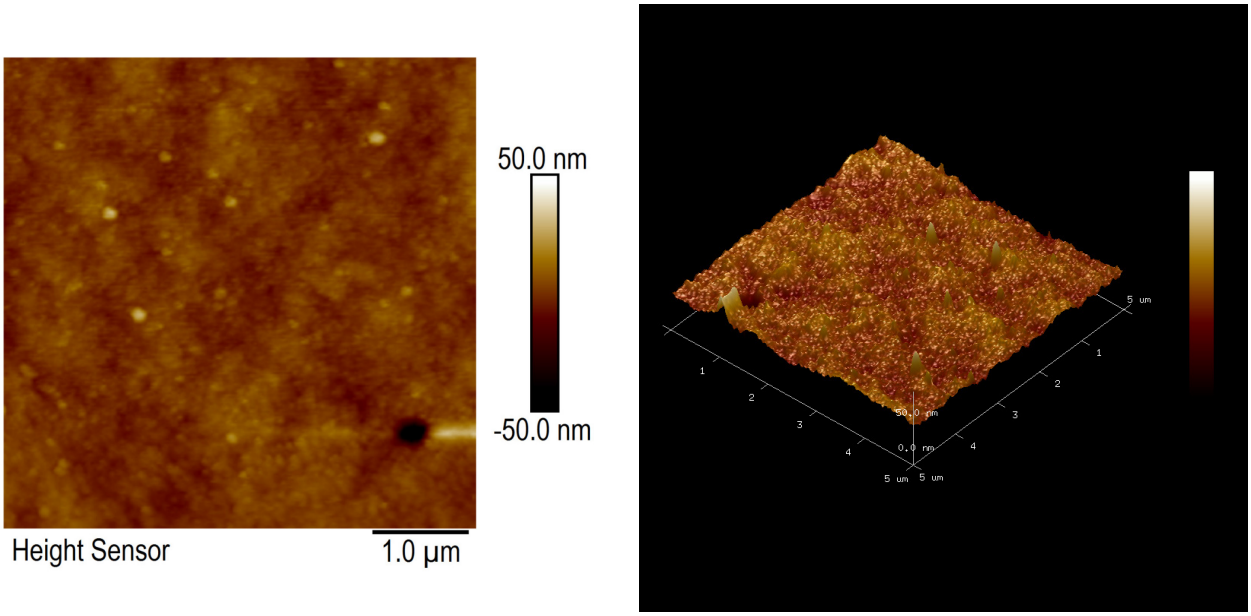

Figure 3.1: AFM roughness profile for membrane #1

3.2.1.2 Contact Angle Measurements

Contact angle measurements of the membrane surface are a property that can be measured and show the hydrophobicity and hydrophilicity (water droplet on the membrane) and also the oleophobicity and oleophilicity (oil droplet on the membrane) of that surface. This property gives an indication into why some membranes perform better during the fouling experiment than other membranes. Membranes with more hydrophilic properties tend to allow the water to easily pass through the membrane and thus have a high permeate flux [Hartland (2004)]. On the other hand, dissolve organics in the process water can potentially be attracted to more oleophilic membrane surfaces and cause the fouling process on the membrane to occur faster. The droplets make an angle with the membrane surface at the three phase interface (liquid droplet – air – solid membrane). The measured angles are dependent on the interfacial tension between the surface and droplet and can vary depending on membrane surface properties. The membrane surface properties that affect the contact angle are roughness and membrane material composition.

Another property is the membrane surface charge when the membrane is immersed in a fluid and the droplet is allowed to contact the membrane surface. In our study, the contact angles were measured for each clean membranes using DI water, synthetic process water, and diluted bitumen. The instrument used is a Dataphysics Instrument GmbH contact angle system (Model TBU 95) using the sessile drop method. After the fouling experiments, the contact angles are again measured for the membranes with the three different fluids. The contact measurements are all done in air and at 23^{o}C. The same procedure is repeated for all measurements where a 4μL drop of the fluid is placed on the flat membrane surface and the droplet is allowed to stabilize and after 10 seconds, a digital image is captured. The image is then analyzed to determine the contact angle. The contact angle measurements of the clean membranes are shown in Table 3.2.

Table 3.2: Contact angle measurement on clean membranes

Membrane #	Mean Contact Angle		
	DI Water	Process Water	Diluted Bitumen (70:30)
1	9.77±2.62	8.62 ± 2.95	62.17 ± 1.88
2	21.47±0.87	26.50 ± 0.78	80.50 ± 4.56
3	30.77±3.64	31.55 ± 2.08	101.98 ± 5.18
4	16.88±1.14	14.20 ± 2.15	60.95 ± 1.15
5	59.00±2.75	52.45 ± 2.16	80.40 ± 3.04
6	55.17±2.71	55.98 ± 2.16	72.57 ± 3.04

The contact angle measurements indicate that out of the polyamide type membranes (#1 to #4), the most hydrophilic membrane is membrane #1. This would indicate higher permeate flux due to the membrane's affinity for water. Looking at the diluted bitumen contact on the polyamide type membranes, membrane #3 shows the most oleophobic initial membrane behavior; this could

prevent or reduce the chance of organic fouling on the membrane surface during filtration. The ideal membrane to treated SAGD-PW would be the most hydrophilic (to have the highest permeate flow) and be the most oleophobic (resist organic fouling). Comparing the average roughness and observed contact angle values for polyamide type membranes, there is a relationship between roughness and contact. This is shown in Figure 3.2. As the membrane roughness increases, the membrane becomes more hydrophobic.

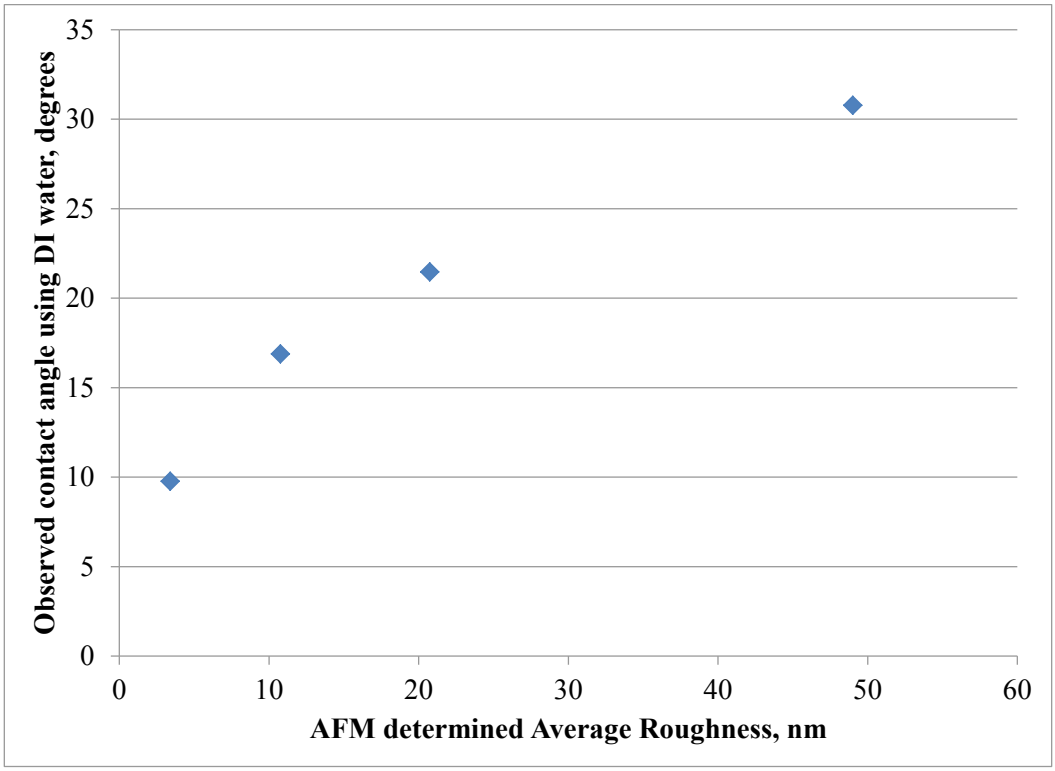

Figure 3.2: Comparison of contact angle using water to roughness for amide type membranes

Assuming that the membrane's surface composition is similar for the polyamide type membranes, Figure 3.2 indicates that as the roughness increases the observed contact angle for

water also increases. This means that a rougher polyamide type membrane is less hydrophilic. An opposite observation is evident for contact angle measurements using dilute bitumen. The rougher the polyamide type membrane, the more oleophobic the clean membrane behaves. If we relate this initial observation to the upcoming fouling experiments, membrane #1 would have the highest permeate flux even though membrane #1 is more oleophilic. Looking at membrane #5 and #6, they both have low average roughness values but were less hydrophilic compared to the polyamide type membranes. This shows that membrane surface material composition plays an important role in determining the membranes affinity for water or oil. Even though membranes #5 and #6 are very smooth, they are more hydrophobic compared to the polyamide type membranes.

3.2.1.3 Attenuated Total Reflectance-Fourier Transform Infrared Spectroscopy (ATR-FTIR)

ATR-FTIR spectroscopy is a method that can provide information on the type of functional groups present and surface material composition on the membrane surface. The penetration depth is typically less than 1 μm. The instrument used is the Thermo Nicolet 6700 FT-IR system using an Attenuated Total Reflectance accessory (Smart Performer- Diamond crystal). The membrane samples are scanned over the range of 500 cm^{-1} to 4,000 cm^{-1} and at 23^{o}C. The ATR-FTIR spectra for the clean polyamide type membranes (#1 to #4) are shown in Figure 3.3. The result shows that these four polyamide type membranes are very similar in composition and the types of functional groups present. This gives more confidence that the initial assumption that membrane #4 (piperazine membrane) and the other polyamide membranes (#1, #2, and #3) are similar in composition and can be grouped in this study as polyamide or amide type of membranes. The peaks at 1,650 cm^{-1} and 1,540 cm^{-1} indicate amide I and amide II for these membranes respectively. Figure 3.4 shows the vibrations responsible for the Amide I and Amide

II where Amide I band is due to carbonyl stretching vibration and for Amide II the vibration is from the NH.

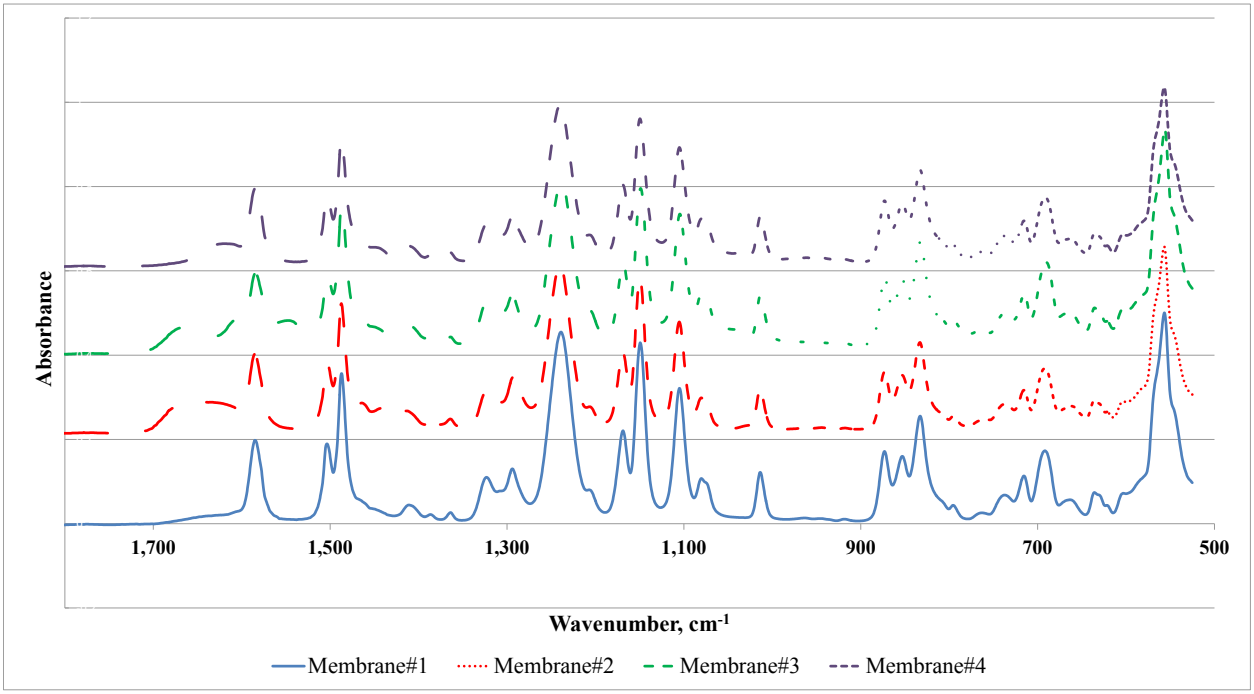

Figure 3.3: ATR-FTIR Spectra for amide type membranes

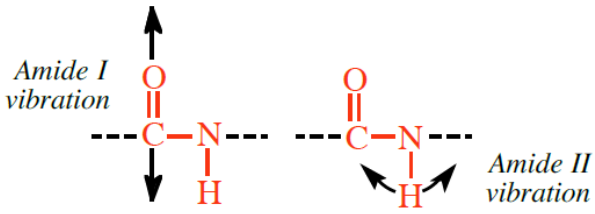

Figure 3.4: Vibrations responsible for Amide I and Amide II bands

The ATR-FTIR spectra comparing a polyamide type (membrane #1) to the non-amide membranes (#5 to #6) are shown in Figure 3.5.

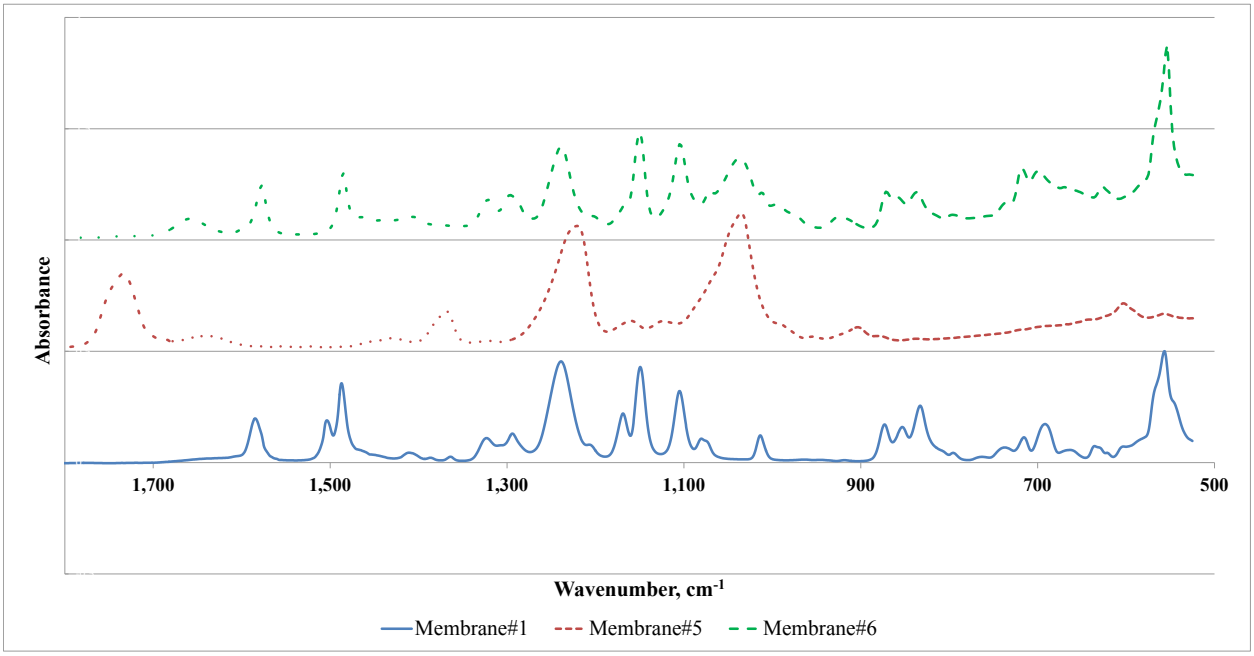

Figure 3.5: ATR-FTIR spectra comparing amide membrane to non-amide membranes

The result from Figure 3.5 shows that the polyamide type membrane is different in surface composition compared to the cellulose acetate membrane (membrane #5) and to the polyethersulfone membrane (membrane #6).

3.2.1.4 Scanning Electron Microscopy-Energy Dispersive X-Ray (SEM-EDX)

The scanning electron microscopy method provided images of the membrane surface morphology prior to and after the fouling experiments. In this method, the membrane is bombarded by a thin electron beam with a certain amount of kinetic energy. The electrons initially hitting the membrane surface are called the primary electrons and possess high energy levels. The reflected electrons by the membrane surface have lower level of energy than the primary electrons and are called the secondary electrons. The SEM images are built by secondary electrons released by the atoms of membrane's surface. The SEM used in this study is a Hitachi S-3000N scanning electron microscope with tungsten filament and the instrument

resolution range was 30x to 300,000x. The membrane samples sizes are approximately 5 mm by 5 mm. Membrane sample preparation is done by sputter coating the membrane surface with gold. The EDX analysis is also done in conjunction with SEM imaging to provide quantitative elemental analysis of the membrane surface. The EDX analysis is done on the membrane samples before and after the fouling experiments. Figure 3.6 shows the SEM images for membrane #1 at 20,000 times magnification.

Table 3.3 shows the EDX analysis for all six membranes. The additional SEM images for all other membranes are shown in Appendix A.

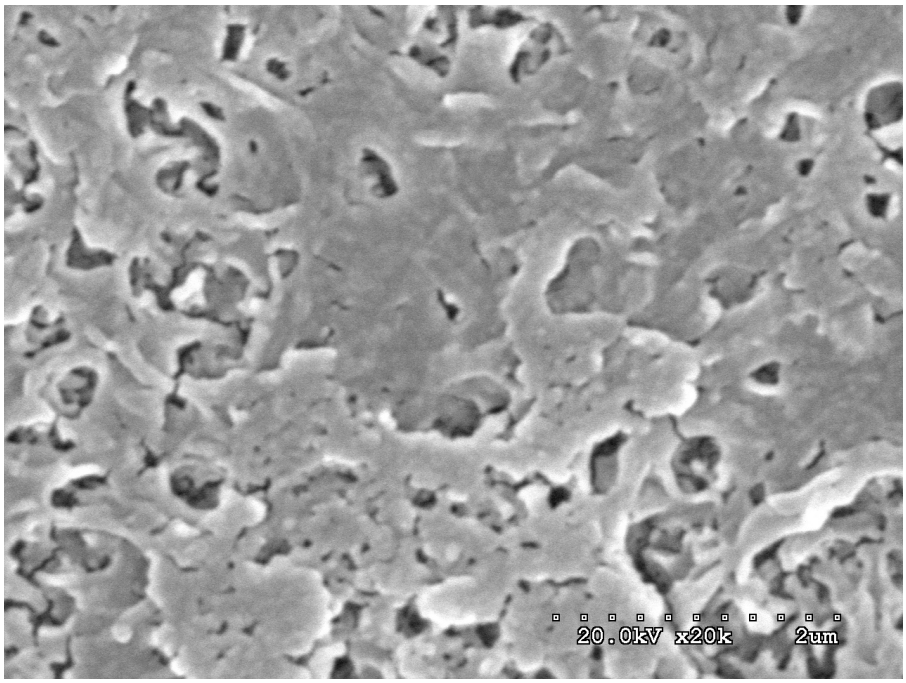

Figure 3.6: SEM image of membrane #1 at 20k magnification

Table 3.3: EDX elemental analysis of membrane surface for all membranes

Membrane #	Concentration, weight %							
	Carbon	Oxygen	Sodium	Magnesium	Aluminum	Silicon	Phosphorus	Sulfur
1	78.42	17.46	0.09	-	0.16	-	-	3.74
2	77.01	20.00	-	-	1.68	0.04	-	0.98
3	67.44	23.10	2.30	-	-	-	0.18	6.76
4	69.81	18.59	2.34	-	0.04	-	0.21	8.77
5	57.31	41.44	0.29	0.04	0.60	0.08	-	0.06
6	66.85	19.08	-	-	-	-	-	14.07

The EDX data shows that membrane #1 to #4 has similar surface elemental composition compared to membranes #5 and #6.

3.2.2 Characterization of Process Fluids

3.2.2.1 Total Organic Content (TOC)

The total organic content (TOC) in the process water, concentrate water samples, and permeate water samples is measured using Shimadzu scientific instrument (Model TOC-LCPM). The organic content is dissolved in the process water. This analyzer uses the combustion catalytic oxidation method at a combustion temperature of 680^{o}C. The detector is a non-dispersive infrared type and the method used is based on ASTM 7573. The sample sizes are 10 µL and measured at 23^{o}C.

3.2.2.2 pH Measurement of Process Water

The pH is a measure of the process water acidity or basicity. The pH of synthetic process water is measured using a pH electrode refillable with Ag/AgCl by Thermo Scientific. The pH meter used is an Orion Star Thermo Scientific.

3.2.2.3 Chloride Content in Water Samples

Chloride ion content in the process water, concentrate water samples, and permeate water samples is determine by ion chromatography (IC). In this method, the ions of interest are separated based on their affinity to the ion exchanger and are separated based on their respective charged group. The instrument used is a Metrohm 861 advance compact IC with Metrohm suppressor module. Samples are diluted with water if needed and the test condition is at 23^{o}C.

3.2.2.4 Sodium Ion Content in Water Samples

The sodium ion content in the process water, concentrate water samples, and permeate water samples is determined using inductively coupled plasma-optical emission spectroscopy (ICP-OES). This method is a quick and sensitive method for determining metal ions in aqueous solutions. The Agilent 5110 instrument is used to measure the sodium content at 23^{o}C. The detector used by the instrument is charged coupled device (CCD). The method used is developed in-house by the Analysis and Testing Services group in InnoTech Alberta (Edmonton, Alberta) where the samples are diluted with HNO_3.

3.2.2.5 Emulsified Oil Droplet Size and Distribution

An acoustic spectrometer is used to measure the emulsified oil droplet size and distribution in the process water. As a note, this process water with the emulsified oil is used in only one fouling experiment to observe the effect of dispersed organics on membrane fouling. The Dispersion Technology Inc (Model DT-100) uses the ultrasound scattering method to measure the particle

size distribution. The particle size distribution is determined from the measured attenuation sounds spectra taking into account particle-particle systems. The frequency range of the instrument is from 1 to 100 MHz. The measurement is made at 23^{o}C. The measured average oil droplet size is 3 μm. The droplet distribution measurement for the 1% emulsified oil process water feed is shown in Figure 3.7.

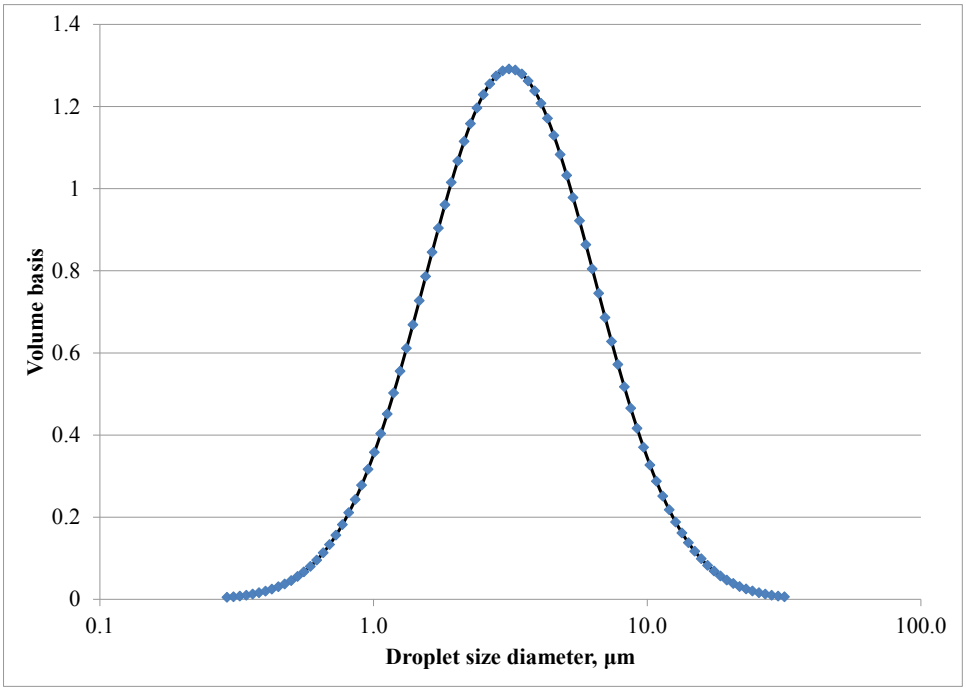

Figure 3.7: Emulsified oil droplet distribution in the synthetic process water

3.2.2.6 Zeta Potential on the Emulsified Oil Droplets

The zeta potential (ζ) on the emulsified oil droplets in the presence of process water is measured using light scattering analysis to determine the electrophoretic mobility of the charged droplet (Brookhaven Instrument Co. ZetaPALS potential analyzer). The zeta potential is then estimated by using Equation 16.

$$\mu_e = \frac{\epsilon_r \epsilon_o \zeta}{\eta} \quad (16)$$

Where μ_e=electrophoretic mobility, ϵ_r=dielectric constant of the bulk medium, ϵ_o=permittivity of free space, and η=dynamic viscosity of bulk medium.

The electrophoresis phenomenon is simply described as motion of dispersed particles or droplets relative to the bulk fluid under the influence of a uniform electric field. The zeta potential represents the potential difference between the continuous process water phase and the layer of charged fluid surrounding the oil droplet. Theoretically, the zeta potential is the electric potential in the electrical double layer at the location of the slipping plane relative to the bulk process water at some point away from the oil droplet. All measurements are made at 23^{o}C. The measured zeta potential for the diluted bitumen droplets in synthetic process water is -93.8 mV with a standard deviation of 4.5 mV.

3.3 IMPLICATIONS FROM THE INITIAL CHARACTERIZATION

The following are the potential implications from the initial characterization on the upcoming fouling experiments presented in the next chapter:

- There is a linear trend in terms of membrane surface roughness and the observed contact angle measurement for the amide membranes. This indicates that surface roughness may play a role in determining the membrane hydrophilicity and oleophilicity tendency.
- The roughness value and measured contact angle for the amide type membranes show that membrane #1 is the most hydrophilic. This could results in higher permeate flux over compared to the other amide membranes. This means less fouling may occur on membrane #1 primarily due to the smoother surface. However, membranes #5 and #6 are

very smooth surface membranes as well and have the potential to resist fouling. The contact angle measurements for these two non-amide type membranes would indicate even lower hydrophilicity compared to the amide membranes. This should result in lower permeate flux even though the membrane surface roughness values are low (5.42 nm and 1.24 nm for membrane #5 and #6 respectively).

- From the ATR-FTIR spectra and EDX surface elemental analysis, membranes #1 to #4 are similar in both spectra and relatively similar in elemental composition. Therefore, the initial assumption that the three polyamide and the one piperazine membranes are similar is valid in this study and can be grouped as amide type membranes.
- The average emulsified oil droplet size of 3 μm and is larger than the pore size of the NF membranes as shown in **Table 1.3**. This indicates that the dispersed oil droplets should not pass through any of the NF membranes tested in this study.
- Knowing the zeta potential of the emulsified oil droplet can possible indicate the affinity of the emulsified oil in the process water for the membrane and this can affect membrane fouling. It is documented that most commercially available NF membranes are negatively charged over a wide range of pH conditions [Elimelech et al. (1994)]. In most cases the surface charges of these membranes is due to their functional groups on the membrane surface. Commercial polyamide type membranes contain carboxylic ($R\text{-}COO^-$) and amine ($R\text{-}NH_3^+$) ionizable groups and these groups contribute to the membrane surface charge [Elimelech et al. (1994), Jacobasch and Schurz (1988)].

4.0 RESULTS AND DISCUSSION OF MEMBRANE FOULING EXPERIMENTS

4.1 INTRODUCTION

In this chapter the results of the fouling experiments are discussed. The specific membrane resistance for all membranes is determined using DI water and these values give an indication of the relative pore sizes between each membrane. For all the fouling experiments, the feed flow rate is set at 500 cc/min, the temperature is 45^{o}C, and the experimental duration is 20 hours. The experiments are operated under a constant pressure mode and allowing the permeate flux to decline over time due to fouling. The fouling experiments are grouped into two categories, a high TMP conditions and at low TMP conditions. For most experiments the process water feed composition is identical. However two additional experiments are conducted at low TMP conditions to observe the effect of sodium chloride and the presence of emulsified oil droplets. In these two special cases, the same membrane #1 was used and the feed process water was different in both cases. Post analysis and characterization results of the collected permeate water and fouled membranes are also discusses in this Chapter. The last part of this Chapter attempts to model the fouling experimental data generated and relate it to the proposed concept of roughness resistance presented in Chapter 1.

4.2 DETERMINATION OF MEMBRANE RELATIVE PORE SIZE

The membrane specific resistance is a function of the membrane pore size distribution and is related to the pressure drop across the membrane at a given water permeate rate. Membranes with smaller pores requires higher pressure drops or TMP to push the permeate water across the membrane compared to membranes with larger pores. To determine the membrane specific resistance, the membranes are conditioned with DI water in the filtration module. The TMP

across the membrane is set and the permeate flux is allowed to stabilize. The TMP and associated permeate flux values are then recorded. Two additional runs with different TMP settings and the corresponding permeate flux values are determined. The permeate flux is plotted as a function of TMP and based on Equation 17 below, the calculated slope results in the membrane resistance (R_M).

$$Permeate\ water\ Flux = \frac{TMP}{\mu_w R_M} \qquad (17)$$

Where μ_w is the water viscosity.

The specific membrane resistance is then determined by knowing the mass of the membrane. A plot of permeate flux versus the TMP for all the membranes is shown in Figure 4.1. The values determined for each membrane studied in this work in presented in Table 4.1. The determined specific membrane resistance is similar in order of magnitude (10^{13} m^{-1}) and in linear trend when the pressure was adjusted for other studies using NF membranes [Sadrzadeh et al. (2015), Hayatbakhsh et al. (2016), Koo et al. (2013), Schafer (2001), Khorshidi et al. (2016)].

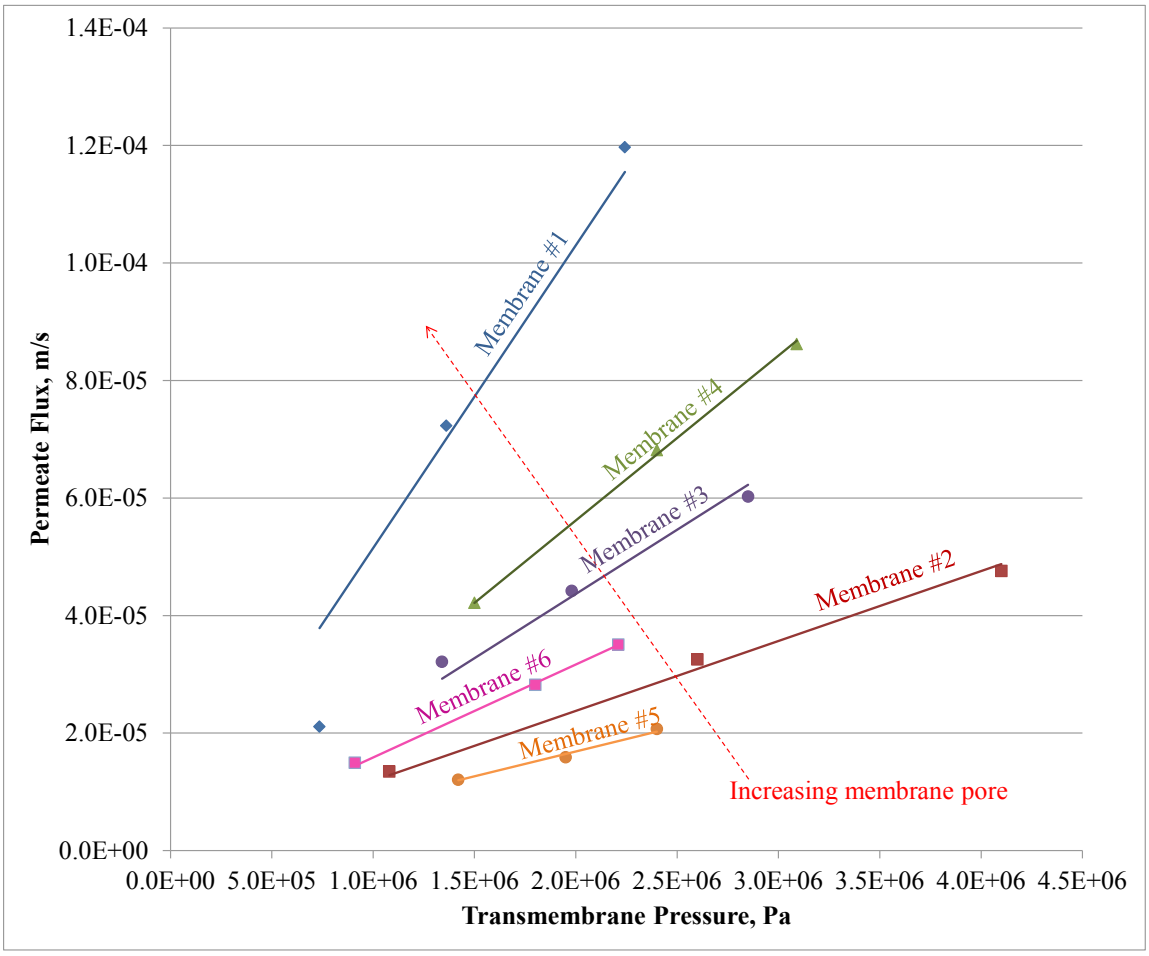

Figure 4.1: Plot of permeate flux versus TMP (Membrane specific resistance)

Table 4.1: Membrane specific hydraulic resistance

Membrane #	R_m, m^{-1}	Specific R_m,m^{-1}/g	Membrane Pore size
1	3.65E+13	5.61E+13	Large pores
4	6.09E+13	9.04E+13	
3	9.14E+13	1.33E+14	
6	9.14E+13	1.03E+14	
2	1.83E+14	2.80E+14	
5	2.29E+14	3.18E+14	Small pores

The results show that membrane #1 has the largest pores compared to membrane #5 which has the smallest pores. The specific membrane resistance values give an indication of the relative pore size distribution for all the membranes. The determined R_m values are used later on in this Chapter during the modelling of the fouling data. To show that the experimental setup and procedure is repeatable, three different samples of membrane #4 are tested with DI water to again determine the specific resistance. Figure 4.2 shows the repeat runs for membrane #4. The repeat runs conducted yielded same specific membrane resistance values (R_m). The results show that the experiment procedure to determine R_m is repeatable.

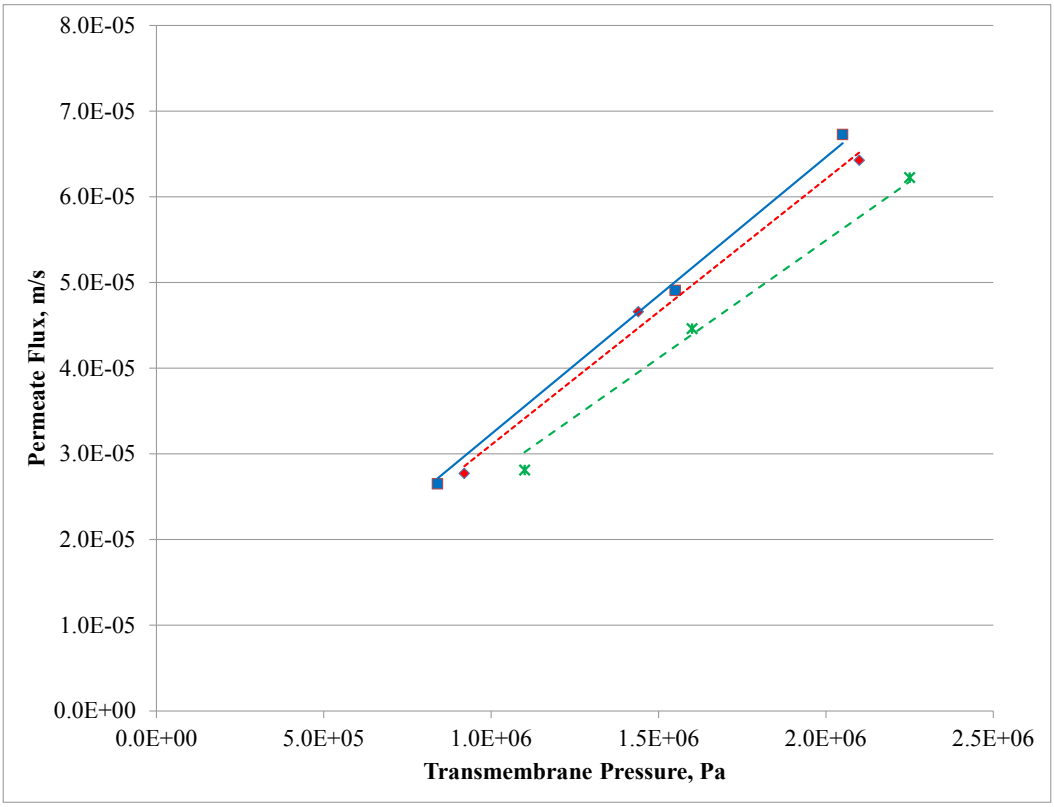

Figure 4.2: Repeat runs for membrane #4 (Membrane specific resistance)

4.3 FOULING EXPERIMENT RESULTS

4.3.1 High TMP Fouling Experiments

The initial starting permeate flux for all high TMP runs is 10 g/min. This is accomplished by adjusting the BPR until the initial permeate flux reached the setting point. Once the desired initial permeate rate is reached, no further adjustments to the BPR is made and the subsequent TMP is recorded. At this point the fouling experiment begins. The synthetic process water feed composition for all the high TMP runs includes DI water mixed with humic acid and sodium chloride. The specific quantity of each component in the water is shown in Table 2.3 back in Chapter 2. Figure 4.3 shows the results of the high TMP fouling runs.

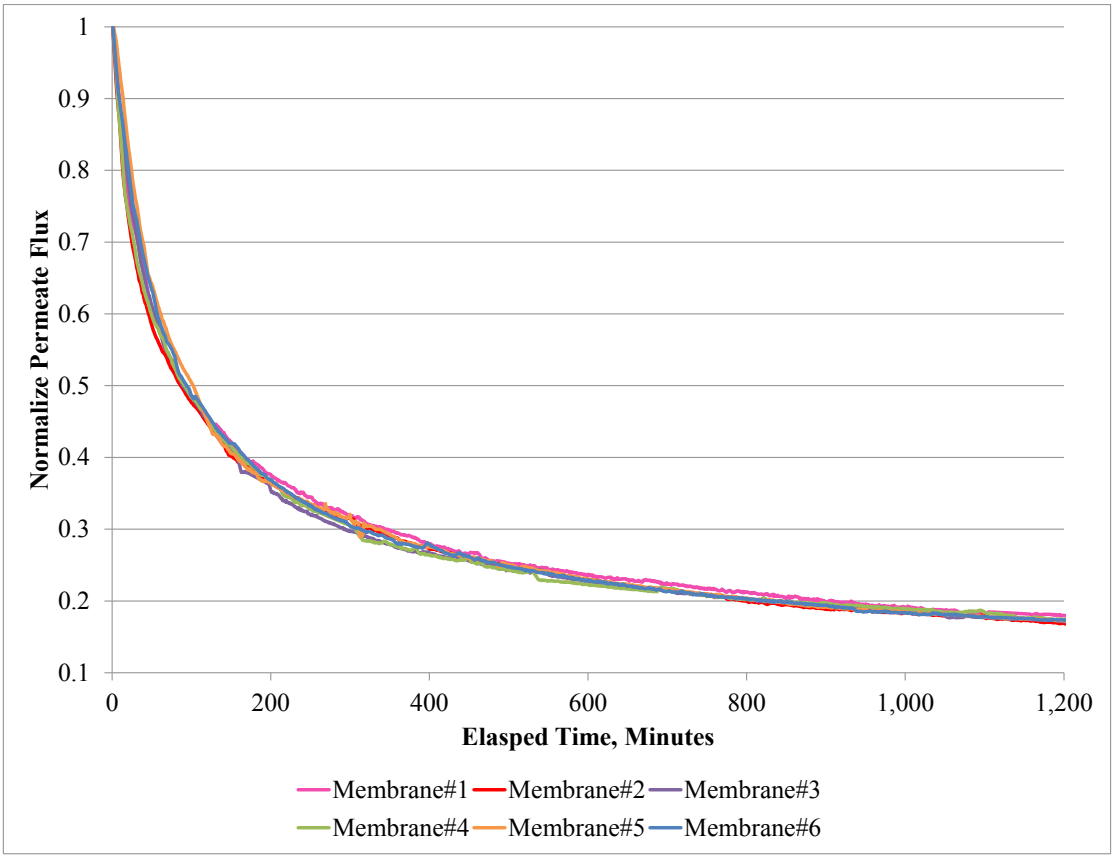

Figure 4.3: High TMP fouling results

The permeate flux values are normalized with the initial permeate flux (10 g/min). Figure 4.3 shows that the fouling behavior and permeate flux decline for each membrane is similar. Initially, there is a sharp decline in the permeate flux within the first 200 minutes of the experiment. After that the permeate flux starts to gradually level off and reach a stable value. The initial stage of fouling have been described by other studies as the initial plugging or blocking of the membrane pores by the foulant and the subsequent second stage of fouling is caused by the forming of layers upon layers of foulant to form the filter cake [Xiao et al. (2011), Koo et al. (2013), Rezaei et al. (2011), Iritani and Katagiri (2016), Hermia (1982), Schafer (2001)]. Figure 4.4 and Figure 4.5 show the fouling data for the initial stages and later stages of the experiments respectively.

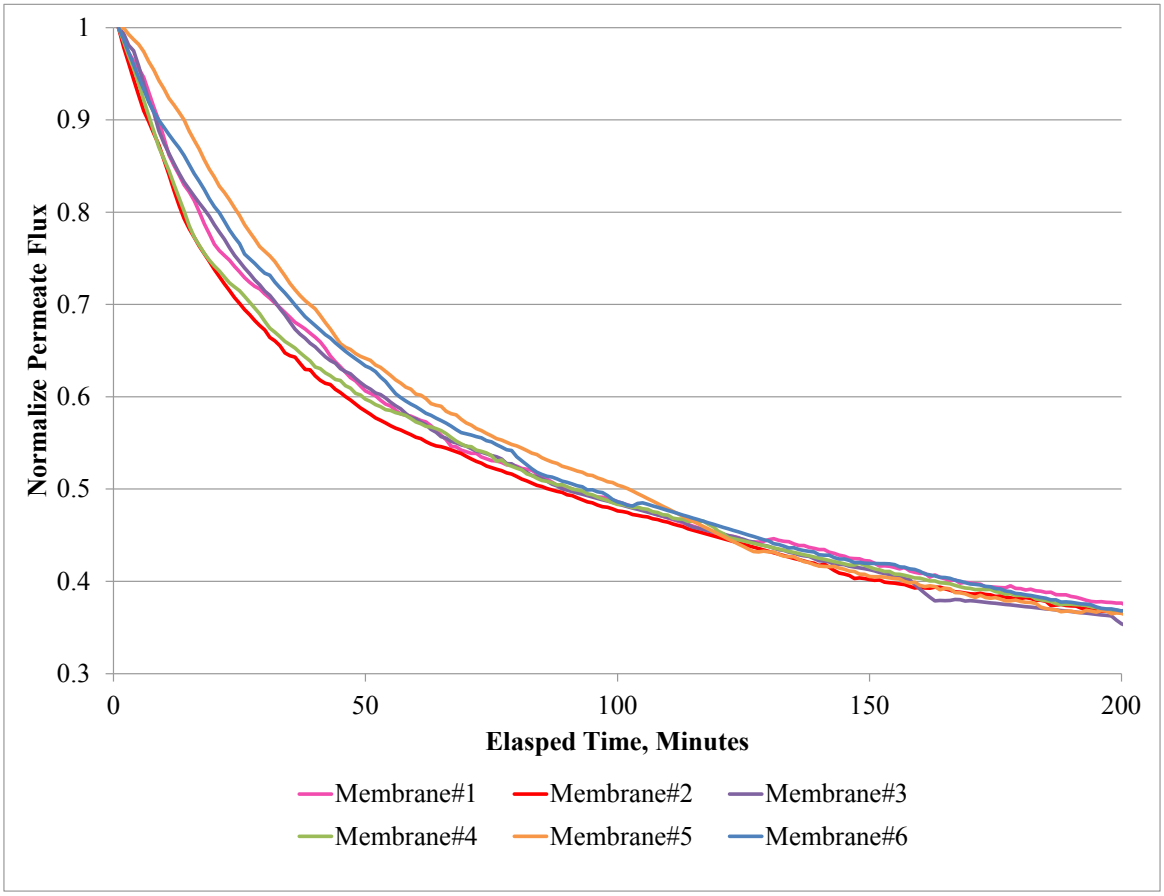

Figure 4.4: Initial stages of high TMP fouling experiments

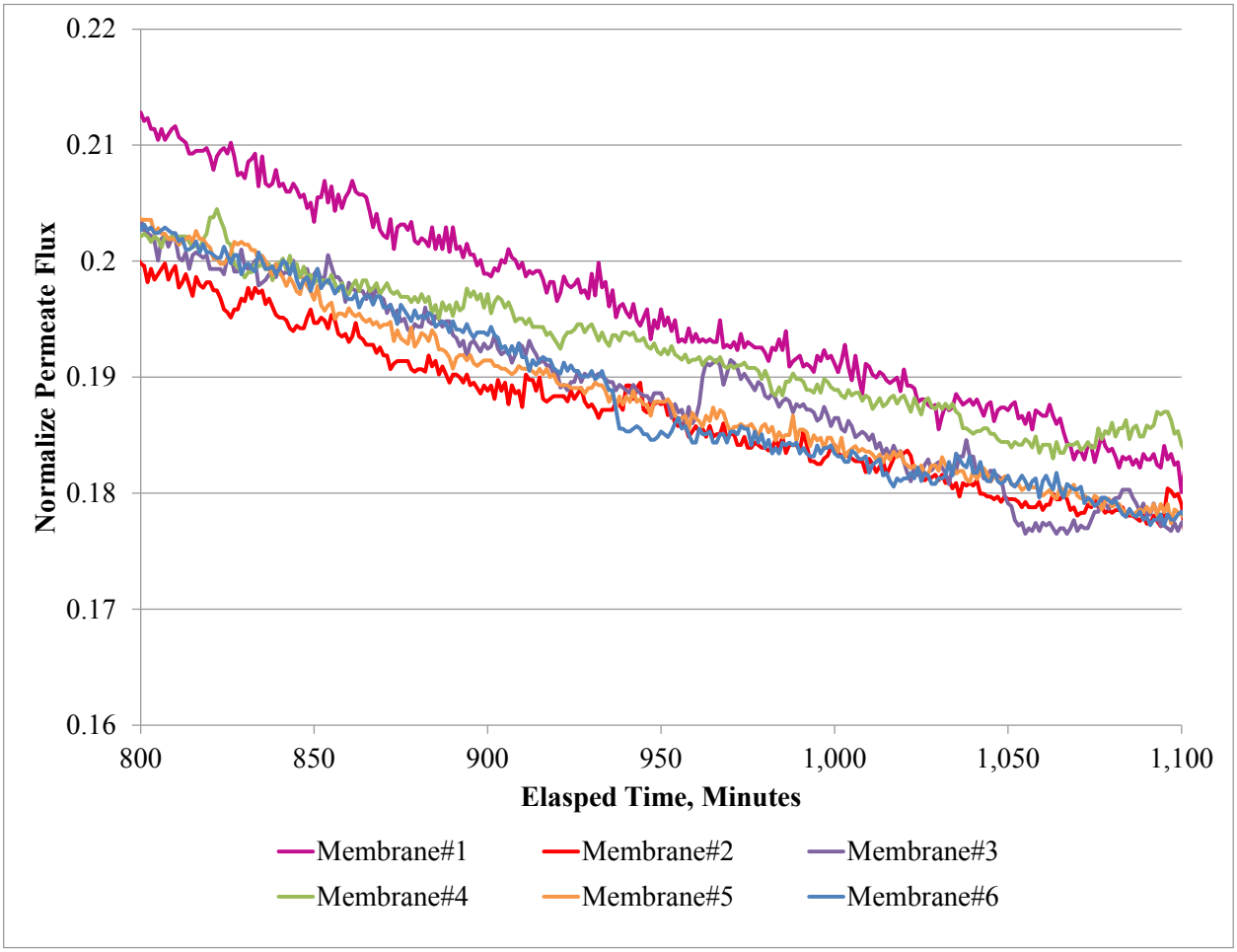

Figure 4.5: Later stages of the high TMP fouling experiments

During the initial stages of the fouling experiments, as mentioned before, pore blocking or pore constriction can occur due to foulant to membrane interactions. Adsorption of foulant on the membrane surface happens initially to cause the sharp permeate flux decline. Once that initial layer of foulant is formed on the membrane surface, more layers of foulant continue to pile on top of each other and the formation of a cake begins and during this stage, the permeate flux decline is much slower and gradual over time. In the later stages of the fouling experiments, the interactions are mainly from foulant to foulant.

The corresponding recorded TMP across each membrane for the high TMP fouling runs is shown in Table 4.2.

Table 4.2: Average TMP for high TMP runs

Membrane #	Average TMP, kPa
1	2,100
2	4,050
3	2,450
4	2,250
5	4,350
6	3,100

The average TMP results show that membrane #1 requires lowest energy requirements (pressure) to operate since the recorded TMP is the lowest value. The average TMP values for each membrane follows the same trend in membrane pore size and the determined specific membrane resistance. Examining Table 4.1 and Table 4.2 shows this trend of relating pore size to the require TMP. If we try to correlate the average TMP values in Table 4.2 with the observed initial roughness of each membrane (Table 3.1) and the observed contact measurements (Table 3.2), there is no observable correlation between them. This is as expected since the TMP is determined initially before theoretically any fouling begins. Once the fouling experiment begins and the membrane is exposed to foulant, then the membrane surface properties (roughness, wettability) become important in determining the rate of permeate flux decline. For our study, the initially set TMP is only a function of the clean membrane pore size distribution.

Post analysis of the collected permeate water samples reveal that all membranes showed high removal of the dissolved organics (humic acid) with all average values >90% TOC rejection. Table 4.3 shows the rejection performance of the membranes during the high TMP runs. This result shows that these NF membranes are capable of filtering out high amounts of dissolved organics. One mechanism for dissolved organic removal is size exclusion. As mentioned earlier in Chapter 2, the range in size of humic acid is between 2 to 18 nm and given the average pore size of the NF membranes is between 1 to 2 nm, it is therefore highly likely that most of the humic acid is rejected due to size exclusion. Another possible rejection mechanism for the dissolved organic is the charge rejection mechanism. If the membrane or foulant cake and the foulant have the same charge then the foulant would be rejected. Other studies have concluded that for NF membranes, the predominate rejection mechanisms are by size and charge exclusion with treating process water with dissolved organics and salt [Sadrzadeh et al. (2015), Hayatbakhsh et al. (2016), Schafer (2001), Mondal and Wickramasinghe (2008), Nghiem et al. (2010), Chang et al. (2011)].

Table 4.3: Salt and TOC rejection for high TMP runs

High TMP Runs		
Membrane #	Average Salt rejection %	Average TOC rejection %
1	65.0	97.6
2	68.8	98.2
3	79.0	97.6
4	66.7	98.7
5	87.5	97.5
6	66.8	96.5

The salt (NaCl) rejection performance for the membranes varies from 65.0% for membrane #1 to 87.5% for membrane #5. The ionic radius of Cl^- ions (0.18 nm) and Na^+ ions (0.1 nm) are smaller than the membrane pore sizes [Marcus (1983)]. This would mean that if no electrostatic interactions are involved, the ions would not be filtered out by the membranes due to size exclusion. Thus, the mechanism of Na^+ and Cl^- rejection is due to electrostatic interactions. Here the interaction between the charged ions and the surface charge on the membrane initially and the charges associated with formed cake later on during the experiments cause ion rejection by the NF membranes. Past studies have highlighted this conclusion in their studies indication electrostatic interactions or charge rejection between membrane and ion species as the primary mechanism for their rejection [Sadrzadeh et al. (2015), Hayatbakhsh et al. (2016), Schafer (2001), Mondal and Wickramasinghe (2008), Nghiem et al. (2010), Chang et al. (2011)]. The surface charge on amide type membranes in the presence of water have been reported to be negatively charged and the negative value is dependent on the composition of the water [Sadrzadeh et al. (2015), Hayatbakhsh et al. (2016), Schafer (2001), Khorshidi et al. (2016), Elimelech et al. (1994)]. Only membrane #3, #4, and #5 salt rejection performance is similar to manufacturer specifications. One possible reason for this discrepancy is that manufacturers use idealizes water feed quality during the testing of the membrane performance.

The contact angle measurements on the fouled membranes are presented in Table 4.4. These membranes were from the high TMP experiments and the contact angle measurements on the fouled membranes were made after the fouling experiments were concluded. All measurements were done in air with a droplet fluid on top of the fouled membrane.

Table 4.4: Contact angle measurement of fouled membrane (high TMP experiments)

Membrane #	Clean Membranes			Fouled Membranes		
	Mean Contact Angle			Mean Contact Angle		
	DI Water	Process Water	Diluted Bitumen (70:30)	DI Water	Process Water	Diluted Bitumen (70:30)
1	9.77±2.62	8.62 ± 2.95	62.17 ± 1.88	58.4±1.23	52.88±2.01	85.83±1.28
2	21.47±0.87	26.50 ± 0.78	80.50 ± 4.56	48.53±2.01	50.25±1.85	99.85±2.18
3	30.77±3.64	31.55 ± 2.08	101.98 ± 5.18	55.42±0.92	55.8±1.28	83.23±2.31
4	16.88±1.14	14.20 ± 2.15	60.95 ± 1.15	50.52±1.21	58.85±1.67	97.17±1.47
5	59.00±2.75	52.45 ± 2.16	80.40 ± 3.04	68.28±2.41	65.72±0.88	62.23±0.98
6	55.17±2.71	55.98 ± 2.16	72.57 ± 3.04	48.15±1.37	34.93±1.18	71.52±2.11

The results show that at the end of the experiment, all membranes except for membrane #6 are less hydrophilic. For membrane #6, the contact angle with water or process water decreased meaning it is slightly more hydrophilic. The decrease in hydrophilicity for most of the membranes is due to the organic cake formed on top of the fouled membrane. Figure 4.6 shows an image of a clean membrane (left) and fouled membrane (right).

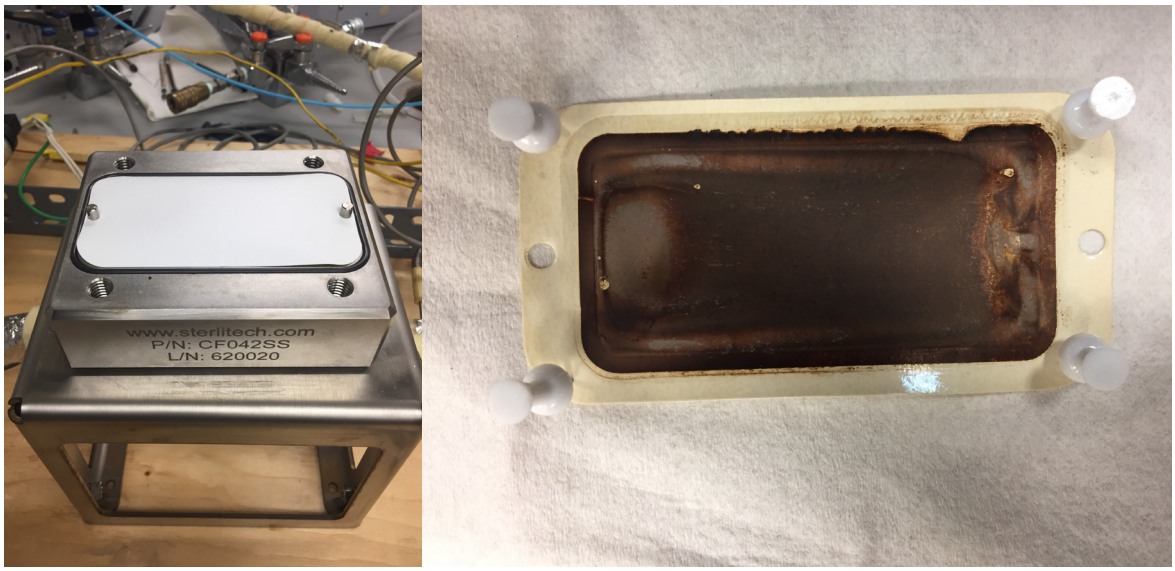

Figure 4.6: Image of clean and fouled membrane

The results from the high TMP experiments are that NF membranes are capable of removing the dissolve organics and salt. From the analysis of the normalized permeate flux decline curve (Figure 4.3), the effect of membrane surface properties (roughness, wettability, material composition) on organic fouling is unclear at this high TMP experimental condition. The initial behavior and overall semi-stable flux at the later stages of the high TMP fouling experiments appear to be similar. This could be due to the high TMP condition and resulting in the organic fouling happening to quickly on the membrane to capture the effects from membrane surface characteristics. One way to prevent fouling from happening too quickly is to lower the pressure drop across the membrane. This leads into the next group of fouling experiment where the TMP is lower and the initial starting permeate rate is reduced.

4.3.2 Low TMP Fouling Experiments

The initial starting permeate flux for the low TMP runs is 5.0 g/min. This is again accomplished by adjusting the BPR until the initial permeate flux reached the setting point. Four membranes are investigated in the low TMP experiments including membranes #1, #3, #5, and #6. Two amide type membranes (#1 and #3) with a wide difference in roughness and two non-amide membranes made of different material compared to the amide membrane are tested. The synthetic process water feed composition for the initial four low TMP runs include DI water mixed with humic acid and sodium chloride which is identical to the feed process water for the high TMP experiments. The specific quantity of each component in the water is shown in Table 7 back in Chapter 2. Figure 4.7 shows the results of the low TMP fouling runs.

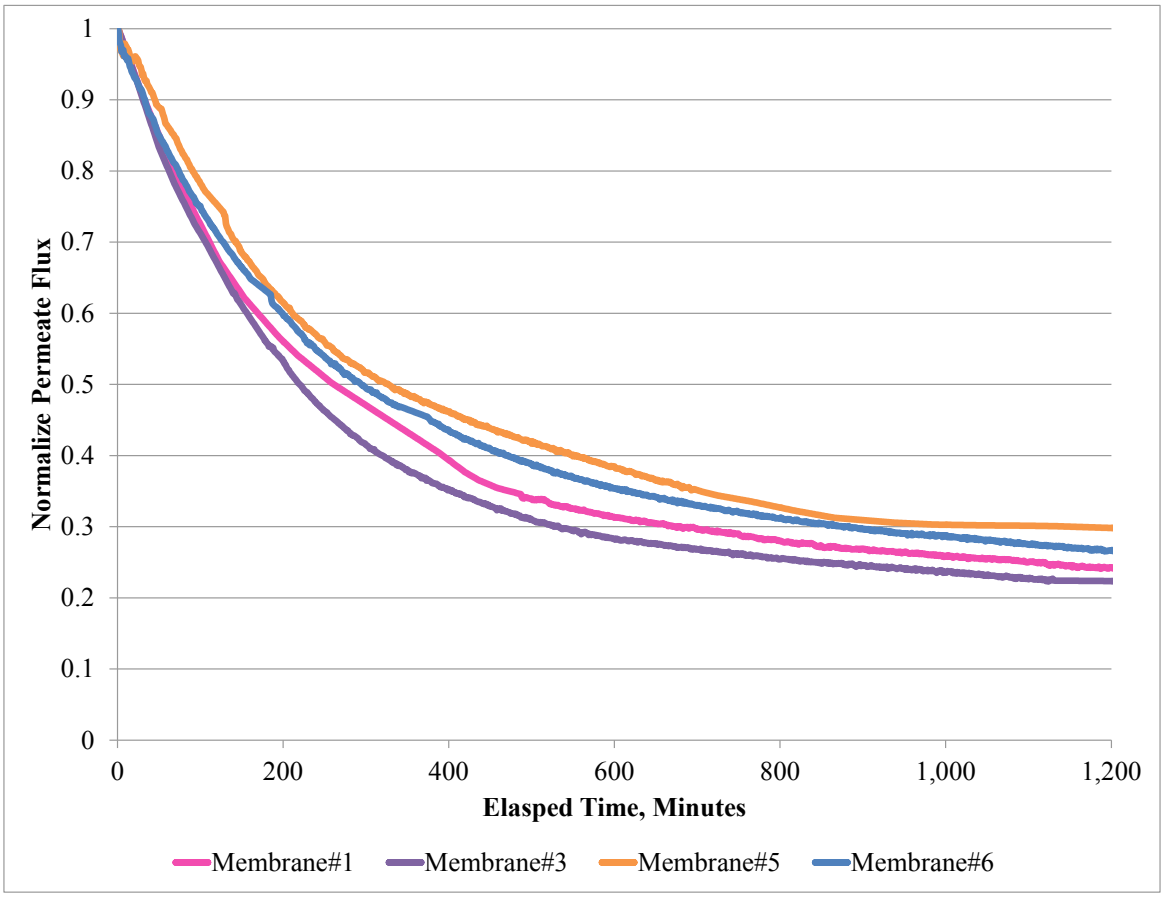

Figure 4.7: Low TMP fouling results

The permeate flux values are normalized with the initial permeate flux (5 g/min). Figure 4.7 shows that the fouling behavior and permeate flux decline for each membrane is similar. However, compared to the high TMP runs (Figure 4.3), there are more differences between the four low TMP runs indicating possible effects from membrane roughness and different membrane material composition. Initially, as seen in the high TMP runs a sharp decline in the permeate flux within the first 200 to 300 minutes of the experiment. After that the permeate flux starts to gradually level off and reach a stable value. Figure 4.8 and Figure 4.9 show the fouling data for the initial stages and later stages of the experiments respectively.

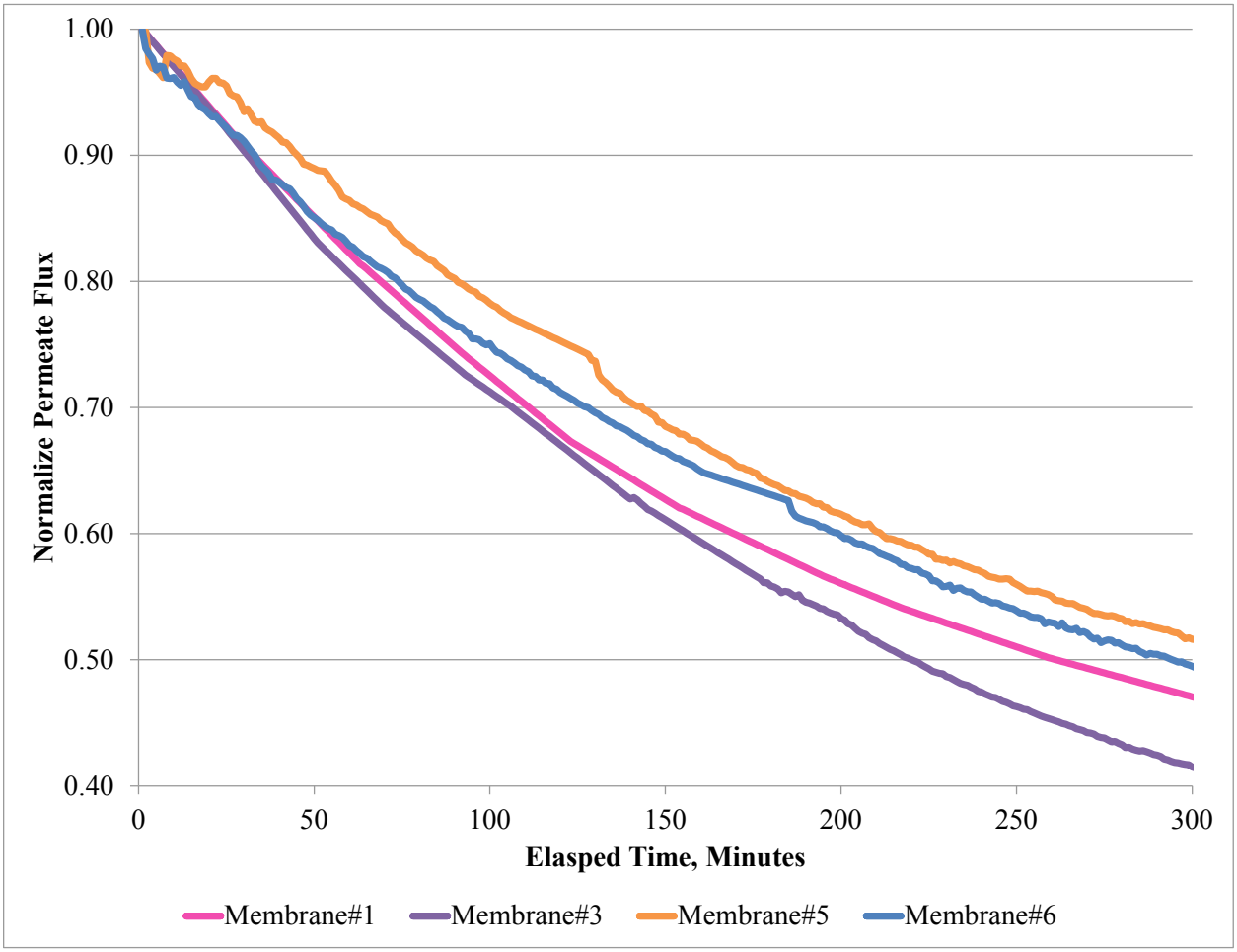

Figure 4.8: Initial stages of low TMP fouling experiments

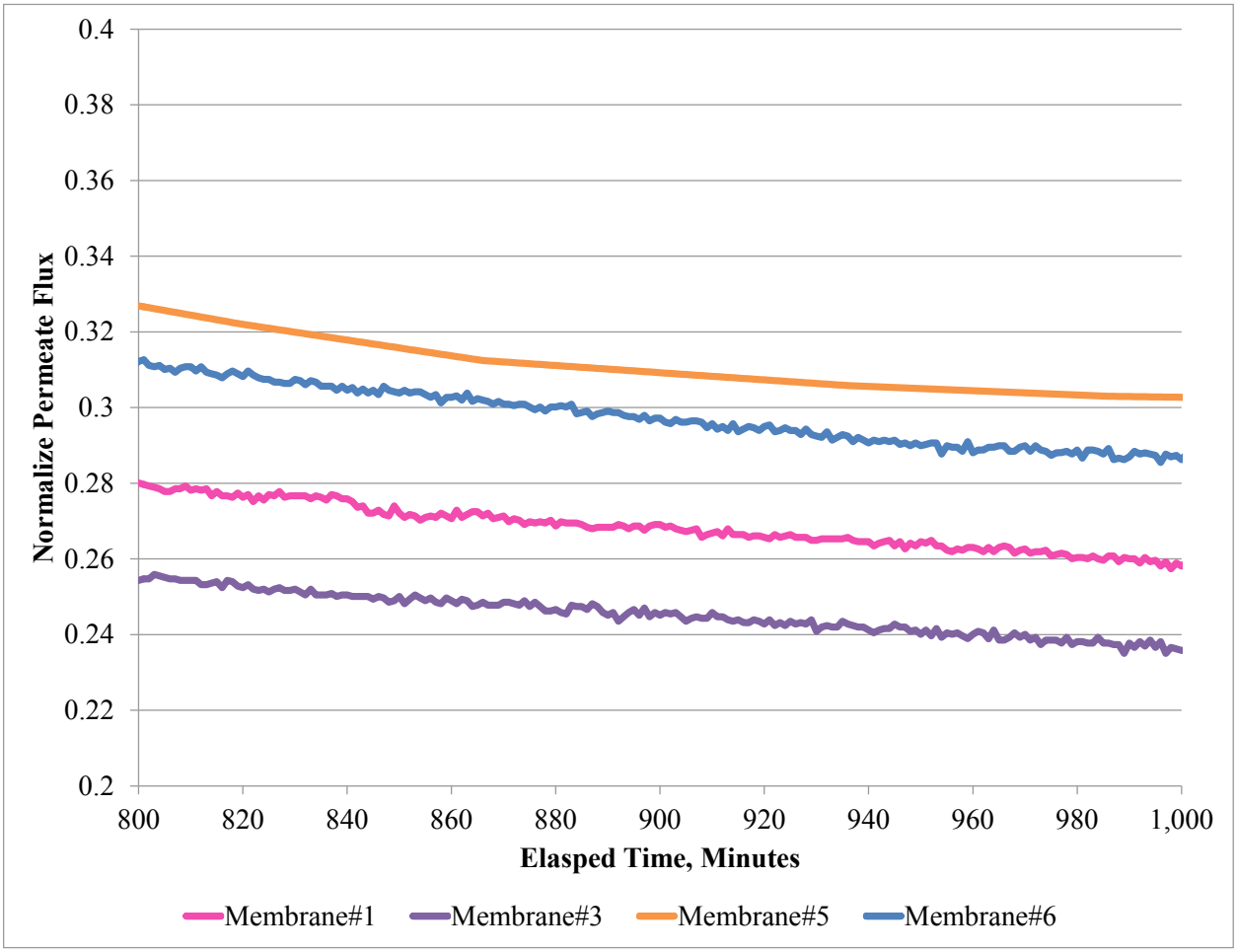

Figure 4.9: Final stages of low TMP fouling experiments

The results show that for the amide membranes (#1 and #3), membrane #1 is performing better with a higher permeate flux at the beginning of the experiment and at the end of the fouling experiments. This difference between membrane #1 and #3 is likely due to the initial surface roughness of the membranes. Membrane #1 is smoother than membrane #3. The rougher membrane surfaces performing poorer when you consider both membranes are composed of similar material. The membrane roughness is not the only factor to consider when evaluating the performance and fouling characteristics. The membrane material composition is also important as evident from the low TMP fouling experiments. The non-amide membranes (#5 and #6)

perform better and foul relatively less than the two amide type membranes. Membrane #1 and Membrane #5 have similar roughness (3.4 nm and 5.42 nm respectively), but their fouling performance is different. This is due to the different material surface composition of the two membranes. In terms of being the smoothest membrane (#6) at 1.24 nm, the expectation is that this membrane should foul the least. Unfortunately, due to the effect from material composition, it performed slightly poorer compared to membrane #5. So there is influence or different interactions between the membrane surface and the foulant present in the process water for membrane #5 and #6. From the results, the amide type membrane seems to have to have higher affinity for the organic foulant in the water compared to membranes #5 and #6.

The corresponding recorded TMP across each membrane for the low TMP fouling runs is shown in Table 4.2.

Table 4.5: Average TMP for low TMP runs

Membrane #	Average TMP, kPa
1	650
3	775
5	2,000
6	1,150

The recorded pressure drops are again following the expected trend with the membrane pore size with membrane #1 requiring the least amount of energy to operate. Even though membrane #5 performed the best in terms of having higher overall permeate flux over the course of the

experiment, the high TMP required makes this membrane the most costly to operate in terms of energy requirements.

Post analysis of the collected permeate water samples reveal that all membranes showed high removal of the dissolved organics (humic acid) with all average values >90% TOC rejection. This is similar to the results in the high TMP runs and Table 4.6 shows the comparison of rejection performance for low and high TMP runs. The main mechanisms as mentioned before for dissolved organic removal are size and charge exclusion.

Table 4.6: Salt and TOC rejection for Low and high TMP runs

Membrane #	Low TMP runs		High TMP runs	
	Average Salt rejection %	Average TOC rejection %	Average Salt rejection %	Average TOC rejection %
1	91.0	97.2	65.0	97.6
3	85.0	97.3	79.0	97.6
5	84.0	95.6	87.5	97.5
6	56.6	96.6	66.8	96.5

The salt (NaCl) rejection performance in the low TMP runs is similar to the results of the high TMP runs with the exception to membrane #1 where the salt rejection improved at lower TMP conditions. The mechanism of Na^+ and Cl^- rejection for low TMP condition is again due to electrostatic interactions. Only membrane #6 salt rejection performance is higher than manufacturer specifications. The other three membranes for low TMP runs have salt rejection performance similar manufacturer specifications.

The contact angle measurements on the fouled membranes are presented in Table 4.7.

Table 4.7: Contact angle measurement of fouled membrane (low TMP experiments)

Membrane	Clean Membranes			Fouled Membranes		
	Mean Contact Angle			Mean Contact Angle		
	DI Water	Process Water	Diluted Bitumen (70:30)	DI Water	Process Water	Diluted Bitumen (70:30)
1	9.77±2.62	8.62 ± 2.95	62.17 ± 1.88	49.8±2.11	51.98±2.00	121.78±2.88
3	30.77±3.64	31.55 ± 2.08	101.98 ± 5.18	43.63±1.74	49.22±2.18	126.47±2.74
5	59.00±2.75	52.45 ± 2.16	80.40 ± 3.04	54.22±1.11	57.37±1.43	67.02±1.88
6	55.17±2.71	55.98 ± 2.16	72.57 ± 3.04	39.13±1.55	43.12±1.22	78.65±1.90

The post measurements of the contact angle on membrane surface are similar to the results observed for high TMP runs. The results show that at the end of the experiment, all membranes except for membrane #6 are less hydrophilic. For membrane #6, the contact angle with water or process water decreased meaning it is slightly more hydrophilic. At either high or low TMP condition, the decrease in hydrophilicity for the membranes is due to the organic cake formed on top of the fouled membrane.

Analysis of the cake formed on top of the fouled membrane using ATR-FTIR is shown in Figure 4.10. This graph compares the clean membrane #1 spectra with the fouled membrane spectra. The two peaks at 1,000 cm^{-1} and 900 cm^{-1} are characteristics of humic acid spectra [Tanaka et al. (2001)].

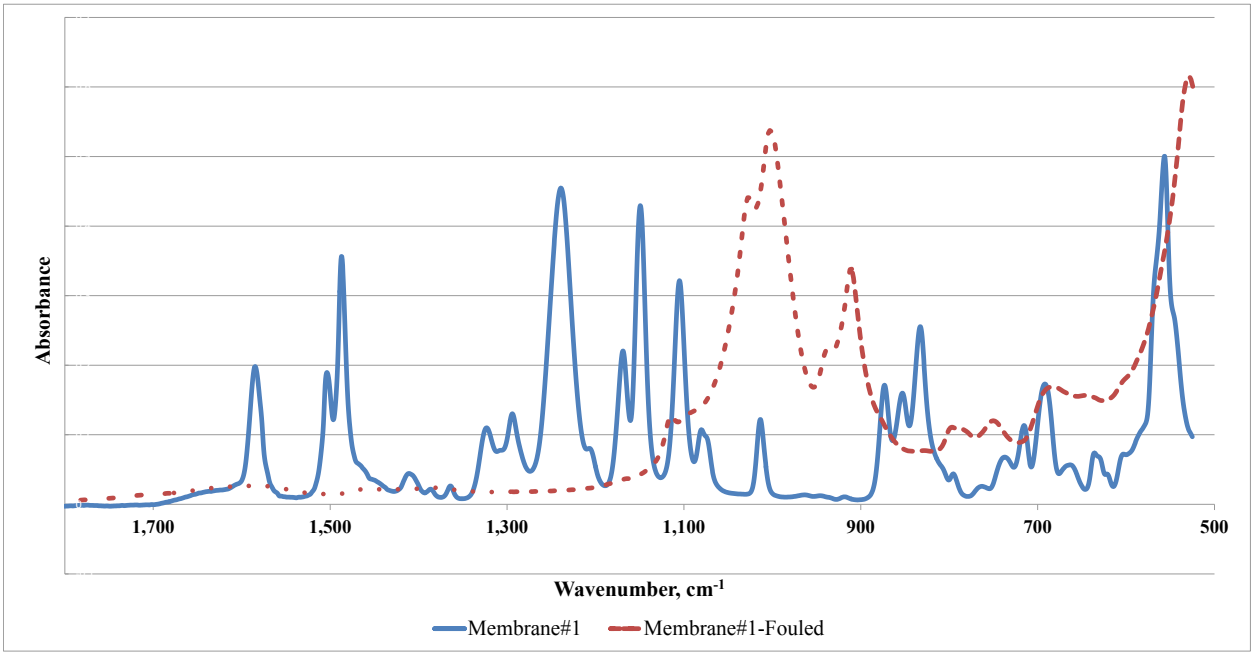

Figure 4.10: ATR-FTIR analysis of foulant cake (Low TMP run)

4.3.2.1 Change in Membrane Surface Characteristic during the Fouling Experiment as a function of time

This next section looks into how the membrane surface characteristic changes during the fouling experiment. The membrane characteristics that are investigated include surface roughness and wettability (hydrophilicity and oleophilicity). One low TMP fouling experiment using membrane #1 is used as the case study. The procedure to investigate the change in surface characteristics during the fouling experiment is as follows. The experiment is conducted at low TMP condition with membrane #1. The change in surface membrane properties study is conducted in three independent runs using three different membrane #1 samples with the assumption that the membrane samples are very similar in initial roughness. The first run is from time 0 hours to 2 hours. The second run is from 0 hours to 8 hours and the third run is from 0 hours to 20 hours. After each run, the surface roughness and the post contact angle measurements are determined.

Also SEM images of the membrane surface for each run are taken. The fouling behavior is similar to the one observed for membrane #1 in Figure 4.7. Table 4.8 shows the results for this specific case study.

Table 4.8: Change in membrane surface properties during the fouling experiment (Low TMP case)

Experiment Duration (hrs)	Membrane #	Average Roughness, RMS (nm)	Clean Membranes			Fouled Membranes		
			Average Contact Angle			Average Contact Angle		
			DI Water	Process Water	Diluted Bitumen (70:30)	DI Water	Process Water	Diluted Bitumen (70:30)
0	1	3.4	9.77±2.62	8.62 ± 2.95	62.17 ± 1.88		-	-
2	1	70.8				46.58±2.33	51.63±1.88	119.82±2.11
8	1	59.6				47.53±1.77	42.93±1.61	119.45±1.81
20	1	54.5				49.8±2.51	51.98±2.00	121.78±2.88

The results show that the membrane fouled surface becomes more hydrophobic and oleophobic compared to the clean membrane surface. The measured contact angles are similar throughout the fouling experiment. Once the initial layer of foulant is formed on the membrane surface, the wettability does not change dramatically. In fact, it stays relatively similar. As for the average surface roughness, initially the clean membrane is smooth with a roughness value of 3.4 nm. At time 2 hours, the average roughness of the membrane surface is 70.8 nm. This is the highest average roughness value measured during the fouling experiment. During this time period, the average roughness jumps to a higher value possibly due to foulant sticking or adsorbing to the membrane surface and to other deposited foulant to form a rougher surface. As the fouling experiment proceeds, we observe that the surface roughness slowly declines from the peak value at 2 hour. During this stage from 2 hours to the end of the fouling experiment, it is conceivable

the additional foulant attaching to the contaminated membrane surface continues to fill in at a higher rate between the peaks on the surface than attaching to the tops of the peaks. This potential filling in phenomena reduces the roughness of the surface gradually. Figure 4.11 shows the AFM and SEM images of the membrane surface as a function of time.

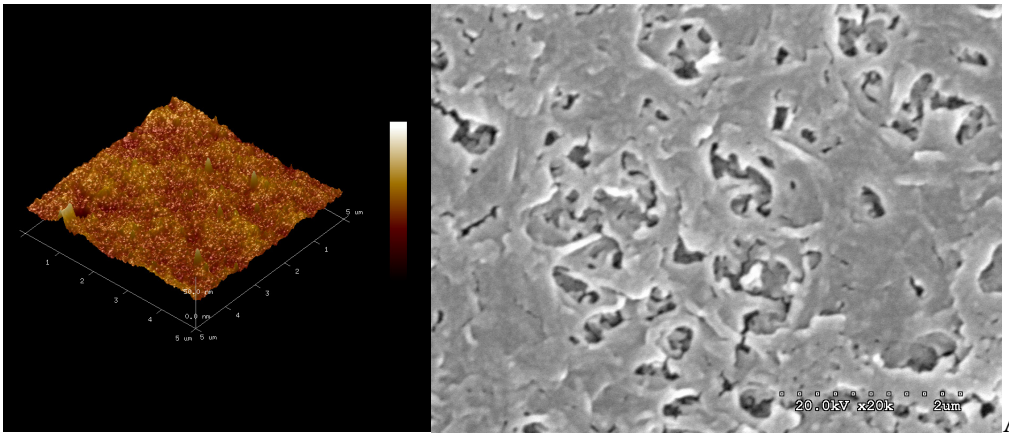

At time 0 hours

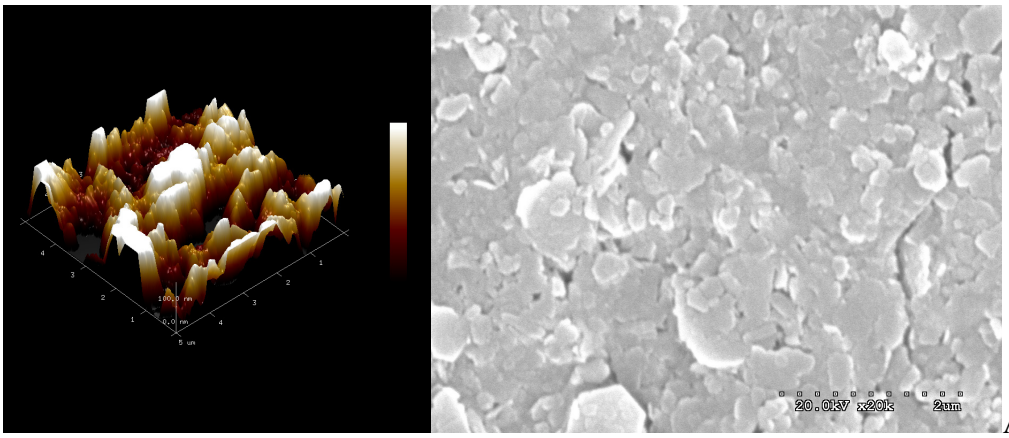

At time 2 hours

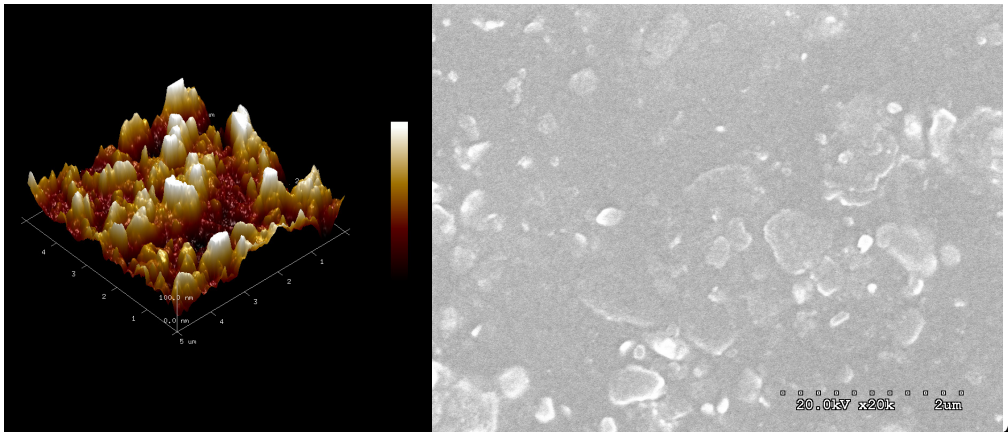

At time 8 hours

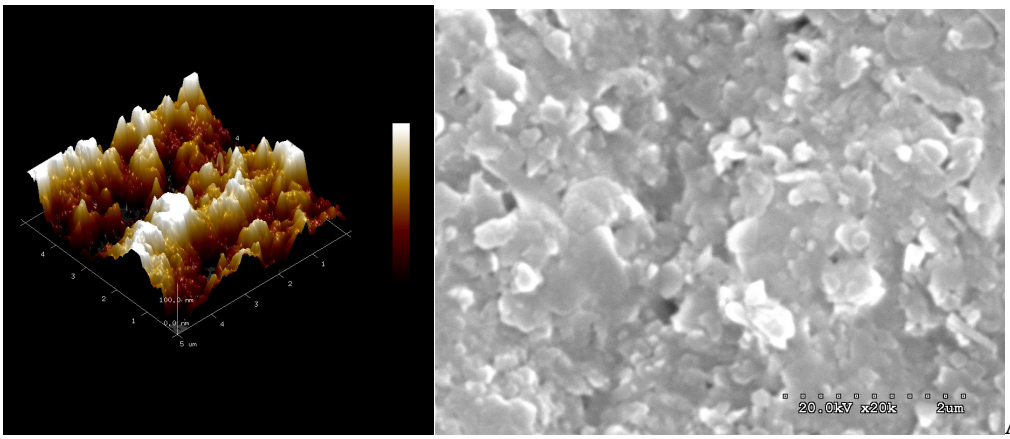

At time 20 hours

Figure 4.11: AFM and SEM images of membrane surface during the fouling experiment

The overall impressions from the low TMP experiments are that membrane surface roughness and membrane material composition have an effect on the fouling performance. For amide type membranes, the increase fouling is attributed to the rougher membrane surface. However, the non-amide membranes (#5 and #6) fouled less compared to the amide membrane (#1) with similar roughness. This is probably attributed to the material composition of the membrane as causing the differences in fouling performance. Another explanation is that the surface charge on these non-amide membranes maybe more negative compared to the amide membranes in the presence of identical feed water. An increase in negativity for the membrane surface charge value can enhance the electrostatic repulsion between foulant and membrane [Hayatbakhsh et al.

(2016)]. This would results in higher permeate rate and less fouling. Even though membrane #5 and #6 had higher permeate rates compared to membrane #1, membrane #1 has the advantage in terms of operating at lower operating pressures. Commercially, membrane would cost the least in terms of operating cost. However there needs to be a balance between performance and cost of operation. Later in section 4.4.4, the performance of the NF membranes are analyzed to determine their volumetric capacity to produce clean permeate water. At the lower TMP condition, the NF membranes are still capable of removing the dissolve organics and salt.

4.3.2.2 Effect of Salt Content in Process Water

This section looks into how the synthetic process water salt content affects the fouling performance of NF membranes. These experiments are conducted at low TMP conditions using membrane #1. The procedure for making the two synthetic process water samples is as follows. Process water #1 is made using DI water, humic acid, and sodium chloride and the composition of humic acid and sodium chloride is shown in Table 2.1. Process water #2 is made using RO water and humic acid and again the composition of humic acid is presented in Table 2.1. The average salt content in process water #1 and #2 is 213 ppm and 10 ppm respectively. Both water samples are pH adjusted between 7 to 8. RO water is used to minimize the amount of ions in the water compared to using DI water. Figure 4.12 shows the results of the two fouling experiments.

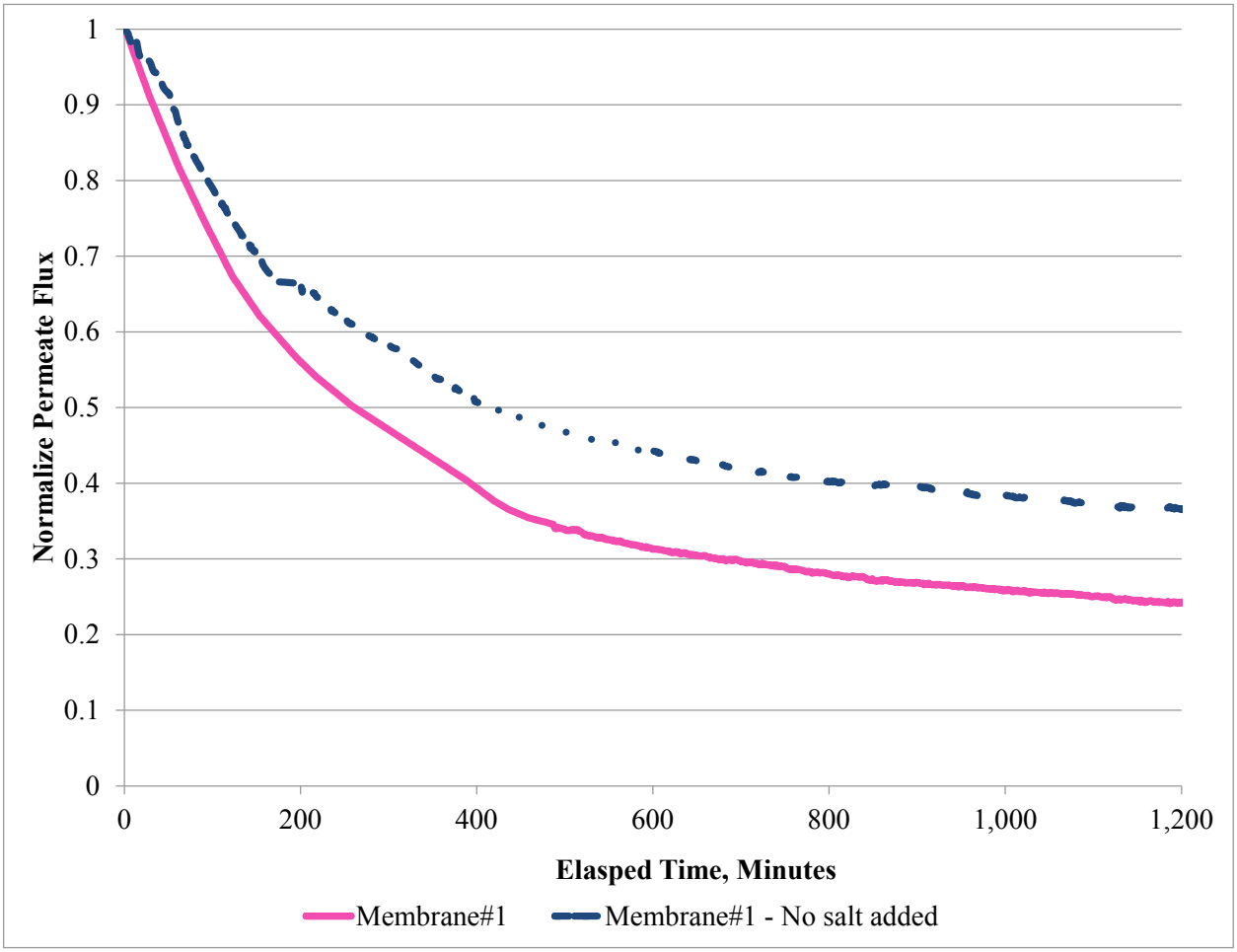

Figure 4.12: Effect of salt content in process water on fouling (low TMP)

The results indicate that the feed water (Process water #2) where no addition salt is added the membrane fouled less. This is due to the reduced ionic strength of the continuous feed water and the interaction forces between the membrane foulant. The higher the ionic strength (higher salt content) of the process water, the smaller the Debye length (λ_D) value. The electric double layer (EDL) repulsive interactions decreases at higher ionic strength conditions and the Van der Waals forces (adhesive forces) dominate. The adhesive forces are between membrane and foulant. The calculated Debye lengths for each water samples are presented in Table 4.9.

Table 4.9: Debye length values and TMP for process water with and without NaCl added

Debye Length, nm	Average Trans Membrane Pressure, kPa	Process water feed compostion
5.0	650.0	Water #1 with DI water, humic acid, and NaCl
11.0	575.0	Water #2 with RO water and humic acid

The Debye length (λ_D) is determined using Equation 18.

$$\lambda_D = \left(\frac{\sum C_{i,o} e^2 Z_i^2}{\varepsilon \varepsilon_o K_B T}\right)^{-0.5} \quad (18)$$

Where $C_{i,o}$ is the molar concentration of ion i, e=elementary charge, Z_i=charge number, ϵ=dielectric constant, ϵ_o=permittivity of free space, K_B=Boltzmann's constant, and T=absolute temperature.

The recorded TMP is also slightly lower for the fouling run where no salt is added. This results indicates that removing as much salt from the process feed water can reduce the amount of fouling and improve the permeate flowrate. For our cases, when salt is added to the process water, the permeate flux at 20 hours of filtration time is 32% lower compared to the case when no salt is added.

4.3.2.3 Effect of Emulsified Oil in Process Water

This section looks into how the presence of emulsified or dispersed organics in synthetic process affects the fouling performance of NF membranes. This experiment is conducted at low TMP conditions using membrane #1. The procedure for making the synthetic process water samples with 1 wt.% emulsified oil is described in Chapter 2. Essentially the process water contains DI

water, humic acid, sodium chloride, and emulsified oil droplet. Figure 4.13 shows the results of the fouling experiments compared the run where no emulsified oil is present in the feed water to the run where dispersed organics are present in the feed water. Figure 4.14 shows the initial stages of this experiment where the permeate flux rapidly drops in the first 10 minutes of the fouling experiment.

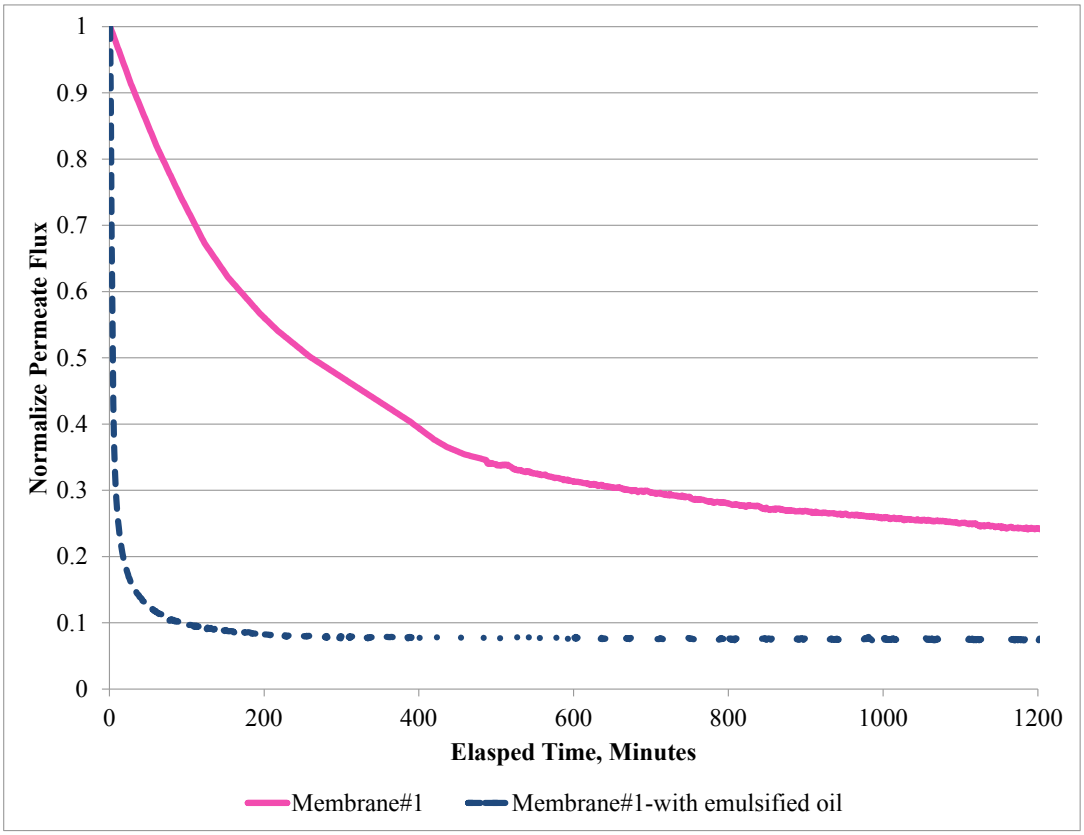

Figure 4.13: Effect of emulsified organics in process water on fouling (low TMP)

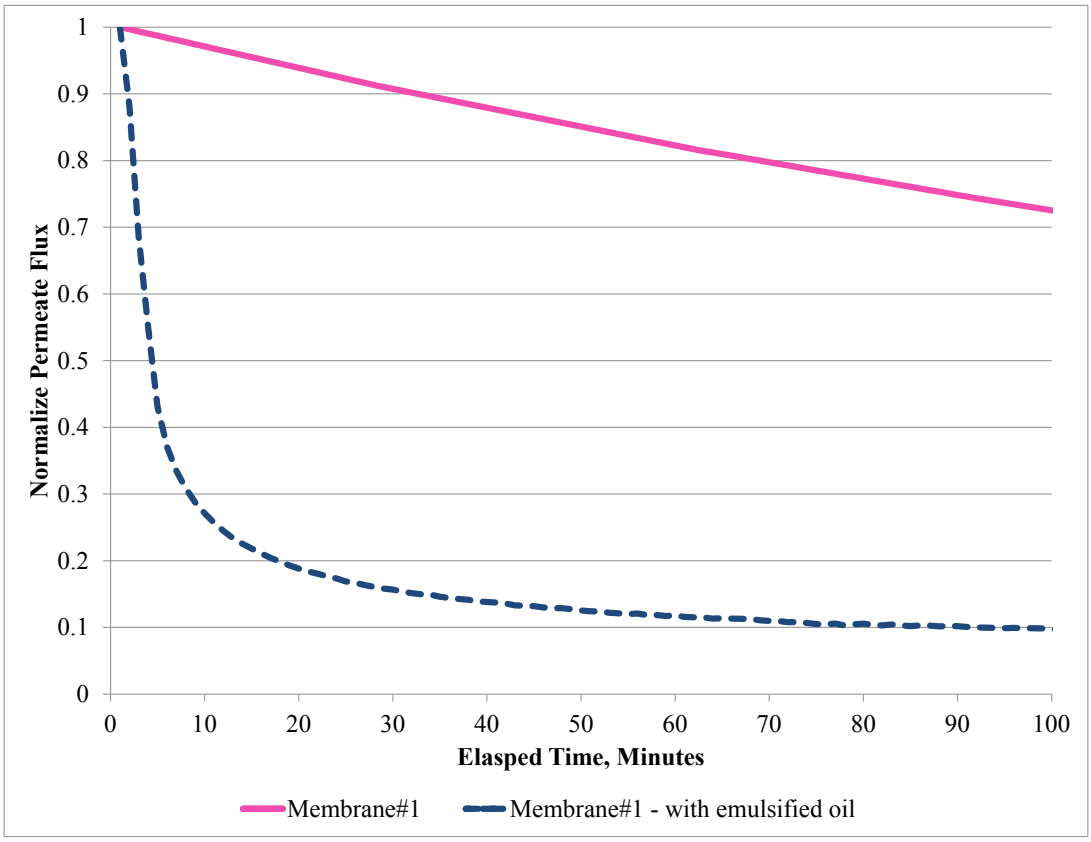

Figure 4.14: Effect of emulsified organics in process water on fouling (low TMP) - Initial stages

The results indicate that when emulsified organics or oil droplets are present in the feed water, the fouling of the membrane occurs rapidly with a dramatic decrease in permeate flux. Comparing the two cases in Figure 4.13, when emulsified oil is added to the process water, the permeate flux at 20 hours of filtration time is 70% lower compared to the case when no emulsified oil is added.

A possible explanation for this dramatic decline in performance and permeate flux is due to the sticky nature of diluted bitumen and the bitumen quickly coating the membrane surface and pores to reduce the permeate flux. Another explanation is that adding 1 wt.% or 10,000 ppm of diluted bitumen to the process water dramatically increased the TOC in the process water (from 500 ppm to >10,000 ppm). The dramatic increase in TOC feed concentration quickly fouled the

membrane leading to a dramatic drop in permeate flux as observed in Figure 4.14. Schafer (2001) also reported similar observations showing the effect of foulant feed water concentration on the permeate rate. As the foulant concentration increases in the feed water, the observed permeate rate is reduced and more membrane fouling is occurring.

Figure 4.15 shows SEM images at 20k time magnification of the clean membrane and the fouled membrane for this emulsified oil case.

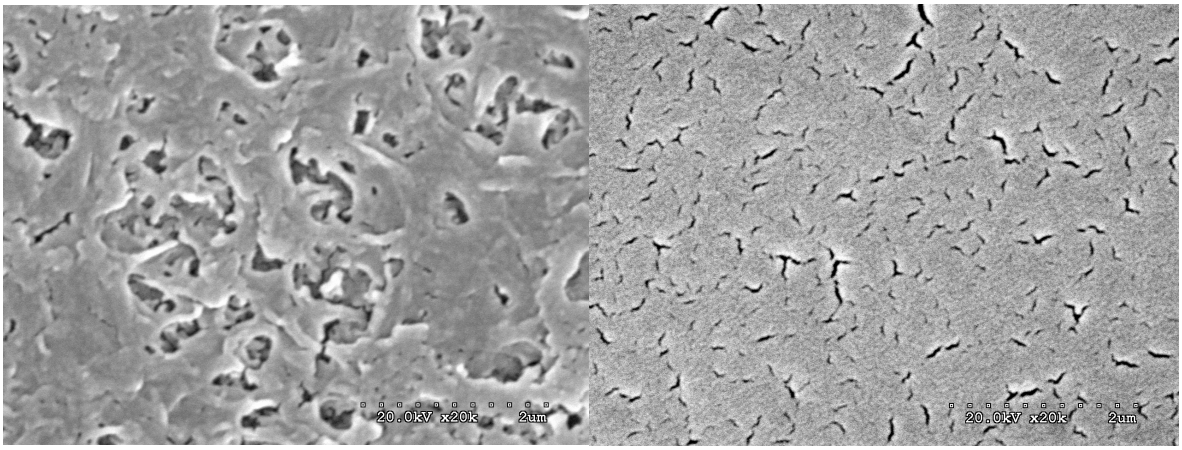

(a) Clean membrane (b) Fouled membrane

Figure 4.15: SEM images of clean and fouled membrane in emulsified oil case

The image (b) shows that the pores are completely covered with foulant (emulsified oil and humic acid) greatly reducing the area for process water to flow through the membrane.

Analyses of the collected permeate water samples showed high removal of the dissolved organics (humic acid) and this is presented in Table 4.10. This is similar to the results in the low TMP runs. This table compares the rejection performance using membrane #1 with three different feed compositions. The first being the normal feed composition (Table 2.1), the second

feed composition with no sodium chloride added to the water (still containing trace amounts of NaCl) and the last feed composition with emulsified oil droplets present in the water.

Table 4.10: Salt and TOC rejection comparison with feed water containing emulsified oil

Low TMP runs		
Average Salt rejection %	Average TOC rejection %	Feed Condition
91.0	97.2	Normal feed
91.9	97.1	Feed with not salt added
84.3	96.2	Normal plus emulsified oil

Analysis of the cake formed on top of the fouled membrane using ATR-FTIR is shown in Figure 4.16. This graph compares the clean membrane #1 spectra, the fouled membrane spectra (emulsified oil case), and the bitumen only spectra. The fouled membrane spectrum shows two peaks at 1,452 cm^{-1} and 1,375 cm^{-1} representing the bitumen accumulation on the filter cake.

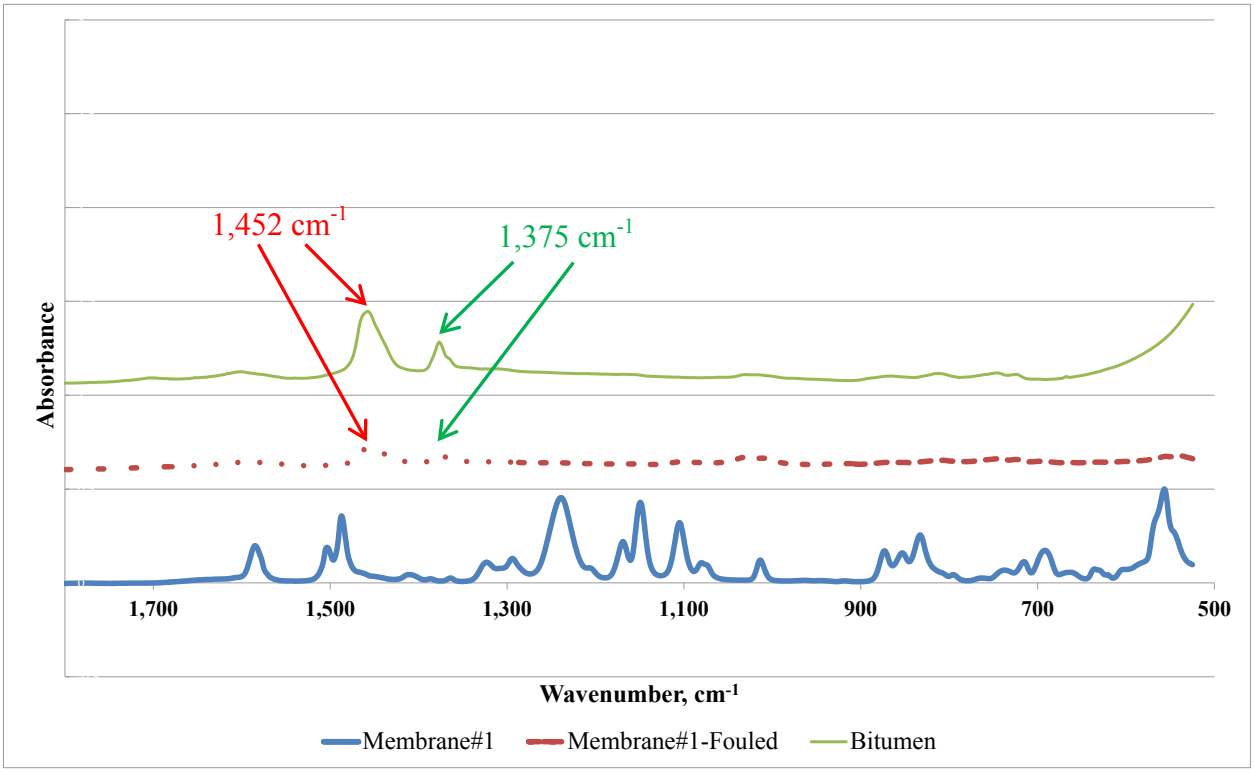

Figure 4.16: ATR-FTIR analysis of foulant cake (Low TMP run with emulsified oil)

EDX analysis of the filter cake for the low TMP run with normal feed water composition (Table 2.1) and the feed water composition with emulsified oil is presented in Table 4.11.

Table 4.11: EDX analysis of fouled membrane exposed to emulsified oil feed water

Condition	Membrane #	Concentration, weight %					
		Carbon	Oxygen	Sodium	Aluminum	Silicon	Sulfur
Clean	1	78.42	17.46	0.09	0.16	-	3.74
Fouled with humic acid and NaCl	1	41.55	47.82	0.52	4.94	4.81	0.01
Fouled with humic acid, NaCl, and emulsified oil	1	90.08	5.82	0.28	0.25	0.18	3.10

The results show that increase in carbon % due to the presence of bitumen in the filter cake compared to original clean membrane and also the case with the membrane was fouled due to humic acid.

The highlights from the low TMP experiments are that NF membranes are capable of removing the dissolve organics and salt similar to the high TMP conditions. From the analysis of the normalized permeate flux decline curve (Figure 4.7), the effect of membrane surface properties (roughness, wettability, material composition) on organic fouling is more evident compared to the results at higher TMP conditions. The results show that both membrane initial surface roughness and membrane material composition affects the fouling tendency of the membrane. From the amide type membranes, the tendency is for the rougher surface membranes to foul more and result in lower permeates flux. Comparing the material composition of the membranes, the non-amide type membranes fouled less and had higher permeate fluxes compared to the amide type membranes. Analysis of the membrane surface properties during the fouling experiment revealed that the surface roughness initially peaks at a higher value during the initial stages and then the roughness declines gradually as the filtration experiment proceeds. This is attributed to and initial adsorption or attachment of the foulant to the membrane surface and then followed by a gradual fill in of the foulant over the course of the fouling run. The influence of sodium chloride showed that at higher ionic strength (high salt content in the water), the more fouling occurring on the membrane and resulting in reduced permeate flux. The presence of emulsified oil in the feed water showed dramatic flux decline due. Even though TOC and salt rejection is excellent and similar to other runs, the presence of emulsified oil in the feed water makes the filtration performance undesirable due to low permeate water flux. This means less

clean water is being produced over a given period of time and therefore, NF membranes are not suitable for use under dispersed organic feed conditions.

The fouling data for high and low TMP experimental cases shows an initial sharp flux decline followed with a gradually decline in the permeate flux. The fouling mechanisms at the initial stages compared to the later stages of the runs should be different since the permeate flux decline behavior is different. In the next section the fouling data is modelled to help determine the type of membrane pore blocking mechanism present during the fouling experiments. The effect of membrane surface roughness on fouling is also modeled in this next section.

4.4 MODELLING OF FOULING DATA

4.4.1 Determining the Fouling Mechanism

Membrane filtration and modelling the fouling behavior have been study for decades with the original cake filtration theory proposed and established back in the 1930s and 1940s by Ruth (1935, 1946). Later, the blocking filtration laws were developed to describe the four potential physical blocking mechanisms that can control membrane pore blocking and fouling [Iritani and Katagiri (2016), Hermia (1982), Hermans and Bredee (1936)]. The blocking filtration laws describe four physical mechanisms that control membrane pore blocking and the cake filtration model. These blocking filtration laws were originally developed for unstirred dead end filtration. However, studies have shown that these laws are applicable to crossflow filtration in the early stages to describe the progressive pore clogging [Murase and Ohn (1996), Johnson et al. (1996), Keskinler et al. (2004)].

A detailed description of the theory and graphical representation of the mechanisms was presented earlier in this study in Chapter 1.

To analyze the fouling data presented in previous sections, the methodology to determine the blocking mechanism is based using the Equation 7 to 10 in

Table 1.4 and plotting the graphs presented in Figure 1.5 for a given fouling experiment data set. The experiment case study chosen for this analysis is the low TMP experiment with membrane #1 with the standard synthetic water feed composition (Table 2.1). Figure 4.17 shows the plots to model the filtration laws for this data set over the entire time period.

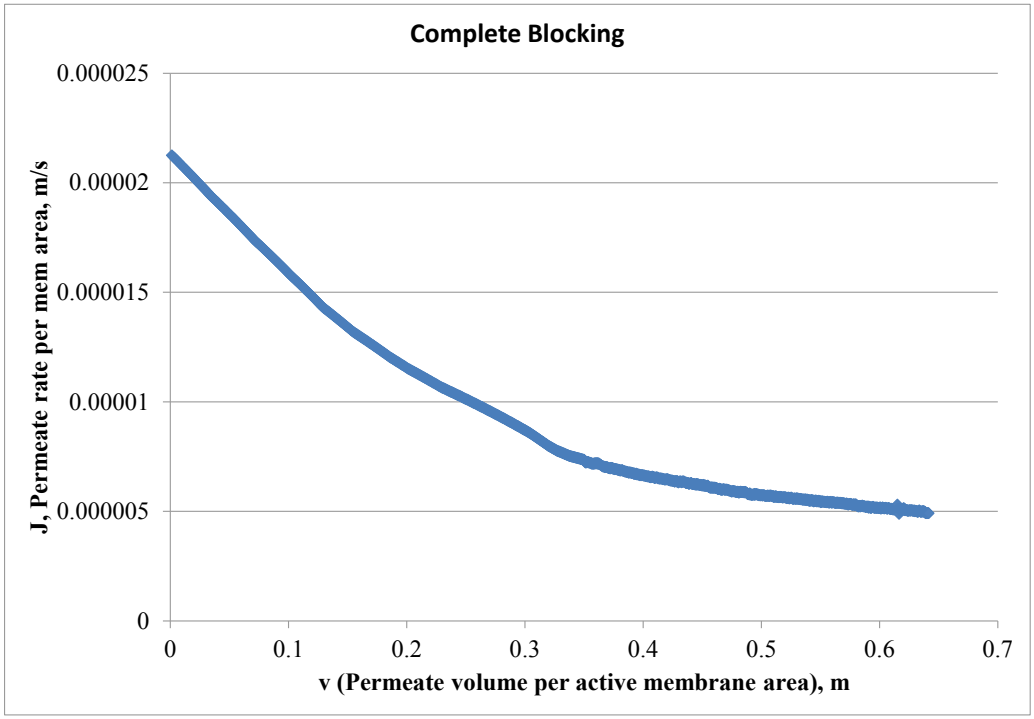

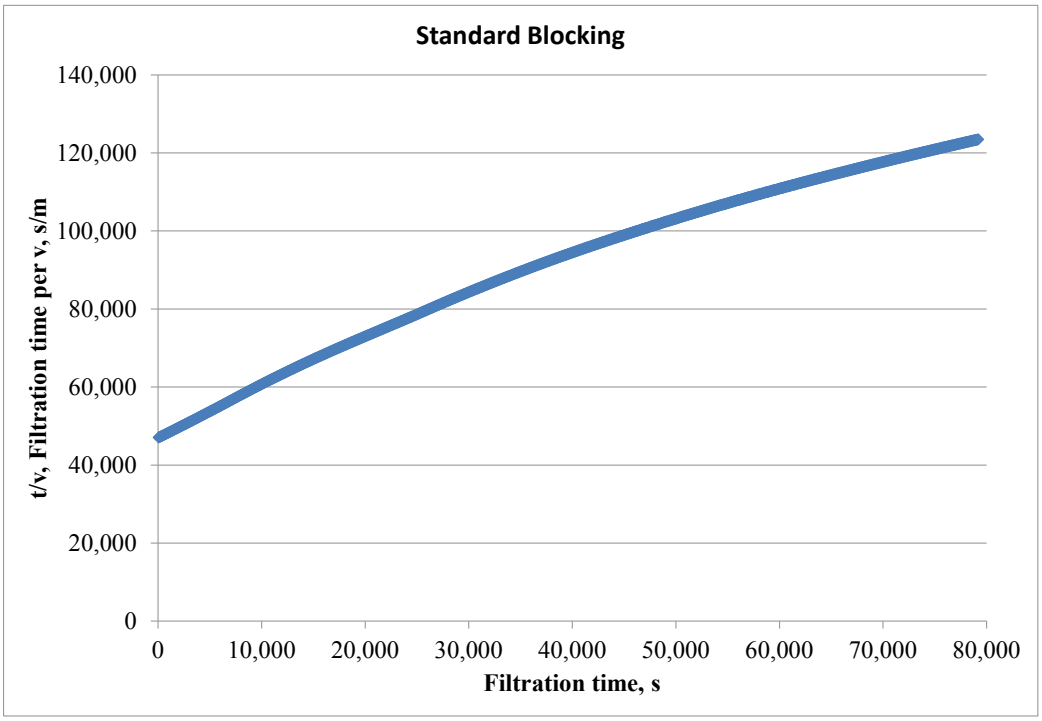
Standard Blocking
140,000
120,000
100,000
80,000
60,000
40,000
20,000
0
t/v, Filtration time per v, s/m
0
10,000
20,000
30,000
40,000
50,000
60,000
70,000
80,000
Filtration time, s

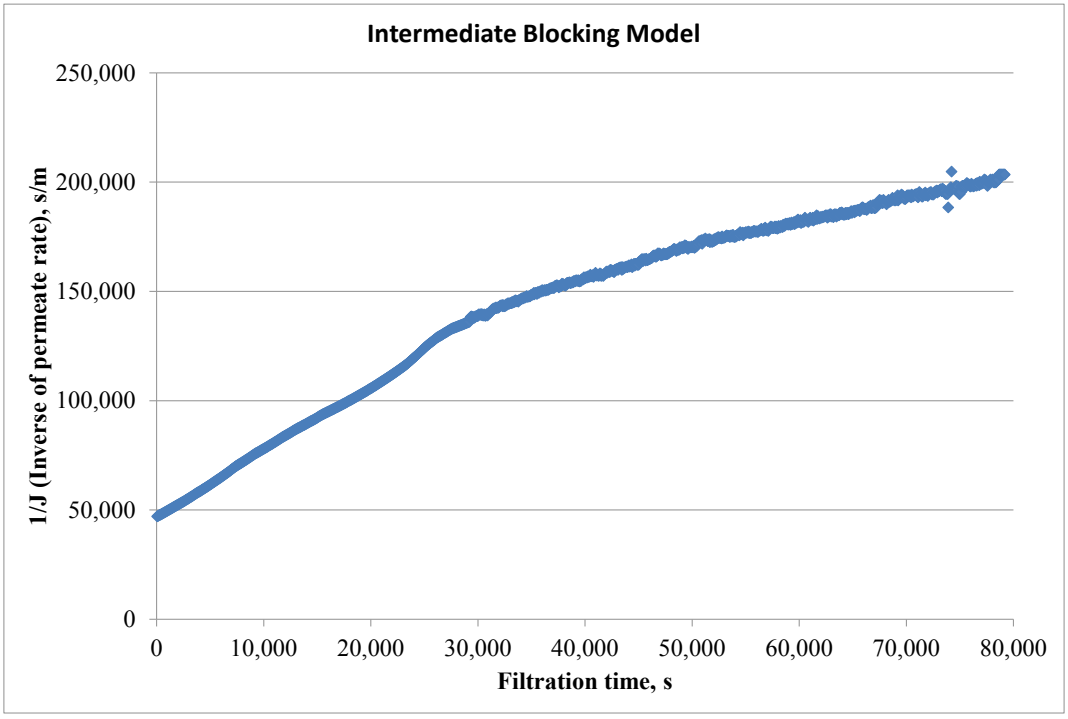
Intermediate Blocking Model
250,000
200,000
150,000
100,000
50,000
0
1/J (Inverse of permeate rate), s/m
0
10,000
20,000
30,000
40,000
50,000
60,000
70,000
80,000
Filtration time, s

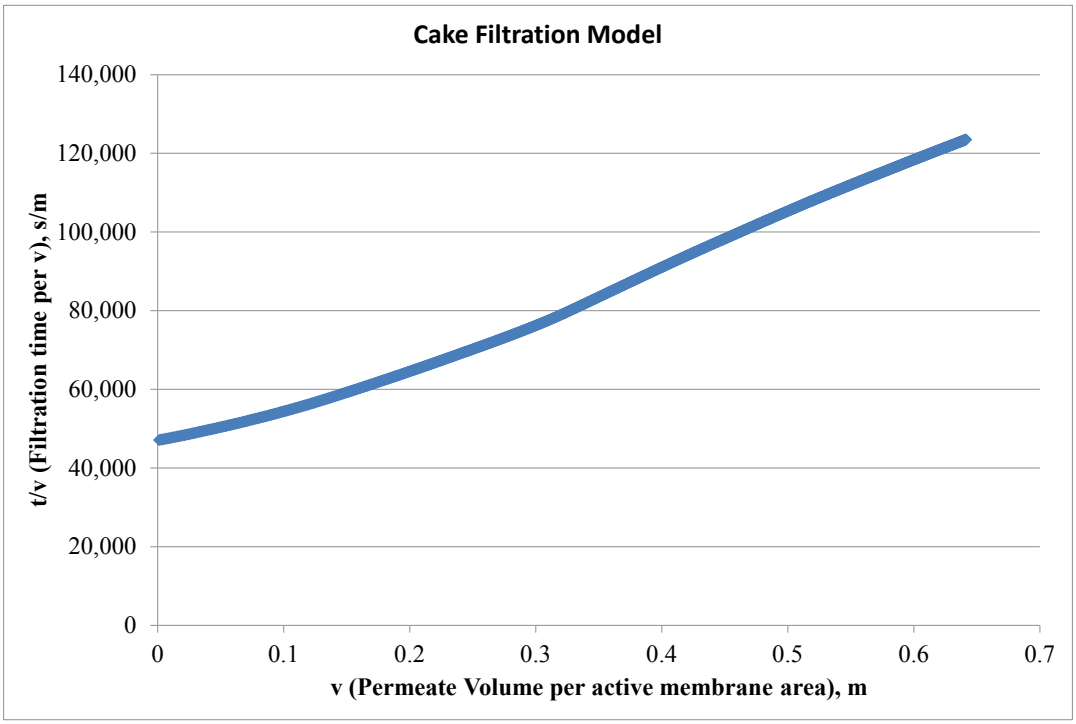

Figure 4.17: Filtration low plots for low TMP fouling experiment

Before analyzing the plots in Figure 4.17, standard blocking is ruled out as the pore blocking mechanism since the average size of the organic foulant (humic acid) is larger than the NF membrane pore size. Therefore, pore constriction due to foulant depositing on the pore wall is not very likely. The analysis of the fouling mechanism involves looking at the initial stages (0 to 200 minutes) of the fouling where there is a sharp decline in the permeate flux and the later stages (200 to 1,200 minutes) where the permeate flux gradually declines. This idea of membrane fouling occurring in two stages has been described by many other studies where pore blockage or constriction is followed by the long term fouling due to gradually accumulation of foulant on the filter cake [Iritani and Katagiri (2016), Hermia (1982), Schafer (2001), Juang et al. (2010), Ozdemir et al. (2012)]. For the initial stage of fouling, the intermediate blocking model has the highest R^2 value (0.9992) when fitting a linear correlation through the data for the initial

200 minutes of the experiment compared to the other blocking mechanism data. Figure 4.18 shows this initial stage data range for the intermediate blocking law.

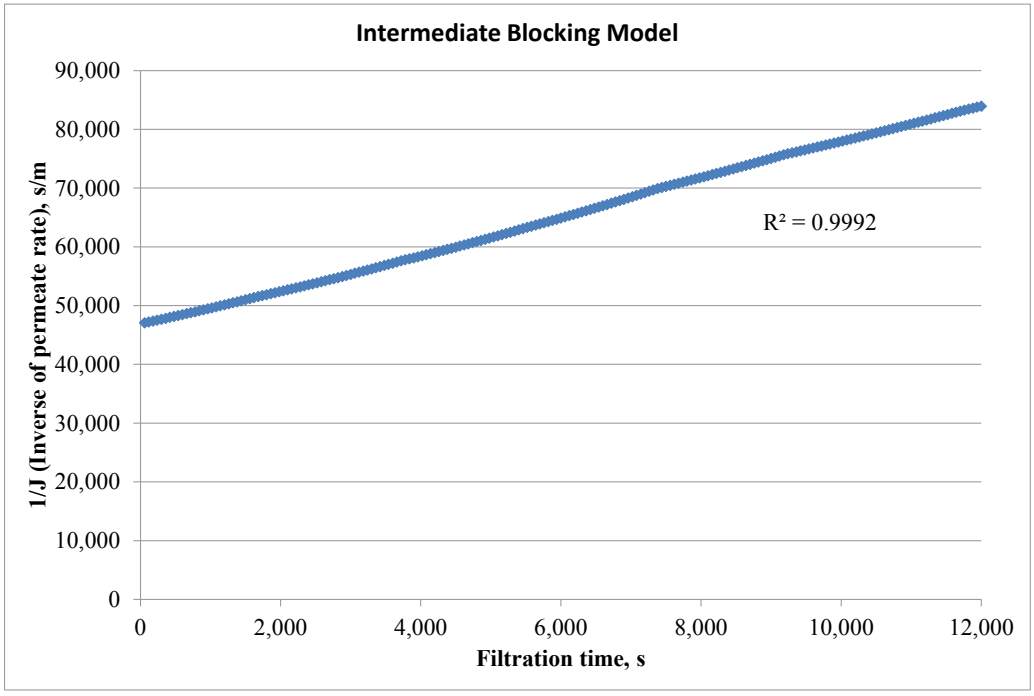

Figure 4.18: Intermediate block model for initial stage of fouling experiment

The correlation that best fits a linear fit is the potential blocking mechanism that is occurring during that time period. For the later stages (data from 200 minutes to 1,200 minutes) of the fouling experiment, the cake filtration has the highest R^2 values (0.9985) compared to intermediate and complete blocking plots. Figure 4.18 shows this later stage data range for the cake filtration law.

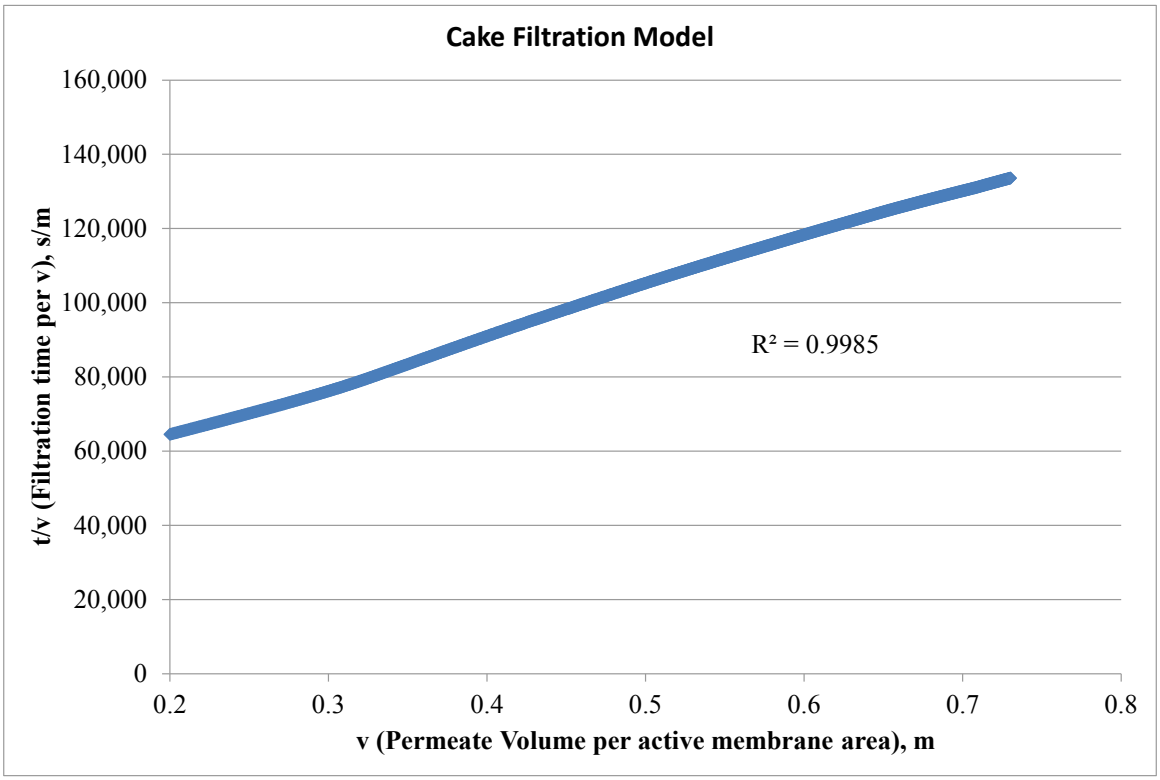

Figure 4.19: Cake filtration model for later stage of fouling experiment

Therefore, for our fouling experiment, intermediate blocking is initially occurring and this is followed by cake filtration.

4.4.2 Development of a New Roughness Resistance Parameter

As mentioned in Chapter 1, to capture the wettability effects (i.e. surface roughness influence) of the membrane during the filtration process, a third resistance term labelled R_r (Roughness resistance) is proposed to be included in the conventional filtration theory. The denominator in Equation 3 presented earlier in this study would become $1/(R_m + JIt + R_r)$. Thus proposed modified form of the conventional filtration theory is presented Equation 13.

The modelling of the effect of surface roughness begins with first determining the total resistance R_{tot} using the fouling data and using Equation 19. Here R_{tot} is the equal to the sum of the resistances (R_m + JIt + R_r). Here R_m is a constant value and JIt and R_r change over time.

$$J = \frac{Q}{A} = \frac{\Delta P}{\mu R_{tot}} \quad (19)$$

Where is J=permeate rate.

At every time step during the fouling experiment, the permeate rate (J) and the TMP is known. Therefore we can determine the total resistance (R_{tot}) at each time step. In order to determine R_r at each time step, we need to determine the cake resistivity, I, and then calculated the JIt term. The cake resistivity is determined from the cake filtration model plot presented in Figure 4.19. The determined cake resistivity, I, is a single constant value for this experiment. Here the slope of this plot is related to the cake resistivity and Equation 20 shows this relationship.

$$Slope = \frac{K_c}{2} = \frac{\mu I}{2\Delta P A^2} \quad (20)$$

Where K_c is the cake filtration constant and A is the membrane surface area.

At each time step we know the R_{tot}, JIt, and R_m. Thus it is possible to calculate R_r.

Figure 4.20 shows a plot of the instantaneous R_r value during the course of the fouling experiment.

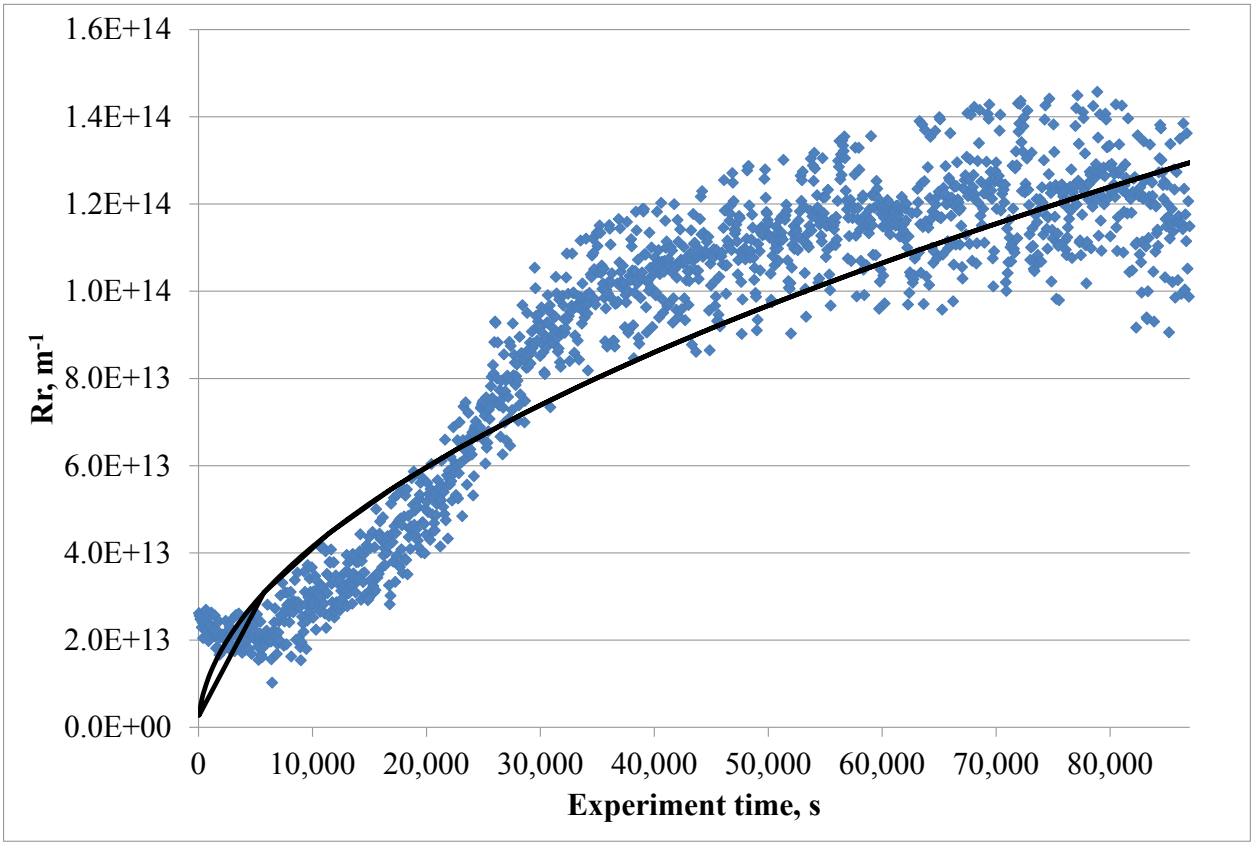

Figure 4.20: Instantaneous R_r values during the fouling experiment

A regression was done on the plot and the initial fit was based on the power law correlation. The next Figure 4.21 shows the instantaneous R_r at three different time periods (2, 8 and 24 hours) during the fouling experiment and the corresponding measured surface roughness at those time periods.

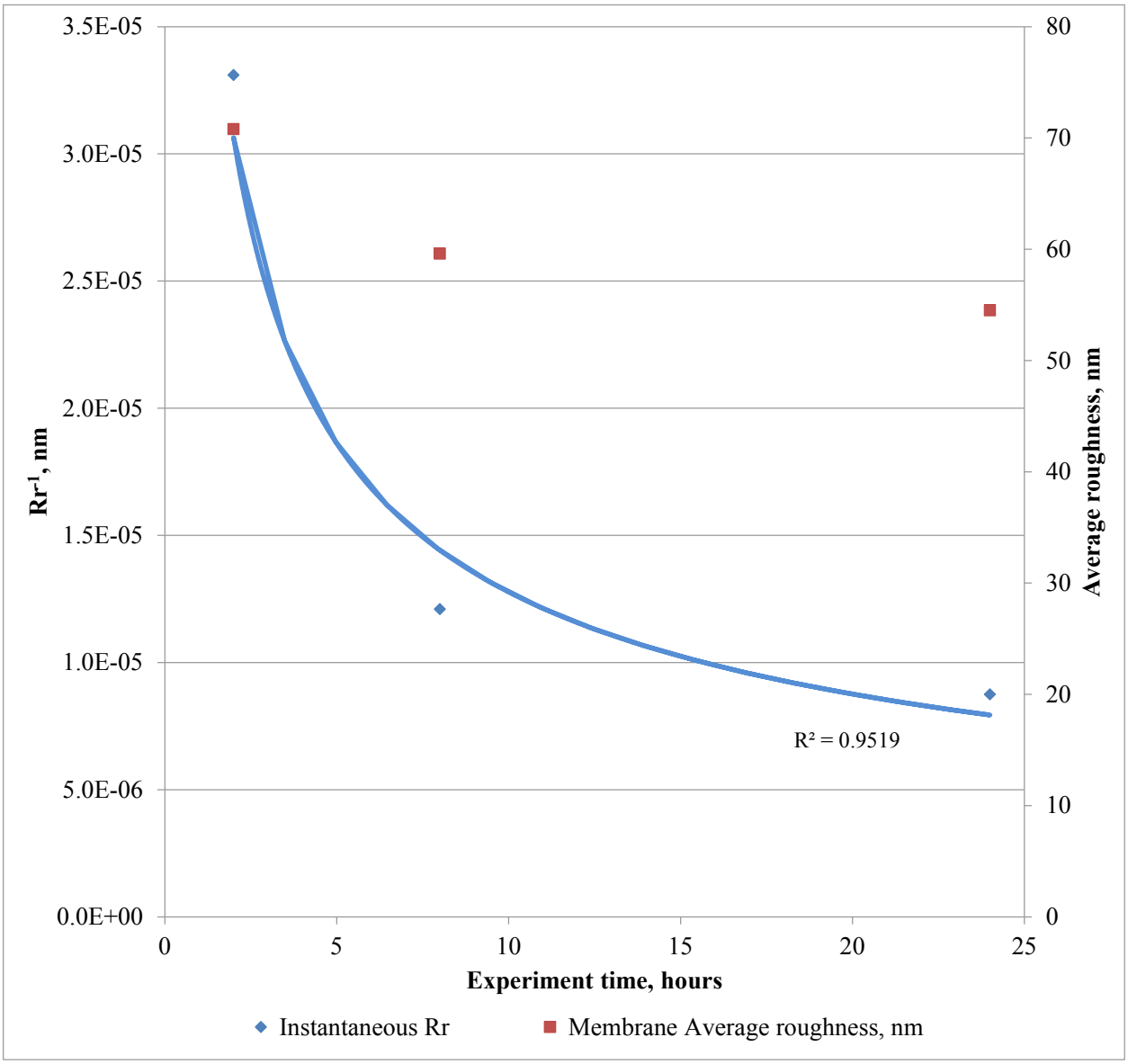

Figure 4.21: Change in Rr and membrane surface roughness during the fouling experiment

This Figure shows that the R_r values over the course of the experiment is again represented by the power law correlation. Here as the surface roughness value peaks at 2 hours and begins to fall during the fouling experiment, the roughness resistance (R_r) declines as well. Figure 4.22 compares the calculated instantaneous R_r and the calculated cake resistance (R_c = JIt) during the experiment.

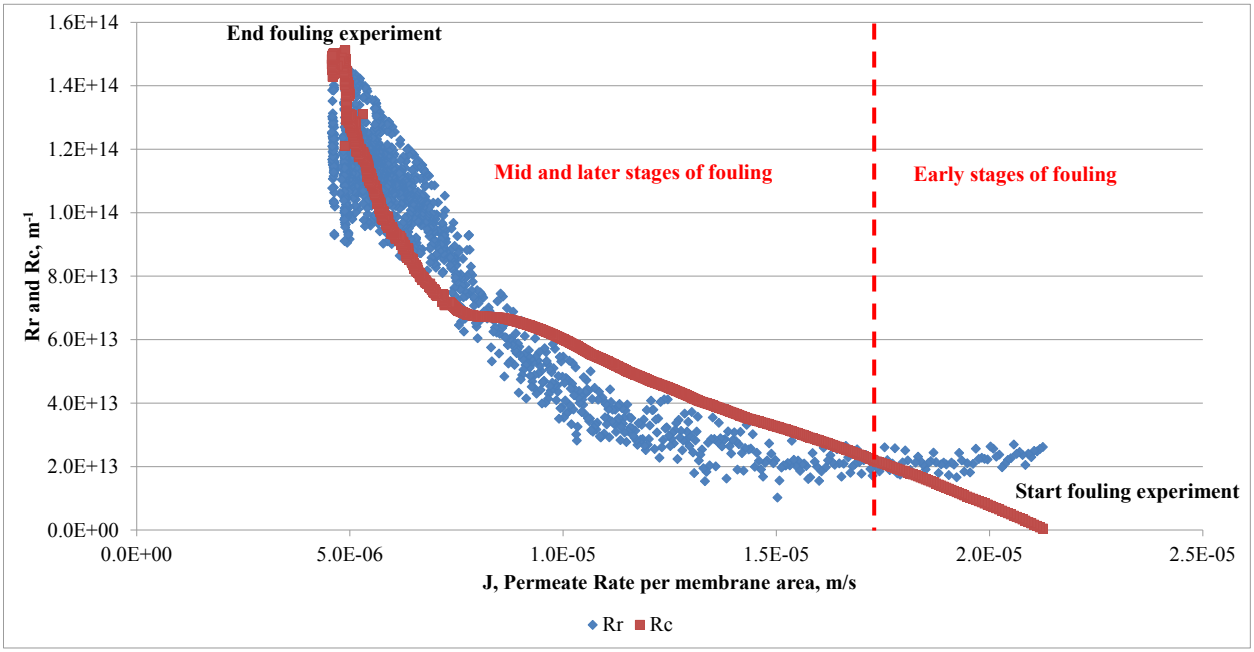

Figure 4.22: Calculated instantaneous R_r and R_c values during the experiment

The interesting observation from Figure 4.22 is that during the initial stages of the fouling experiment, the roughness resistance is more significant and as the experiment progress, the cake resistance starts to become a factor or as important as the roughness resistance.

The next step in attempting to model the roughness resistance is to find a way to relate roughness resistance to the initial surface roughness for all amide type membranes (#1, #2, #3, and #4). The previous roughness resistance data (Figure 4.19, Figure 4.20, Figure 4.21, and Figure 4.22) is for specifically membrane #1 which is an amide type membrane treating the standard process water feed (Table 2.1) under low TMP condition. The average R_r over the entire time period of the experiment can be determined for each low and high TMP experiments for the amide type membranes treating the same process water. Figure 4.23 relates the initial surface roughness to the average roughness resistance including both low and high TMP experiments for only amide type membranes.

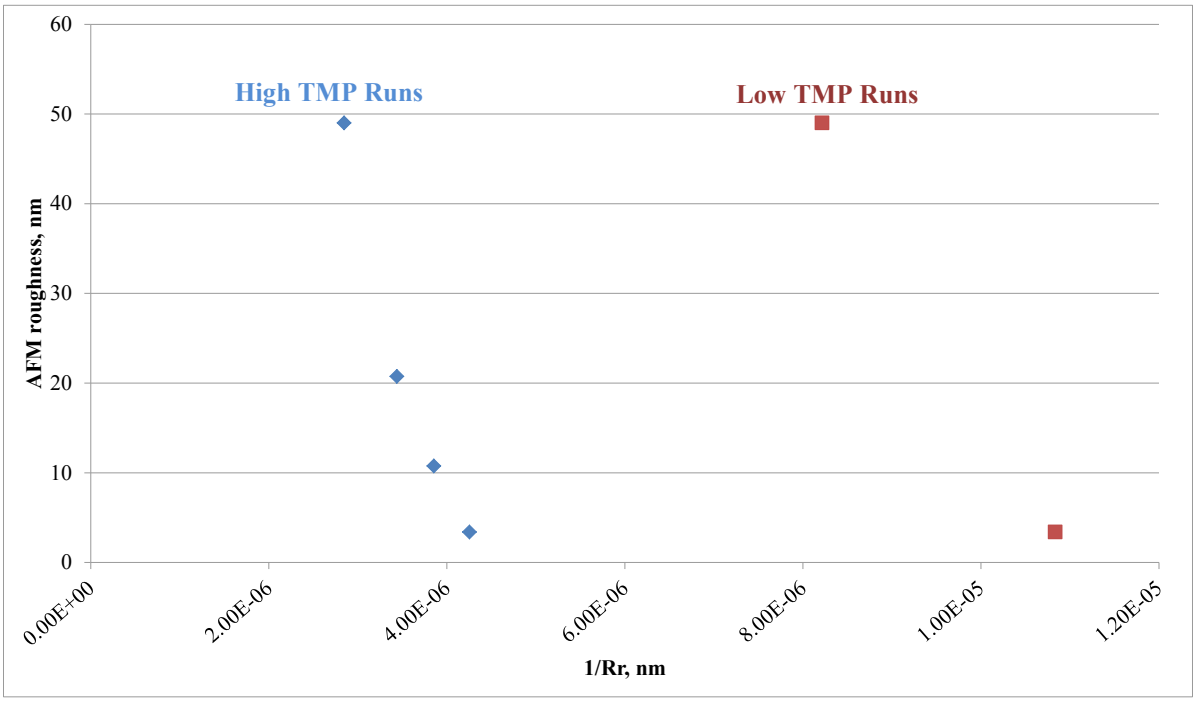

Figure 4.23: Initial membrane roughness and calculated average R_r^{-1} for low and high TMP

The low and high TMP datasets from Figure 4.23 is then normalized with the high R_r value under each TMP condition. This reason for doing this is to collapse the two TMP datasets for the amide type membranes into one general relationship relating initial surface roughness to an average R_r at any TMP condition. Figure 4.24 shows this general relationship for amide type membranes.

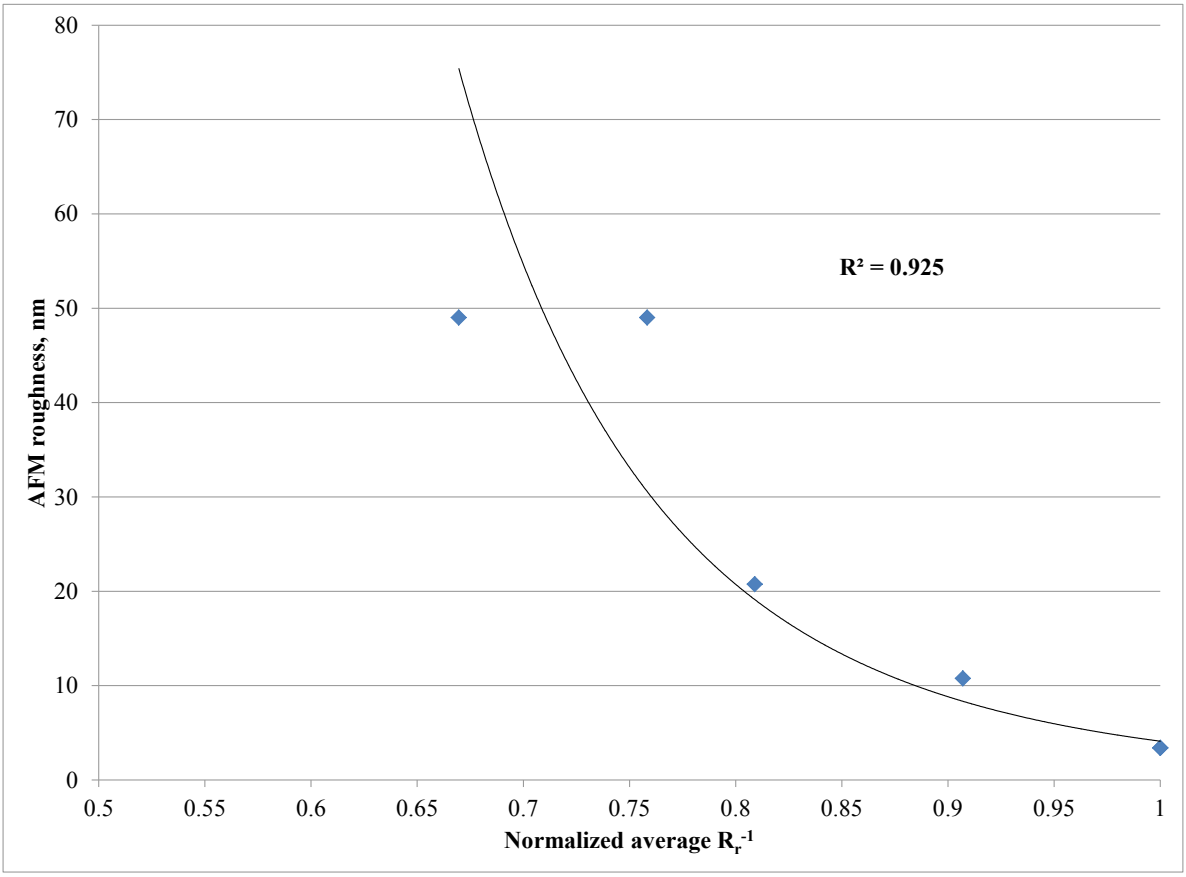

Figure 4.24: Correlation relating initial surface roughness to normalized average R_r

The results in Figure 4.24 are again initially represented by the power law correlation to relate initial surface roughness to a normalized average roughness resistance. The resulting correlation from this graph is shown in Equation 21.

$$R_r^{-1} = 3.62x10^{-5}\left(\frac{4.1076}{AFM\ roughness\ (nm)}\right)^{\frac{1}{7.255}} \text{ in nm} \qquad (21)$$

The calculation of an average R_r using the experimentally determined Equation 21 can then be used in the proposed modified form (Equation 13) of the conventional filtration theory.

4.4.3 Comparison of Roughness Resistance Model to Other Models

This next section tests and compares the predictive behavior of the new modified form of the conventional filtration theory using Equation 13 and Equation 21 to other correlations and models. This new model is called the roughness resistance model (R_r). To also compare the validity of the R_r model, a combined fouling model presented in the study by Rezaei et al. (2011) is also used to predict the fouling behavior. In this combined model, the intermediate blocking and cake filtration mechanisms are incorporated into a single equation to better predict the permeate volume and rate. Equation 22 shows this combined model.

$$V = \frac{1}{K_i} ln\left(1 + \frac{K_i}{K_c J_o}\left(\sqrt{1 + 2K_c J_o^2 t} - 1\right)\right) \qquad (22)$$

Where V is the total permeate volume accumulated at time t.

Figure 4.25 shows the fouling experimental data using membrane #1 at low TMP conditions and the predicted fouling behavior using the conventional filtration theory, the combined model, and the R_r model. Figure 4.26 shows the validation of the observed permeate rate and the predicted permeate rate using the R_r model.

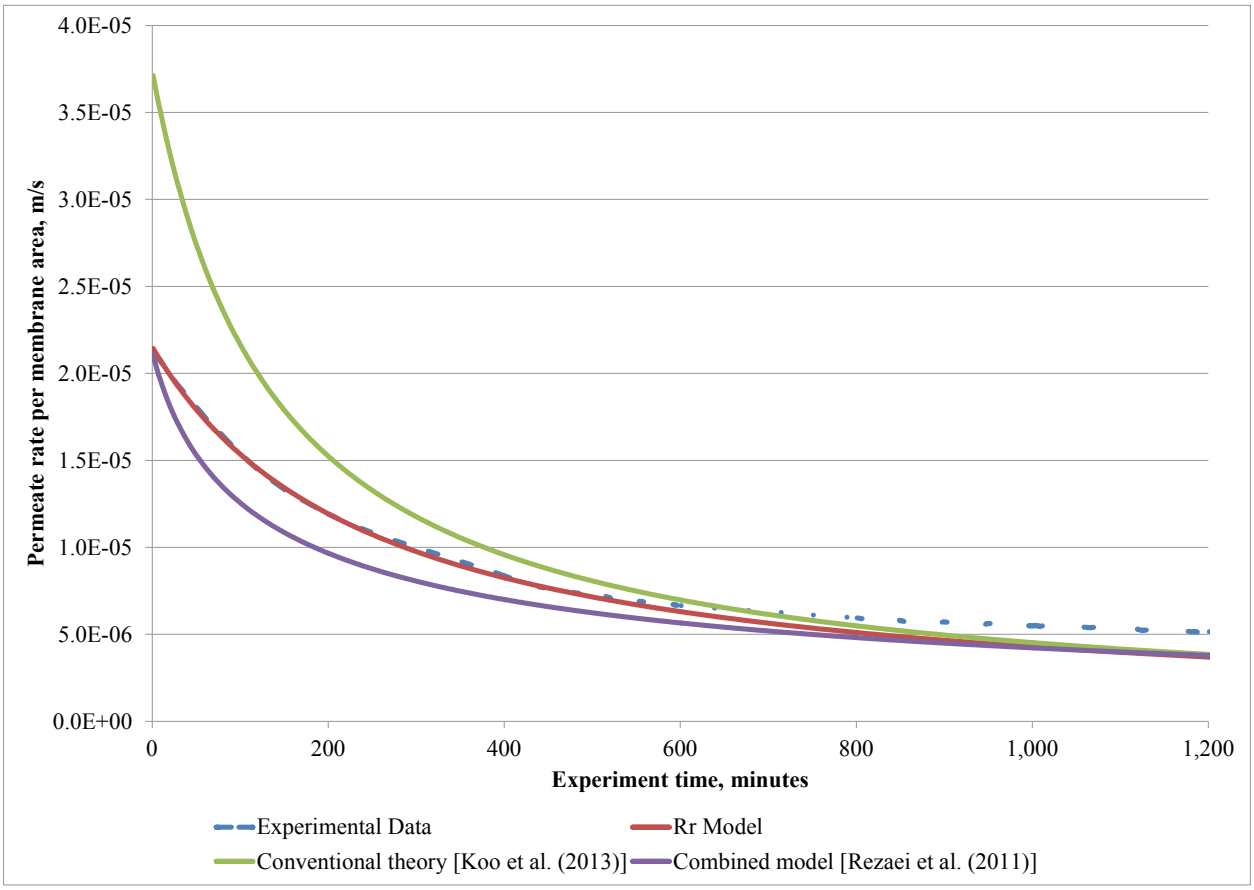

Figure 4.25: Experimental fouling data and predicted fouling data by R_r model at low TMP condition

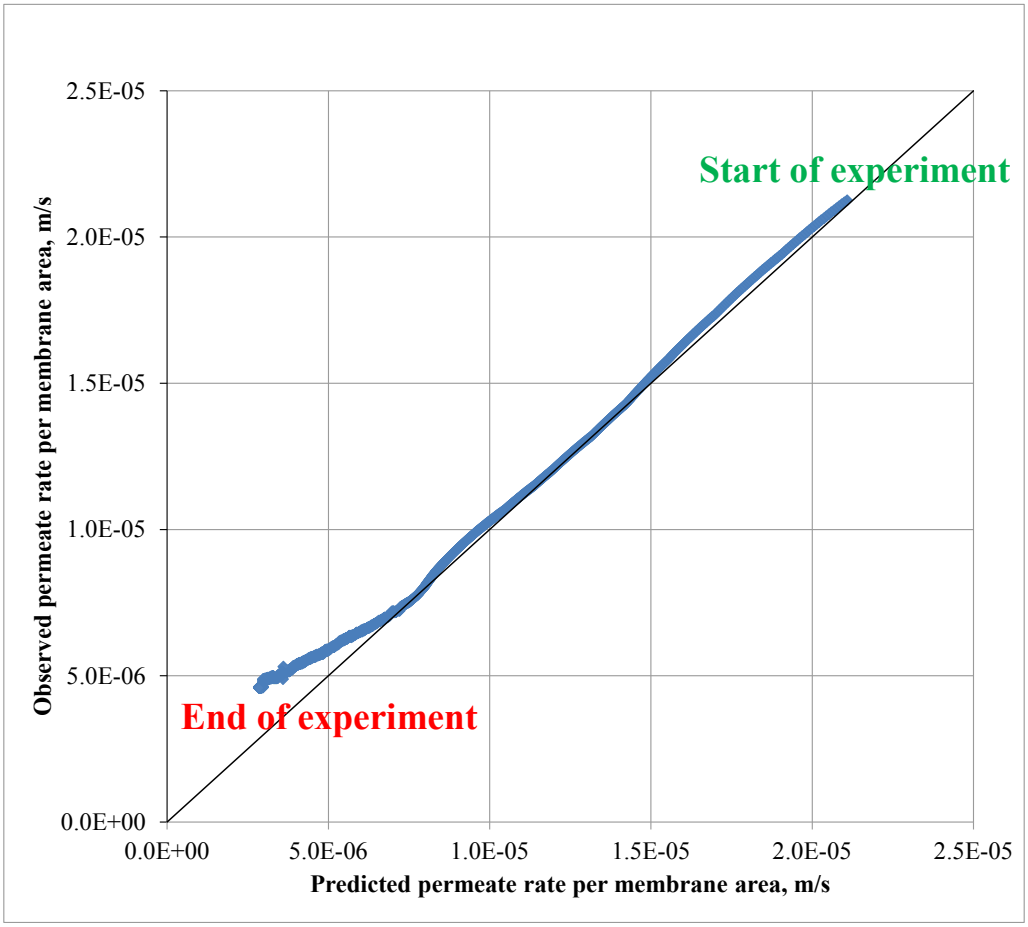

Figure 4.26: Validation of the observed permeate rate and the predicted rate by the R_r model

The results show that the conventional filtration theory does not adequately predict the fouling behavior of our system. This is probably due to the fact that this conventional theory was originally developed for filtration of hard spherical particles or foulant. The combined model predicted the experiment results better than the conventional theory but during the initial stages, the predicted permeate rate was lower than observed in the experiment. The R_r model predicted better the initial stages of the fouling experiment compared to the combined model and did an adequate job in predicting the later stages. The impression of the R_r model is that it is an improvement to the conventional theory and the combined model under the low TMP condition.

The improvement is noticed the most during the initial stages of the experiment where possibly the roughness plays an initial important role. So how do the models perform under high TMP conditions? Figure 4.27 shows the fouling experimental data using membrane #1 at high TMP conditions and the predicted fouling behavior using the conventional filtration theory, the combined model, and the R_r model.

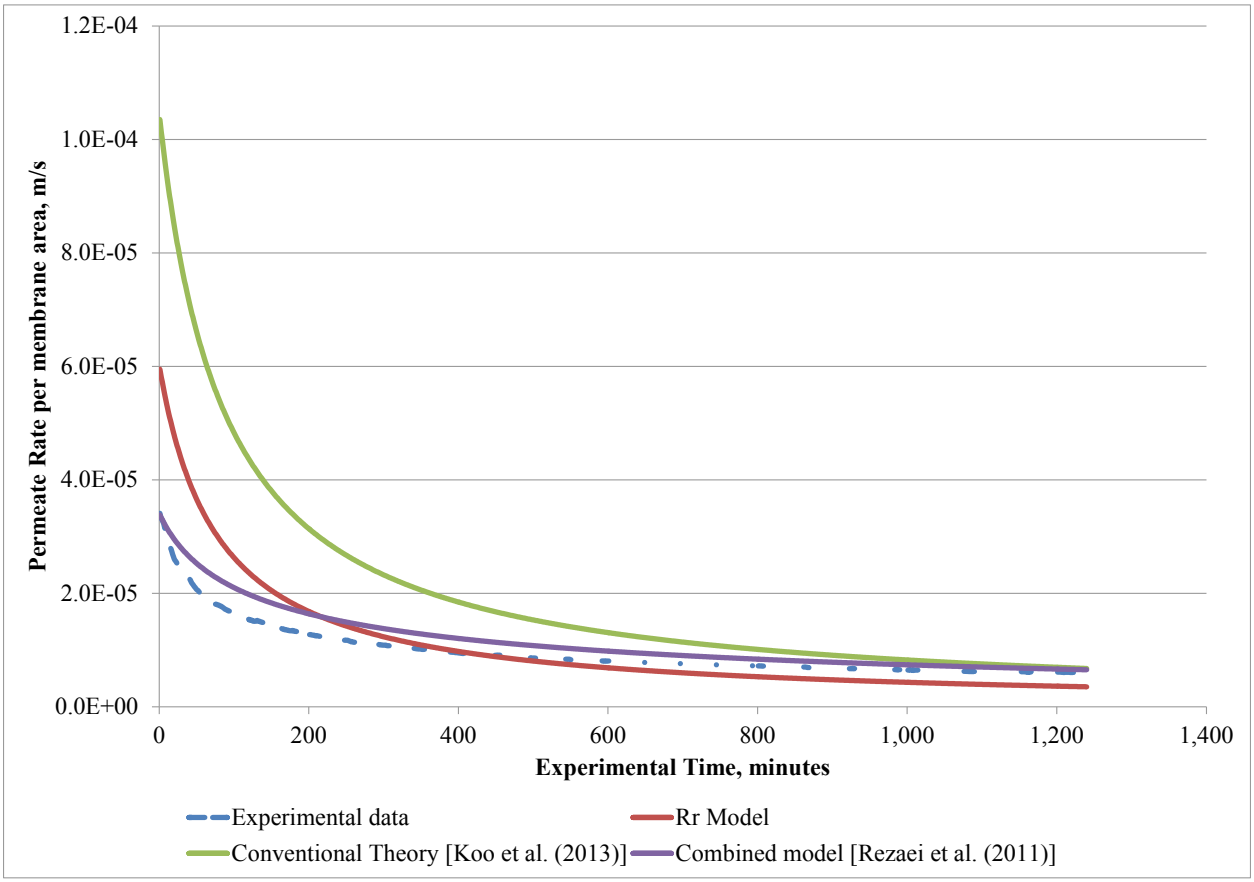

Figure 4.27: Experimental fouling data and predicted fouling data by R_r model at high TMP condition

Predicting the high TMP fouling data is again poor for the conventional filtration theory. As for the combined model, it did a better job predicting initially the fouling compared to the R_r model.

The R_r model did a good job predicting the later stages of fouling experiment. A potential reason for the R_r model to not predict the initial stages of the fouling experiment well is that methodology to generalize the average R_r values for both high and low TMP is not quite effective to cover the range of conditions. Perhaps there needs to be two versions of the R_r model to capture fouling effects are low and high TMP conditions. Also another option, the R_r model may need another variable to capture the TMP condition to better predict a wider range of experimental conditions.

After going through the modelling process of the fouling data and developing a new predictive model, it is credible that the membrane surface roughness plays an important role in membrane fouling. However, this is just an initial attempt at modelling the effect of membrane roughness during fouling process. It is anticipated that further develop on this idea of roughness resistance be explored in subsequent studies.

4.4.4 NF Membrane Performance

The degree of membrane fouling or performance can give insight into how membranes behave and perform during commercial operations. Iritani et al. (2016) presented a series of equations to evaluate the performance of membrane during the fouling process based on the theoretical background of the blocking laws.

For intermediate blocking and cake filtration, the theoretical filtration rate becomes zero at infinite time. Therefore, we define V_y as the permeate volume when the initial permeate rate

decreases by y percent. Equation 23 and Equation 24 is used to evaluate the performance for intermediate blocking and cake filtration mechanism respectively.

$$V_y = \frac{ln\left(\frac{y}{100}\right)}{K_i} \quad (23)$$

Where K_i=intermediate blocking coefficient.

$$V_y = \frac{100-y}{yK_cJ_o} \quad (24)$$

Where K_c=cake filtration coefficient.

Table 4.12 summaries the performance of all low TMP experiments described in section 4.3.2 for membranes #1, #3, #5, and #5 with the standard synthetic water feed composition (Table 2.1).

Table 4.12: Summary of performance for low TMP experiments

Membrane #	Feed water condition	Filtration Models		Performance of NF membrane		
		Initial stage: Intermediate blocking constant, K_i, m^{-1}	Later stage: Cake Filtration constant, K_c, s/m^2	Based on initial permeate flux declining to 90% signifying the membrane has reached it's capacity		
				Vy, m^3 permeate/m^2 of membrane area	Total mass of permeate at membrane capacity, kg	% of permeate mass @ 20 hr filtration time
1	DI water, NaCl, humic acid	3.17	2.76E+06	1.89E-02	4,453	6.0
1	RO water and humic acid (no salt added)	2.24	1.13E+05	4.50E-02	10,588	3.4
1	DI water, NaCl, humic acid, 1% Emulsified oil	26.74	2.98E+06	1.82E-03	427	13.3
3	DI water, NaCl, humic acid	3.56	3.59E+05	1.49E-02	3,498	6.9
5	DI water, NaCl, humic acid	2.51	1.88E+05	2.78E-02	6,549	4.6
6	DI water, NaCl, humic acid	2.50	2.03E+05	2.49E-02	5,864	5.1

The intermediate and cake filtration constants are determined from the experiment data and using the appropriate equation presented Chapter 1. The results from Table 4.12 show that membrane #1 with a feed water contain little to no NaCl in it has the best performance in terms of having the highest mass of permeate (10,588 kg) before the membrane reaches it 90% capacity. This means that membrane #1 at this water feed condition can filter out 10,588 kg of permeate water before the permeate flux reaches 10% of the original starting value. Also for this case, at 20 hours of filtration time, only 3.4% of the total capacity (10,588 kg) has been reached at this time. When emulsified oil is present in the water, the same membrane #1 can only filter out 427 kg of permeate water before the permeate flux rate reached 10% of the original starting value.

5.0 CONCLUSIONS AND RECOMMENDATIONS

5.1 SUMMARY OF CONCLUSIONS

In this study, six NF polymeric membranes were investigated using a cross flow filtration setup for the treatment of SAGD-PW. Characterization of the membrane surface properties was done before and after the filtration experiment to observe changes in the surface properties. The effect of membrane surface properties during the fouling process was studied. Synthetic feed water was generated to mimic certain components of SAGD-PW and to target the effect of mainly dissolved organics present in the water. The fouling data was analyzed and a new roughness resistance model was developed to represent the effect of membrane surface roughness during the filtration process. The following conclusions are draw from this study:

- NF membrane are capable of removing high amounts of dissolved organics from process water (>90%). The main mechanisms of removing dissolved organics are size and charge exclusion. For our fouling experiments, the blocking mechanism during the initial stages of fouling is due to intermediate blocking where foulant larger than the membrane pores. During the later stages of fouling, the main mechanism of fouling is due to cake filtration where layers upon layers of foulant form on top of each other. As the thickness increases the filtration efficiency diminishes.
- Both membrane initial surface roughness and the membrane material composition play a role in overall performance and fouling behavior.
- The feed composition also plays a role in the fouling of membranes.
    - Addition of NaCl in the feed water tends to promote earlier onset of fouling.

- The presences of emulsified oil droplets (dispersed organics) in the feedwater fouls the membrane almost immediately and greatly reduces the permeate flowrate. The result means less process water being treated.

- The R_r model is an improvement over the conventional filtration theory model and the combined blocking model at low TMP conditions. However, at higher TMP conditions, the R_r model tends to initially over predict the permeate flowrate but follows the experimental data in the later stages. There still needs to be improvements to the R_r model and more validation are needed. However, based on the data, it is conceivable that the membrane surface roughness plays an important role in membrane fouling.
- The work from this thesis can help the development or improvement of existing NF membranes for treating SAGD-PW. In this work, we observed the changes in membrane surface properties during the fouling experiments and the permeate flux decline. The membrane surface properties and foulant present in the water can affect the performance of these NF membranes. Understanding the permeate flux decline is useful for commercial operators to determine the frequency of replacing or cleaning the membranes for continued water treatment.

5.2 RECOMMENDATIONS AND FUTURE WORKS

The following are the recommendations and proposed future works:

- In our present study, the synthetic water used was an idealized case to specifically target the impact of dissolved organics during the fouling process. It is recommended that future studies add more complexities to the feed water composition and eventually using real SAGD-PW samples to evaluate performance and fouling characteristics. By gradually adding more components to the feed water, individual and combined mechanisms can be

better identified as the impact on fouling. A step by step approach may unlock new ways to make membranes more fouling resistance and make membrane filtration technology a viable option to treat SAGD-PW.

- The interactions of membrane surface to foulant and foulant to foulant in the presence of SAGD-PW is another topic for future studies. This topic can provide more insight into these interactions that can effect fouling. The Atomic force microscopy (AFM) can be used to measure these extremely sensitive and important interactions. This information can be used to support past conclusions on the mechanism of organic fouling and also may provide insight into possibly new mechanisms.
- The use of flat sheet membranes in a cross flow filtration setup is a good way to investigate fouling mechanism and changes in membrane surface properties. To scale up the membrane filtration process and bring the technology closer to pilot scale testing, it is recommended that subsequent studies should integrate spiral wound membrane elements into their lab testing facility. These membrane modules have larger membrane active areas and are of similar construction and design to commercial application. This will allow for better understanding of the performance and membrane fouling capacity on a larger scale.
- It is recommended that futures studies further develop the concept of a roughness resistance and further validate and improve the roughness resistance (R_r) model developed in this study. This current model has potential limitations in predicting fouling in a wide range of TMP conditions. More data is also need to refine the model and make it more universal. Also, since this model was developed using only amide type

membranes, there could be limitation for use in cases where the NF membrane is non-amide.

BIBLIOGRAPHY

1. "TriSEP corporation: technical manual", TripSEP – The specialty membrane company, Revision B, Oct 17, 2016.
2. Allen, E.W., "Process water treatment in Canada's oil sands industry: II. A review of emerging technologies", Journal of environmental engineering & science, 7, Pages 499 – 524, 2008.
3. Baker, R.W., "Membrane technology and applications, John Wiley & Sons, 2012.
4. Boussu, A., Belpaire, A., Volodin, A., Van Haesendonck, C., Van der Meeren, P., Vandecasteele, C., and Van der Bruggen, B., "Influence of membrane and colloid characteristics on fouling of nanofiltration membranes", Journal of membrane science, 289 (1-2), 2007.
5. Chang, E.E., Chang, Y.C., Liang, C.H., Huang, C.P., and Chiang, P.C., "Identifying the rejection mechanism for nanofiltration membranes fouled by humic acid and calcium ions exemplified by acetaminophen, sulfamethoxazole, and triclosan", Journal of hazardous materials, 221-222, Pages 19-27, 2011.
6. Chin, Y.P., Aiken, G., and O'loughlin, E., "Molecular weight, polydispersity, and spectroscopic properties of aquatic humic substances", Environmental science and technology, 28, Pages 1853-1858, 1994.
7. Clifford, D.A., "Ion exchange and inorganic adsorption", In letterman RD (ed.), Water quality and treatment, McGraw-Hill, 1999.
8. D.K. Pingale, "Role of weak acid cation resin in water treatment", Chemical weekly – Bombay, 50, Pages 201-208, 2005.

9. Daniel, A.J., Langhus, B.G., and Patel, C., “Technical summary of oil & gas produced water treatment technologies”, NETL, 2005.
10. Elimelech, M., Chen, W.H., and Waypa, J.J., “Measuring the zeta potential of reverse osmosis membranes by a streaming potential analyzer”, Desalination, 95, Pages 263-286, 1994.
11. Elsayed, N.A., Barrufet, M.A., and El-Halwagi, M.M., “An integrated approach for incorporating thermal membrane distillation in treating water in heavy oil recovery using SAGD”, Journal of unconventional oil and gas resources, 12, Pages 6 – 14, 2015.
12. Hartland, S., “Surface and interfacial tension: measurement, theory, and applications”, New York; Basel: Marcel Dekker, 2004.
13. Hayatbakhsh, M., Sadrzadeh, M., Hajinasiri, J., Pernitsky, D. and Bhattacharjee, S.,”Treatment of an in situ oil sands produced water by polymeric membranes”, Desalination and water treatment, 57, Pages 14869-14887, 2016.
14. Hermans, P.H. and Bredee, H.L., “Principles of the mathematic treatment of constant pressure filtration”, Journal of the society of chemical industry, 55T, Pages 1-4, 1936.
15. Hermia, J., “Constant pressure blocking filtration laws – application to power law non-Newtonian fluids”, Transaction of the institution of chemical engineers, 60, Pages 183-187, 1982.
16. Hoek, E.M.V. and Tarabara, V.V., “Encyclopedia of membrane science and technology” Wiley, Volume 3, Pages 2219-2228, 2013.
17. Igunnu, E.T. and Chen, G.Z., “Produced water treatment technologies”, International journal of low carbon technologies, 9, Pages 157-177, 2014.

18. Iritani, E. and Katagiri, N., “Developments of blocking filtration model in membrane filtration”, Kona Powder and Particle Journal, No. 33, Pages 179-202, 2016.
19. Jacobasch, H. and Schurz, J., “Characterization of polymer surfaces by means of electrokinetic measurements”, Progress in Colloids & Polymer Science, 77, Pages 40-48, 1988.
20. Johnson, G., Pradanos, P., and Hernandez, A., “Fouling phenomena in microporous membranes: Flux decline kinetics and structural modification”, Journal of membrane science, 112, Pages 171-183, 1996.
21. Juang, R.S., Lin, S.H., and Peng, L.C., “Flux decline analysis in micellar enhanced ultrafiltration of synthetic waste solutions for metal removal”, Chemical engineering journal, 161, Pages 19-26, 2010.
22. Karanfil, T., Schlautman, M.A., Kilduff, J.E., and Weber, W.J., “Adsorption of organic macromolecules by granular activated carbon: influence of molecular properties under anoxix solution conditions”, Environmental science and technology, 30, Pages 2187-2194, 1996.
23. Kauppinen, J.K., Moffatt, D.J., Mantsch, H.H., and Cameron, D.G., “Fourier self deconvolution – a method for resolving intrinsically overlapped bands”, Appl. Spectroscopy, 35, Pages 271-276, 1981.
24. Keskinler, B., Yildiz, E., Erhan, E., Dogru, M., Bayhan, Y.K., and Akay, G., “Crossflow microfiltration of low concentration nonliving yeast suspensions”, Journal of membrane science, 233, Pages 59-69, 2004.
25. Khorshidi, B., Bhinder, A., Thundat, T., Pernitsky, D., and Sadrzadeh, M., “Developing high throughput thin film composite polyamide membranes for forward osmosis

treatment of SAGD produced water", Journal of membrane science, 511, Pages 29-39, 2016.

26. Koo, C.H., Mohammad, A.W., Suja, F., and Meor Talib, M.Z.,"Setting up of modified fouling index (MFI) and crossflow sampler modified fouling index (CFS-MFI) measurement devices for NF/RO fouling", Journal of Membrane Science, 435, Pages 165-175, 2013.
27. Lin, T., Lu, Z., and Chen, W.,"Interaction mechanisms and predictions on membrane fouling in an ultrafiltration system, using the XDLVO approach", Journal of Membrane Science, 461, Pages 49-58, 2014.
28. Lokare, O.R., Tavakkoli, S., Khanna, V., Vidic, R.D., and Wadekar, S., "Fouling in direct contact membrane distillation of produced water from unconventional gas extraction", Journal of membrane science, 524, Pages 493 – 501, 2017.
29. Low, Z.X., Wang, Z., Leong, S., Razmjou, A., Dumee, L.F., Zhang, X., and Wang, H.,"Enhancement of the antifouling properties and filtration performance of polyethersulfone ultrafiltration membranes by incorporation of nanoporous titania nanoparticles", American Chemical Society, Industrial & Engineering Chemistry Research, 54, Pages 11188-11198, 2015.
30. Malmali, M., Fyfe, P., Lincicome, D., Sardari, K., and Wickramasinghe, S.R., "Selecting membranes for treating hydraulic fracturing produced waters by membrane distillation", Separation science and technology, Vol. 52, No.2, Pages 266 – 275, 2017.
31. Marcus, Y., "Ionic radii in aqueous solutions", Journal of solution chemistry, Vol. 12, No. 4, Pages 271-275, 1983.

32. Maruf, S.H., Wang, L., Greenberg, A.R., Pellegrino, J., and Ding, Y.,"Use of nanoimprinted surface patterns to mitigate colloidal deposition on ultrafiltration membranes", Journal of Membrane Science, 428, Pages 598-607, 2013.
33. Masliyah, J., Zhou, J., Xu, Z.,Czarnecki, J, and Hamza, H.,"Understanding water based extraction from Athabasca oil sands", Canadian Journal of Chemical Engineering, 82, Pages 628-654, 2004.
34. Mondal, S. and Wickramasinghe, S.R., "Produced water treatment by nanofiltration and reverse osmosis membranes", Journal of membrane science, 322, Pages 162-170, 2008.
35. Murase, T. and Ohn, T., "New decline pattern of filtrate flux in cross flow microfiltration of dilute suspension, AIChE Journal, 42, Pages 1938-1944, 1996.
36. Nghiem, L.D., Coleman, P.J., and Espendiller, C., "Mechanisms underlying the effects of membrane fouling on the nanofiltration of trace organic contaminants", Desalination, 250, Pages 682-687, 2010.
37. Ozdemir, B., Saatci, A., and Yenigun, O., "Evaluation of cake filtration biological reactors (CFBR) vs. membrane biological reactor (MBR) in a pilot scale plant", Desalination, 288, Pages 135-144, 2012.
38. Perez Estrada, L., Martin, J., El-Din, M.G., Zubot, W., and Martin, J.W.,"Naphthenic acids speciation and removal during petroleum coke adsorption and ozonation of oil sands process affected water", Sci. Total Environment, 409, Pages 5119-5125, 2011.
39. R. Singh, "Hybrid membrane systems for water purification: technology, system design and operations", ebook, Elsevier Science, 2006

40. Razi, M., Thundatt, T., Waghmare, P.R., Sinha, S., and Das, S., "Effect of steam-assisted gravity drainage produced water properties on oil/water transient interfacial tension", Energy & Fuels, 30, Pages 10714-10720, 2016.
41. Rezaei, H., Ashtiani, F.Z., and Fouladitajar, A., "Effects of operating parameters on fouling mechanism and membrane flux in cross flow microfiltration of whey", Desalination, 274, Pages 262-271, 2011.
42. Ruth, B.F., "Correlating filtration theory with industrial practice", Industrial & engineering chemistry, 38, Pages 564-571, 1946.
43. Ruth, B.F., "Studies in filtration: III. Derivation of general filtration equations", Industrial & engineering chemistry, 27, Pages 708-723, 1935.
44. Sadrzadeh, M., Hajinasiri, J., Bhattacharjee, S. and Pernitsky, D.,"Nanofiltration of oil sands boiler feed water: Effect of pH on water flux and organic and dissolved solid rejection", Separation and Purification Technology, 141, Pages 339-353, 2015.
45. Schafer, A.I., "Natural organics removal using membranes – principles, performance, and cost", Technomic publishing company, 2001.
46. Souhaimi, M.K. and Matsuura, T., "Membrane distillation: principles and applications", ebook, Elsevier, 2011.
47. Strathmann, H., "Ion exchange membrane separation processes, Elsevier, Amsterdam, Page 166, 2004.
48. Swenson, P., Tanchuk, B., Bastida, E., An, W., and Kuznicki, S.M., "Water desalination and de-oiling with natural zeolite membranes – Potential application for purification of SAGD process water", Desalination, 286, Pages 442 – 446, 2012.

49. Tanaka, T., Ogawa, H., and Nagao, S., “Attenuated total reflection fourier transform infrared (ATR-FTIR) spectroscopy of functional groups of humic acid dissolving in aqueous solution”, Analytical sciences, Vol. 17, Pages 1081-1084, 2001.
50. Thakurta, S.G., Bhattacharjee, S., Maiti, A., and Pernitsky, D.J., “Dissolved organic matter in steam assisted gravity drainage boiler blow-down water”, Energy & fuels, 27, Pages 3883 – 3890, 2013.
51. Thakurta, S.G., Maiti, A., Pernitsky, D., and Bhattacharjee, S.,”Dissolved organic matter in steam assisted gravity drainage boiler blow down water”, Energy Fuels, 27, Pages 3883-3890, 2013.
52. Wang, S., Axcell, E., Bosch, R., and Little, V.,”Effects of chemical application on antifouling in steam assisted gravity drainage operations, Energy Fuels, 19, Pages 1425-1429, 2005.
53. Xiao K., Wang, X., Huang, X., Waite, T.D., and Wen, X.,”Combined effect of membrane and foulant hydrophobicity and surface charge on adsorptive fouling during microfiltration”, Journal of Membrane Science, 373, Pages 140-151, 2011.
54. Zioui, D., Tigrine, Z., Aburideh, H., Hout, S., Abbas, M., and Merzouk, N.K.,”Membrane Technology for water treatment applications”, International Journal of Chemical and Environmental Engineering, Volume 6, No.3, June 2015.

APPENDIX A: MEMBRANE CHARACTERIZATION

The following figures are 2D and 3D AFM images of the roughness profile for membranes #2 to #6:

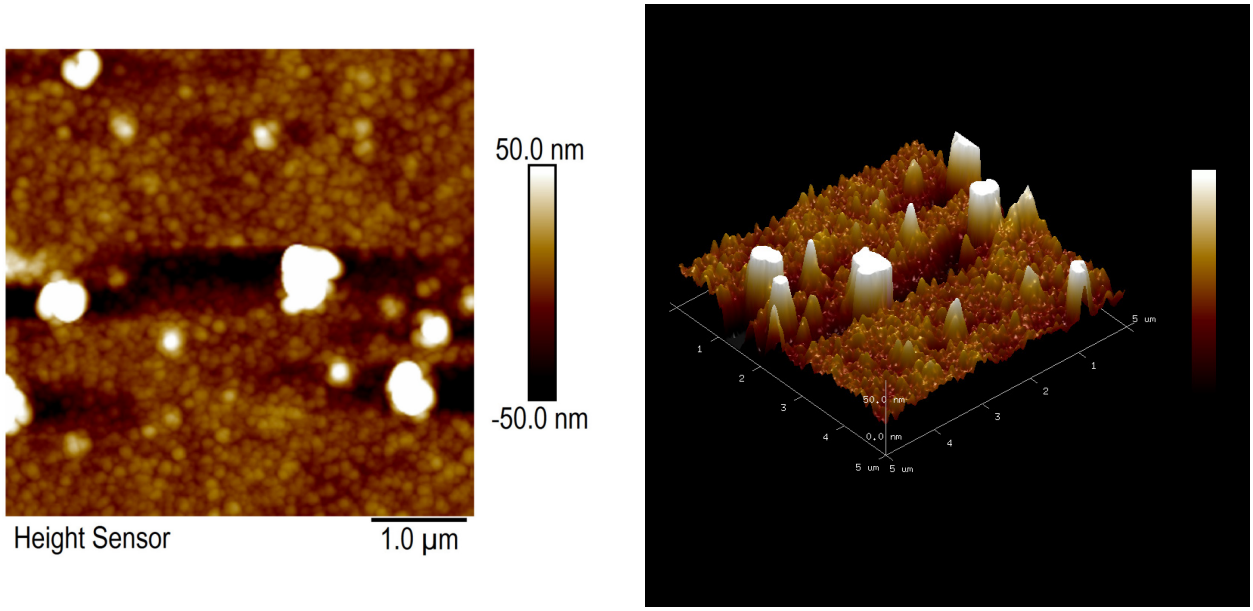

Figure A1: 2D and 3D AFM image of the roughness for membrane #2

The AFM images on Figure A1 shows a number of isolated peaks on the membrane surface which could be the coatings or different molecules that have been grafted onto the membrane surface to give certain surface attributes. The large peaks are surrounded by a smoother membrane surface.

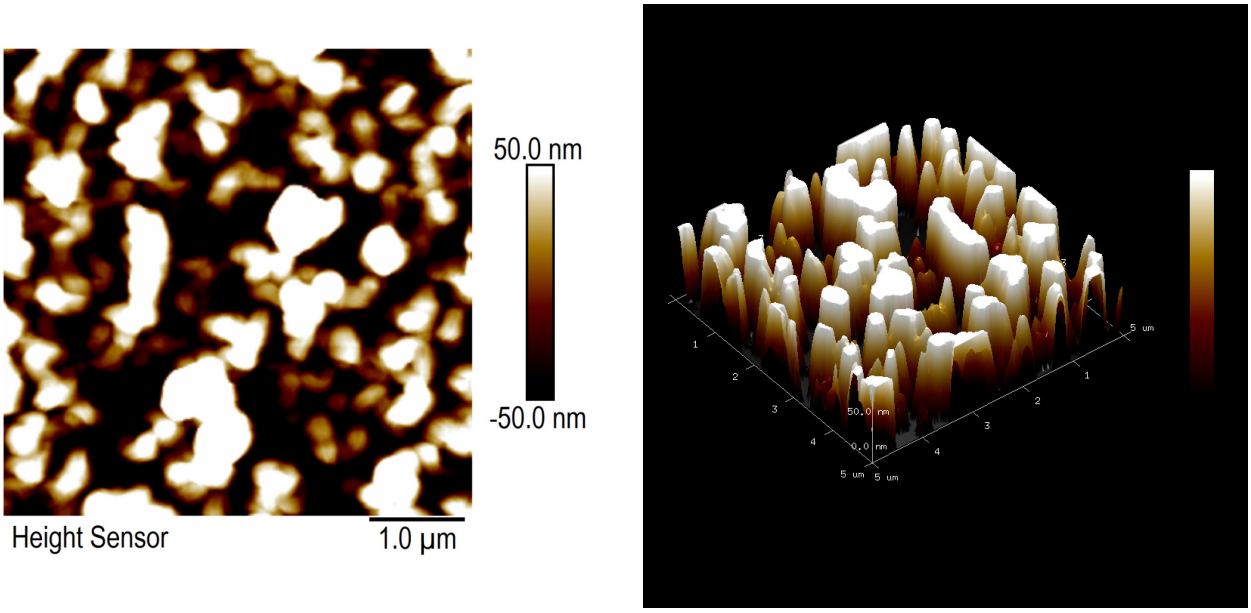

Figure A2: 2D and 3D AFM image of the roughness for membrane #3

In Figure A2, for membrane #3 it shows a much larger number of peaks on the membrane surface which could again be the coatings applied by the manufacturer and is different between each membrane.

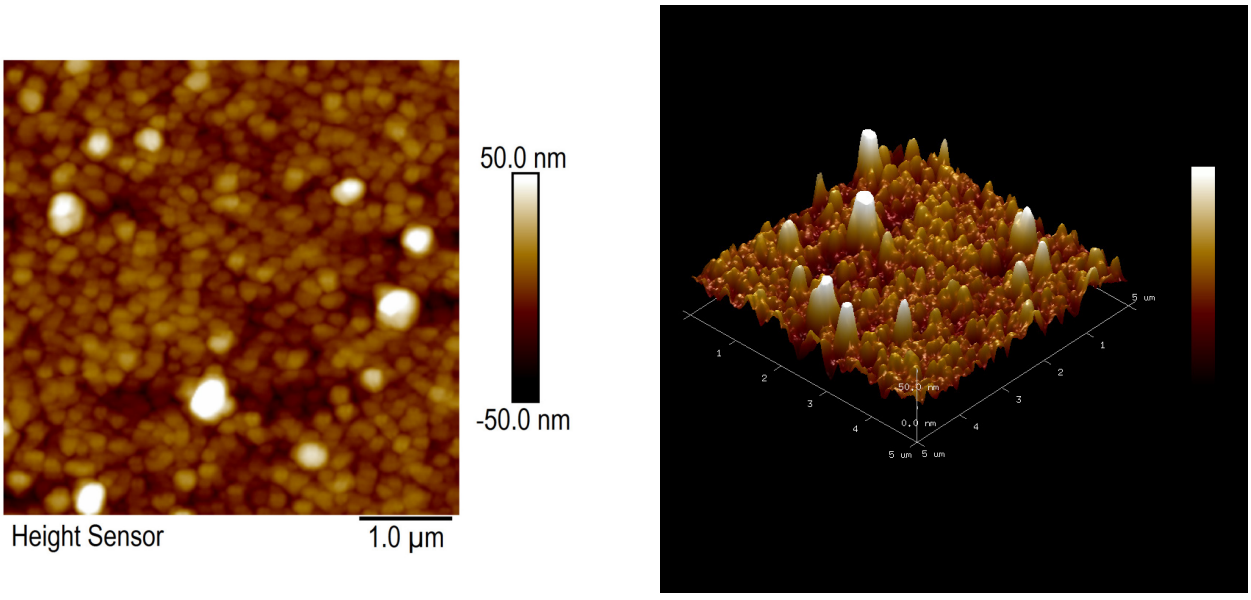

Figure A3: 2D and 3D AFM image of the roughness for membrane #4

Figure A3 for membrane #4 are similar to membrane #2 but the area surrounding the peaks are rougher than observed in membrane #2.

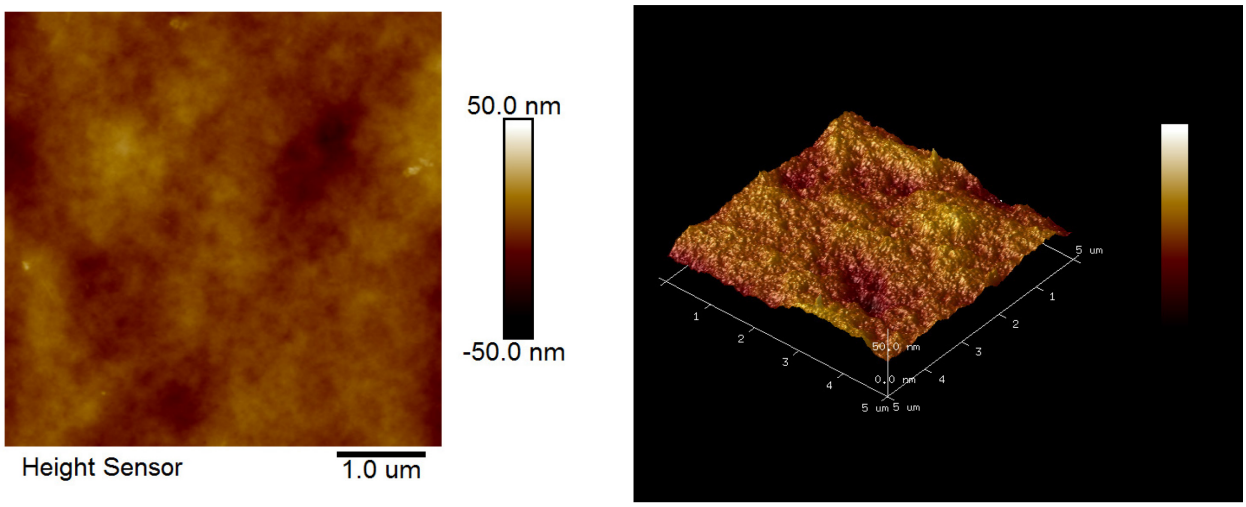

Figure A4: 2D and 3D AFM image of the roughness for membrane #5

Figure A4 for membrane #5 shows no larger peaks like membrane #2, #3, and #4. Only a smooth membrane surface is observed.

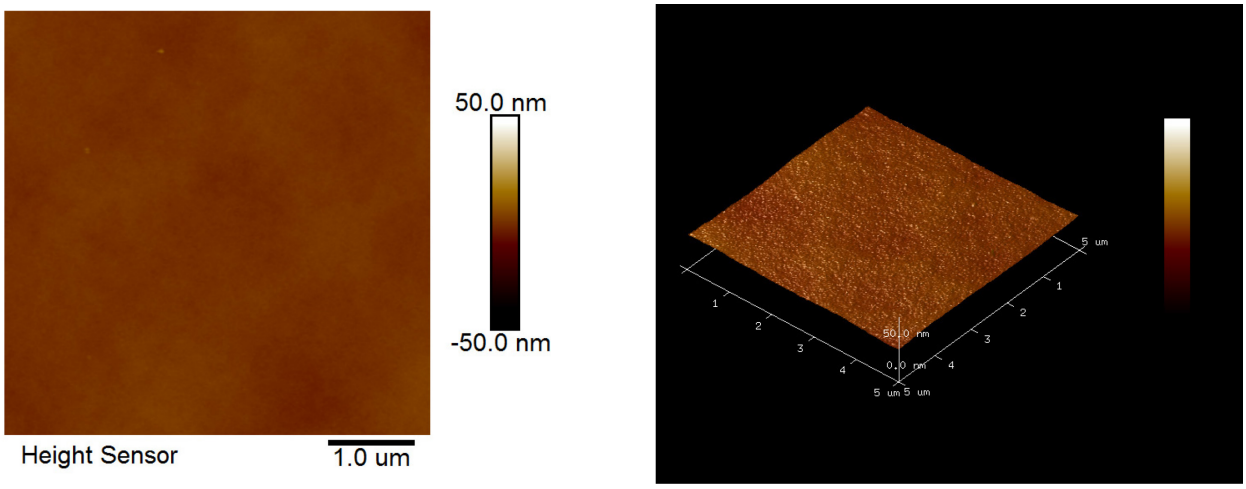

Figure A5: 2D and 3D AFM image of the roughness for membrane #6

Figure A6 for membrane #6 shows again no larger peaks like membrane #2, #3, and #4. However this membrane is the smoothest out of all the membranes tested.

The following figures are additional SEM images of membranes #2 to #6:

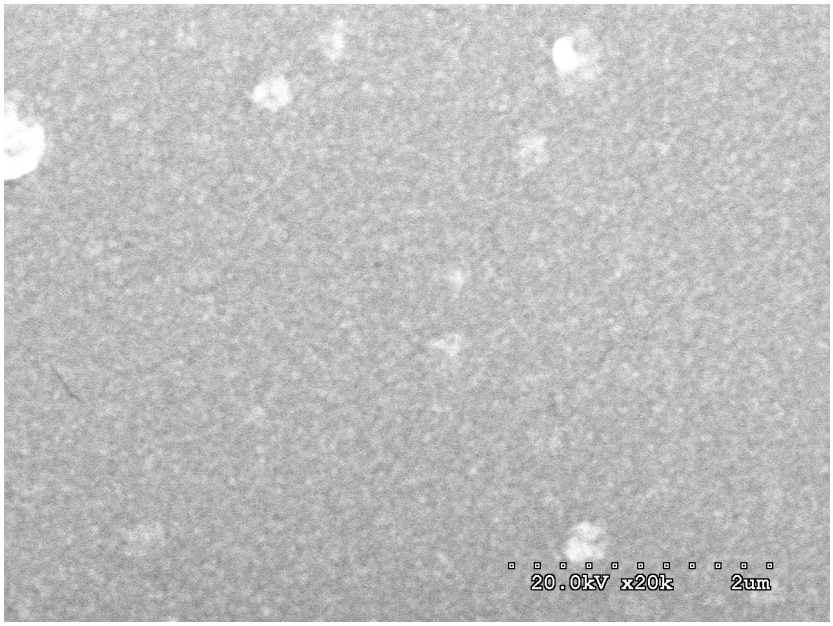

Figure A6: SEM image (20k magnification) of the surface morphology for membrane #2

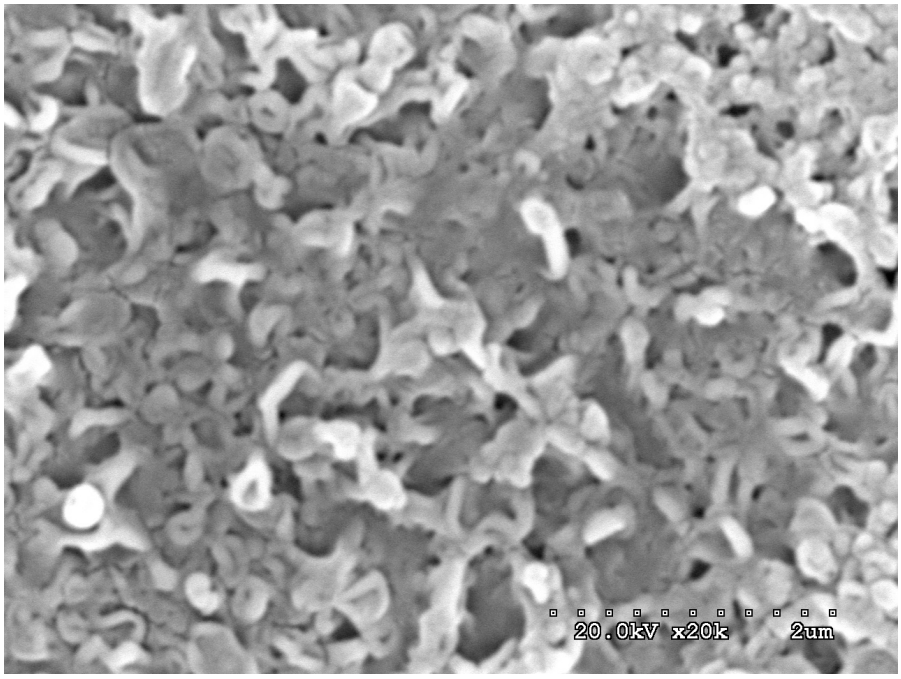

Figure A7: SEM image (20k magnification) of the surface morphology for membrane #3

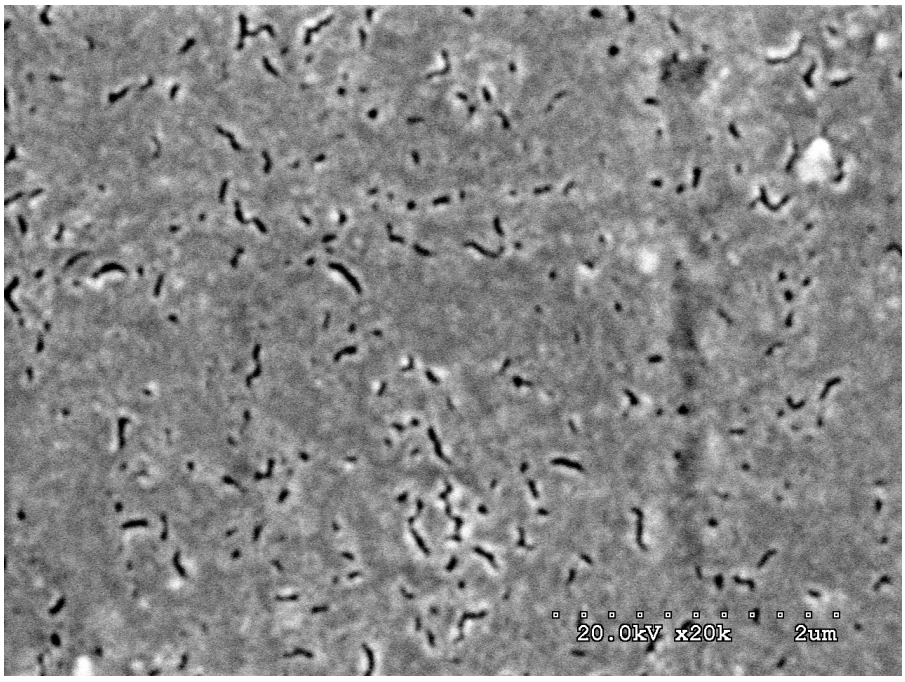

Figure A8: SEM image (20k magnification) of the surface morphology for membrane #4

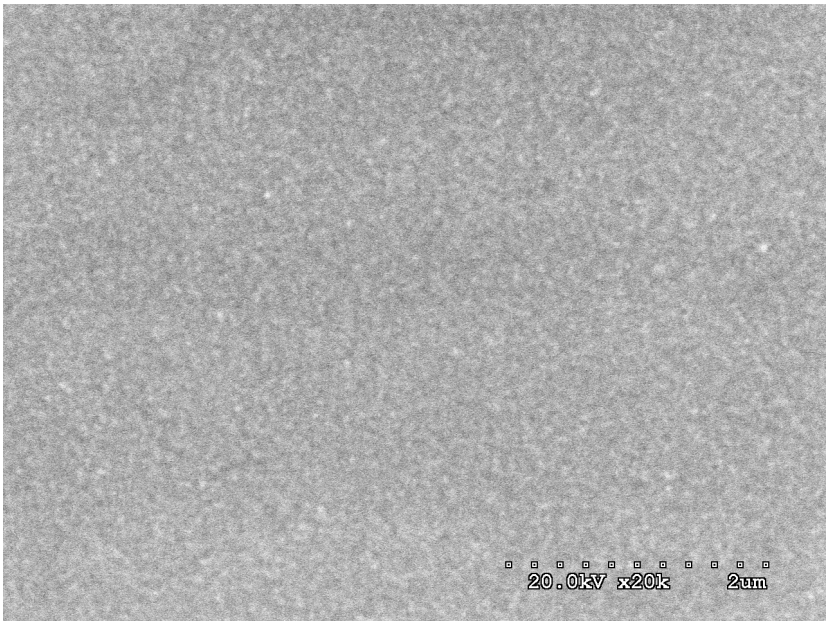

Figure A9: SEM image (20k magnification) of the surface morphology for membrane #5

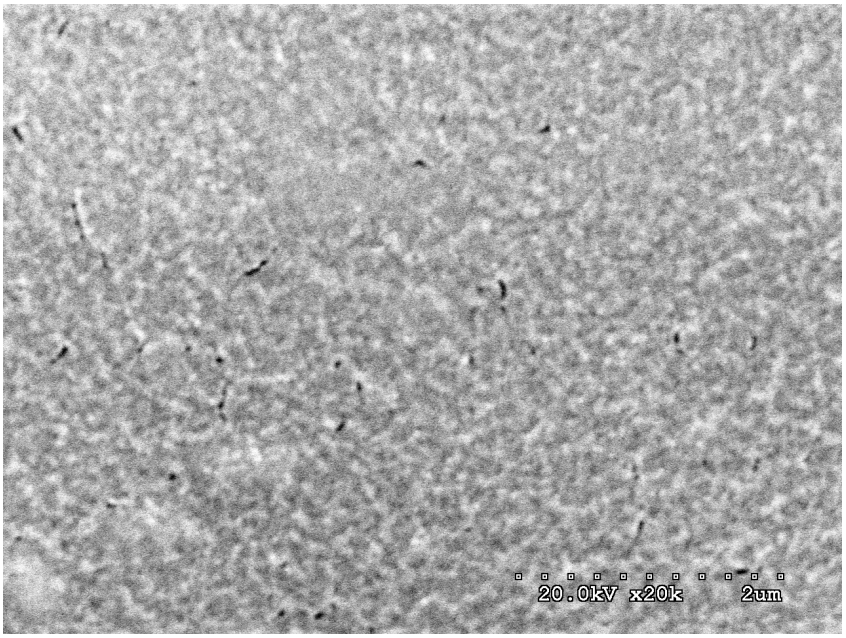

Figure A10: SEM image (20k magnification) of the surface morphology for membrane #6